# Changes in the lysosomal proteome under stressed conditions

Kaela O'Connor

A thesis submitted in partial fulfillment of the requirements for the
Master's degree in Cellular and Molecular Medicine

Department of Cellular & Molecular Medicine
Faculty of Medicine
University of Ottawa

# Abstract

Autophagy is a critical cellular process that is implicated in a vast array of human diseases, including amyotrophic lateral sclerosis (ALS). The targets of this degradative mechanism are frequently altered depending upon the inducing condition, however exactly how these targets change has rarely been explored on a proteomic level. To assess the targets of autophagy, this project analyzed the proteome of lysosomes collected by immunoprecipitation from cells undergoing starvation or recovering from oxidative stress. Oxidative stress induces stress granule formation and is frequently used as a cellular model for ALS. Our results show that while lysosomes from these two conditions retain a similar array of traditionally lysosomal proteins, they nevertheless display substantial differences indicating that their autophagic targets differ. Using Ingenuity Pathway Analysis (IPA) as well as gene ontology (GO) term analysis, the purine biosynthesis pathway was identified as being significantly enriched in lysosomes collected from sodium arsenite treated cells. The enrichment of the purine biosynthesis pathway was heavily dependent on ATG7, indicating these proteins localized to the lysosome primarily through macroautophagy. IMPDH2, the rate-limiting enzyme for guanylate production in the purine biosynthesis pathway drew particular attention due to its significant enrichment in sodium arsenite lysosomes, and its partial dependence on ATG7. Due to this discovery, and the presence of KFERQ-like sequences within the protein, our data suggests that IMPDH2 may localize to the lysosome through both macroautophagy and chaperone-mediated autophagy.

Furthermore, numerous ALS-linked proteins were identified to be enriched in sodium arsenite lysosomes including SOD1, DCTN1, PFN1, TUBA4A, SQSTM1, VCP, CHMP2B, TDP-43, VAPB and TMEM106B. Their presence within the lysosome strengthens arguments that autophagy plays a key role in ALS. Overall, this project confirms the changing substrates of autophagy depending on the environmental

condition and highlights the purine biosynthesis pathway as being involved in the cellular response to oxidative stress.

# Statement of Contributions

This thesis was written by me, Kaela O'Connor, and edited by Dr. Derrick Gibbings prior to submission. Derrick Gibbings conceptualized the initial project. All experimental procedures were performed by myself, except for those listed below.

The StemCore Laboratories performed sequencing to confirm the sequence of my sgRNAs.

Alexandre Savard acquired microscopy images validating the expression of the LysoIP construct using the Zeiss AxioImager M2.

Charlotte Manser performed immunofluorescent staining on cells I treated with bafilomycin $A_1$, sodium arsenite or HBSS to assess their stress response. These were then imaged by Stephen Baird.

Liquid-chromatography mass spectrometry was performed by Zhibin Ning, after I had prepared the samples.

# Acknowledgments

This thesis is dedicated to my grandfather, Dr. Nicolas Steinmetz, for being my fierce supporter and for being the first to ignite my passion in science. Thank you for showing me the importance of how science interacts with society, and for living your life with intelligence, kindness, and acceptance. I hope to be half the person you are one day.

The length of these acknowledgments are a testament to the size and strength of my support network, and to my innate tendency to ramble. I suppose I could distill the following words down to the following: Thank you. You all helped get me here, and I am so fortunate to have you in my life. But I won't.

To my supervisor, Derrick Gibbings, thank you for sticking with me through changing projects and a global pandemic. I appreciated your advice and guidance throughout. Thank you for letting me explore various novel techniques, challenging me to think through my problems, being incredibly patient during the writing process and for teaching me to be a better student. I am also grateful to my TAC members, Maxime Rousseaux and Baptiste Lacoste, for always being understanding and providing key feedback during our yearly meetings. You both helped encourage me more than you know.

To the past (Maisa Alkailani, Huishan Guo, Jenna McCann, Daniela Sosa-Mirandes, Kristofferson Tandoc, James Taylor) and present (Kallol Dutta, Charlotte Manser, Olanta Negeri, Ryan Reshke, Alexandre Savard, Yunping Xue, Adnie Etienne) members of the Gibbings lab, thank you all for your support and your willingness to always help when it was needed. In particular, I need to thank my afternoon squad, Charlie & Ryan, for keeping me (somewhat) sane while working nights, always listening to me, and providing crucial TV show recommendations. I genuinely don't think I could have gotten through this degree without your support. Charlie – I expect regular phone calls, lunches and drinks to help us both survive the rest of grad school. I'm so grateful this lab introduced us to each other. Olanta & Daniela – thank you for seeing me through the entirety of this degree (and introducing me to MooShu) your support through my many projects was vital.

To my family, thank you for nurturing my curiosity, and continuously reminding me that I can do whatever I set my mind to. To Grandma, Nana & Zeke thank you for believing in me, supporting me and for ensuring that kindness was a core pillar on both sides of the family.

Mom and Dad, thank you for raising me to believe I am limitless. Thank you for never stopping me from pursuing something new (except singing, and for that I am grateful), and always being my biggest supporters. Mom, you live every day of your life as I aim to, with pure kindness, grace, intelligence, and compassion. Dad, I hope

one day to have your diligence, wit, organization, and ability to see the positive even when your family is hangry in a foreign country. I am so grateful to have been raised by both of you, and I am proud to be your daughter.

Matt, you are the bravest and strongest person I know. Thank you for always being by my side, for making me a better person, and for getting me through my math homework in elementary school. Your perseverance, creativity and intelligence inspire me. Your ability to instill humour into the toughest of situations is admirable, and I can only hope that whenever I face a roadblack I can be as bada** as my little brother.

To my non-lab friends, Caro, Barbara and Arielle – thank you for helping me grow up. You have all been there for me through thick and thin and I don't know where I would be without you. Thank you for taking classes with me, for travelling with me, for celebrating our wins and mourning our losses. You are the best friends anyone could ever ask for.

Piers, thank you for being there with me every day, for listening to me complain and for reassuring me day in and day out. Thank you for dealing with my stresses day to day, for being my shoulder to lean on and for filling our lives with laughs and smiles. Thank you for letting me know that scientific figures do not align with design principles, for choosing the font this thesis is written in and for allowing me access to your Adobe Suite. You are my partner in life, and I couldn't have gotten through this without you. Thank you for believing in me, even when I do not believe in myself. And for feeding me - you may be the only thing standing between me and a severe nutrient deficiency.

And Jim & Diana - thank you for bringing up Piers to be the person he is today. Thank you for always having our backs, for being quick to laugh, and for being my second set of parents. There is no one I would rather be stuck on a deserted island with - because who better to make our escape raft!

Finally, to all of my friends and family, thank you for listening to me ramble about my work, for always asking questions and showing interest. It means more to me than you know, and I never tire of answering.

# Table of Contents

# List of Figures

# List of Abbreviations

**ADSS2**: Adenylosuccinate Synthetase

**AICAR**: 5-aminoimidazole-4-carboxamide ribonucleotide

**ALS**: Amyotrophic lateral sclerosis

**ATG**: Autophagy-related

**ATIC**: AICAR transformylase/inosine monophosphate cyclohydrolase (ATIC)

**ATP**: Adenosine triphosphate

**BECN1**: Beclin-1

**Bnip3**: Bcl-2/E1B-19K

**C9ORF72**: Chromosome 9 open reading frame 72

**ACN**: Acetonitrile

**CLEAR**: Coordinated Lysosomal Expression and Regulation

**CMA**: Chaperone-mediated autophagy

**CNS**: Central nervous system

**DMEM**: Dulbecco's Modified Eagle Medium

**DTT**: Dithiothreitol

**ER**: Endoplasmic reticulum

**ESCRT**: Endosomal sorting complexes required for transport

**FBS**: Fetal bovine serum

**FDR**: False discovery rate

**FIP200**: FAK family kinase-interacting protein of 200 kDa

**FUNDC1**: FUN14 domain-containing protein 1

**FUS**: FUsed in Sarcoma

**G3BP**: Ras GTPase-activating protein-binding protein

**GABARAP**: Gamma-aminobutyric acid receptor-associated protein

**GAP**: GTPase activating protein

**GAPDH**: Glyceraldehyde-3-phosphate dehydrogenase

**GATOR1**: GAP activity toward RAGs 1

**GDP**: Guanosine diphosphate

**GO**: Gene ontology

**GTP**: Guanosine triphosphate

**GTPases**: Guanosine triphosphatases

**HA:** Hemagglutinin

**HBSS**: Hanks' Balanced Salt Solution

**HEK293**: Human embryonic kidney 293

**HOAc**: Glacial acetic acid

**HSC70**: Heat shock 70 kDa protein 8

**HSP90**: Heat shock protein 90

**IAA**: Iodoacetamide

**IDT**: Integrated DNA Technologies

**IPA**: Ingenuity Pathway Analysis

**KFERQ-motif**: Lysine-Phenylalanine-Glutamate-Arginine-Glutamine motif

**LAMP1**: Lysosome-associated membrane glycoprotein 1

**LAMP2A**: Lysosome-associated membrane protein 2 isoform A

**LC-MS**: Liquid chromatography mass spectrometry

**LC3B**: Microtubule-associated proteins 1A/1B light chain 3B

**LCDs**: Low complexity domains

**LFQ**: Label-free quantification

**LLPS**: Liquid-liquid phase separation

**LSDs**: Lysosomal storage disorders

**LysoIP**: Lysosomal Immunoprecipitation

**MIST**: Mass spectrometry Interaction Statistics

**mLST8**: Mammalian lethal with Sec13 protein 8

**mTOR**: Mechanistic target of rapamycin

**mTORC1**: Mechanistic target of rapamycin complex 1

**MVBs**: Multivesicular bodies

**NDP52**: Calcium-binding and coiled-coil domain-containing protein 2/ Nuclear dot protein 52

**NUFIP1**: Nuclear fragile X mental retardation-interacting protein 1

**OPTN**: Optineurin

**PABP**: Polyadenylate-binding protein 1

**PAICS**: Bifunctional phosphoribosylaminoimidazole carboxylase/ phosphoribosylaminoimidazole succinocarboxamide synthetase

**PARKIN**: E3 ubiquitin-protein ligase parkin

**PBS**: Phosphate buffered saline

**PE**: Phosphatidylethanolamine

**PEI**: Polyethylenimine

**PFAS**: Phosphoribosylformylglycinamidine synthase

**PI3K**: Phosphoinositide 3-kinasse

**PlaToLoCo**: Platform of Tools for Low Complexity

**PVDF**: Polyvinylidene fluoride

**Raptor**: Regulatory protein associated with mTOR

**RBP**: RNA binding protein

**RHEB**: Ras homolog enriched in brain

**Rho:** Ras homolog

**RhoA:** Ras homolog family member A

**RNA**: Ribonucleic acid

**RNase A**: Ribonuclease A

**sgRNA**: Small guide RNA

**siRNA**: Small interfering RNA

**SMN**: Survival motor neuron protein

**SNAP29**: Synaptosomal-associated protein 29

**SNARE**: SNAP receptor

**SOD1**: Superoxide dismutase

**SPIONs**: Superparamagnetic iron oxide nanoparticles

**SQSTM1/p62**: Sequestosome-1/Ubiquitin-binding protein p62

**STX17**: Syntaxin-17

**TDP-43**: TAR DNA binding protein 43 kDa

**TFA**: Trifluoroacetic acid

**TFEB**: Transcription factor EB

**TIA1**: Cytotoxic granule associated RNA binding protein TIA1

**TMEM192**: Transmembrane protein 192

**TOMM20**: Translocase of outer mitochondrial membrane 20

**TSC complex**: Tuberous sclerosis complex
**TSG101**: Tumor susceptibility gene 101 protein

**ULK1/2**: Unc-51 like autophagy activating kinase

**UVRAG**: UV radiation resistance-associated gene

**VAMP7/8**: Vesicle-associated membrane protein 7/8

**VPS34**: Phosphatidylinositol 3-kinase catalytic subunit type 3

# Chapter 1: Introduction

Autophagy is a highly conserved process that is one of the cell's degradation and recycling mechanisms. Autophagy complements the related, but distinct, ubiquitin-proteasome system which works to degrade proteins through ubiquitination of targeted proteins. Autophagy is capable of degrading both ubiquitinated targets, as well as other forms of selective and non-selective degradation.

Autophagy is crucial for both regular protein and organelle turnover under homeostatic conditions, as well as adapting the cell to potentially detrimental conditions. Depending on the environmental conditions autophagy can play different roles including providing nutrients by breaking down macromolecules or demonstrating a protective effect by selectively eliminating harmful targets[1]. While autophagy occurs constitutively, it is upregulated under stressed conditions[2–5]. The ability of autophagy to adapt to changing conditions is indicative of targets of autophagy changing depending on the cellular needs. Defining what is being targeted by autophagy could provide crucial information into both cellular and degradative alterations specific to different conditions.

Disruption of autophagy has been tightly linked to numerous diseases including neurodegenerative disease, cancer and infection (reviewed by Dikic et al. 2018[1]) One prominent example theorized to contribute to disease states, such as amyotrophic lateral sclerosis (ALS), is the ability of autophagy to degrade stress granules. However, despite knowing that autophagy contributes to an everchanging cellular adaptive response and that its substrates can change depending on the environment, the differences in targets from one condition to another have not been well-defined. Previous work has used the lysosomal immunoprecipitation (LysoIP) system to isolate lysosomes and assess autophagic changes between drug and starvation induced autophagy[6]. This project aims to expand this work by utilizing the LysoIP system

to define the lysosomal proteome under new stressed conditions and assess the differences between them.

## 1.1 Forms of autophagy

Autophagy can be divided into three main and distinct processes: chaperone-mediated autophagy (CMA), microautophagy and macroautophagy. It is the final step of autophagy, degradation within the lysosome, that links CMA, microautophagy and macroautophagy together[7]. Lysosomes are acidic organelles that contain numerous hydrolases capable of breaking down macromolecules including proteins, nucleic acids and lipids[8].

### 1.1.3 Macroautophagy

The most widely studied form of autophagy is macroautophagy, which uses double-membraned vesicles, termed autophagosomes, to transport cargo to the lysosomes. The specifics of this process have been reviewed extensively, and are briefly summarized here, and represented in Figure 1[1,7]. In brief, a phagophore, a double-membrane, is nucleated at a phagophore assembly site, and then elongated until it is sealed around the substrates of autophagy. Upon this sealing it is called an autophagosome. The autophagosome travels to the lysosome where its outer membrane fuses with the lysosome, forming an autolysosome. Subsequently, the inner membrane is degraded, releasing the cargo for degradation by lysosomal hydrolases.

#### *1.1.3.1 Nucleation of the phagophore*

The first stage of macroautophagy is the formation of a phagophore, the initial membrane structure of the autophagosome, at a phagophore assembly site[1]. This initial nucleation is induced by the ULK1/2 complex, composed of ULK1/2, ATG13, FIP200 and ATG101. The phagophore assembly site is typically considered to be localized at the endoplasmic reticulum (ER), however other locations have recently

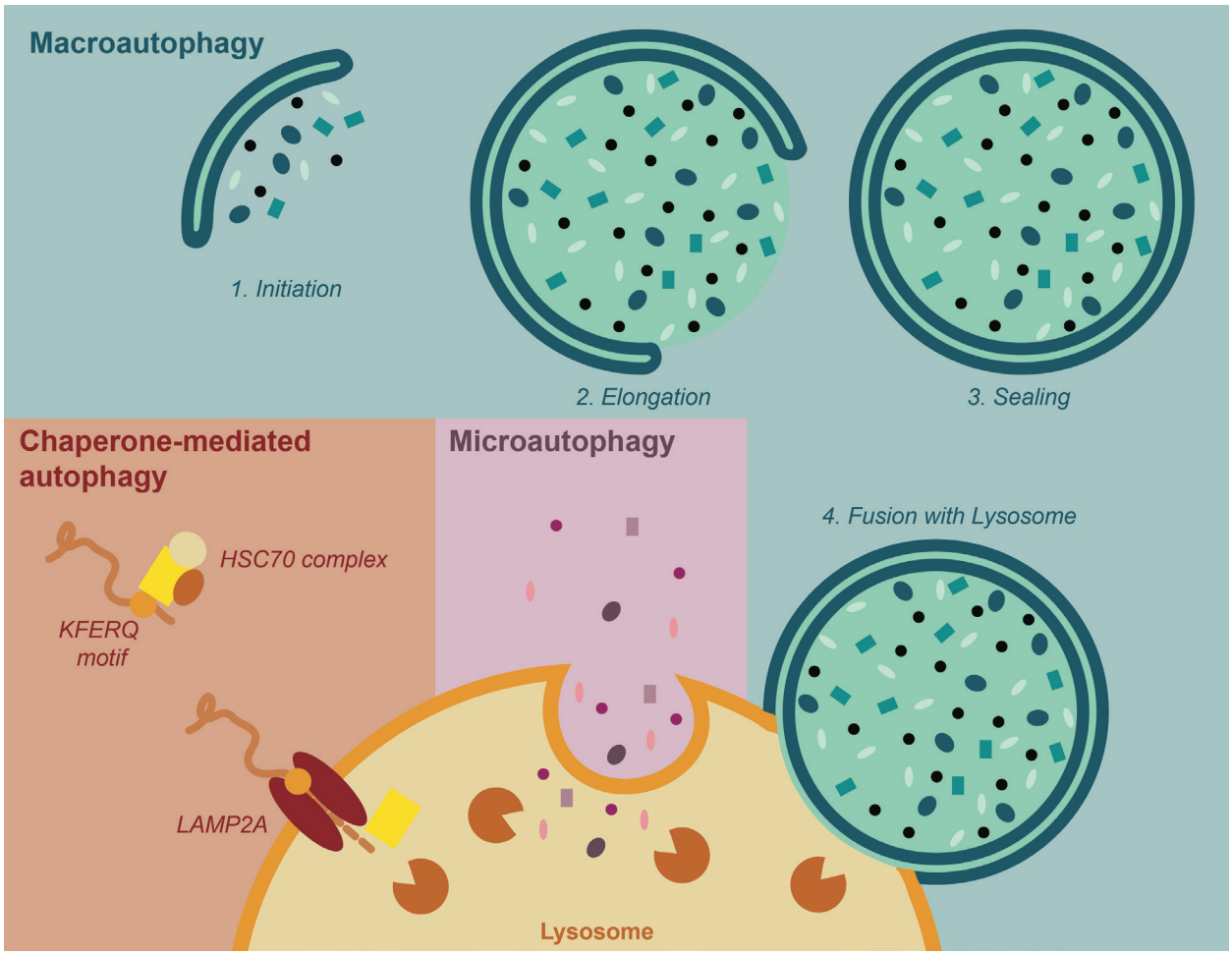


**Figure 1: Schematic of the three primary types of autophagy.** This figure illustrates macroautophagy, chaperone mediated autophagy (CMA) and microautophagy. The multi-step process of macroautophagy is illustrated as four primary steps, beginning with the formation of the phagophore, that then matures into the autophagosome around cargo. This cargo, depending upon the cellular state, may be specific or non-specific. After the autophagosomal formation, the double-membraned vesicle fuses with the lysosome forming the autolysosome. Eventually, the interior membrane is degraded to release the cargo, which is then itself degraded. Comparatively, microautophagy is the direct uptake of cytosolic contents into the lysosome by invagination of the lysosomal membrane. Finally, CMA recognizes specific proteins for degradation that contain a KFERQ-like motif through the HSC70 complex. The proteins are transported to the lysosomal membrane, where LAMP2A proteins facilitate the transport of the proteins across the membrane.

been proposed such as the mitochondria, plasma membrane and the Golgi complex[1]. The phagophore membrane elongates and eventually seals itself around its cargo, becoming an autophagosome.

Following the initiation of this process, the nucleation of the phagophore begins with the recruitment of the Class III phosphoinositide 3-kinase (PI3K) complex, composed of VPS34, PIK3R4 and BECN1. The association of these proteins with ATG14

forms complex I, and the association with UV radiation resistance-associated gene protein (UVRAG) forms complex II[9]. ATG14 is essential for autophagosome formation, while the role of UVRAG is slightly more debated – with some studies showing the PI3K complex II is associated primarily with the endocytic pathway and others showing its role in autophagy[10–12].

#### *1.1.3.2 Elongation of the autophagosomal membrane*

The elongation process is assisted by several proteins, including two conjugates involving ubiquitin-like proteins. The first such example is the ATG12–ATG5–ATG16L complex. To form this complex, ATG12, a ubiquitin-like protein, is conjugated to ATG5 through the actions of ATG7 (an E1-like protein) and ATG10 (an E2-like protein). ATG12–ATG5 then bind ATG16L through ATG5, and the complex dimerizes through ATG16L[13]. The complex binds to the forming autophagosomal membrane but dissociates upon completion of the autophagosome. For this reason, it is not associated with completed autophagosomes or autolysosomes[13]. In yeast, the second ubiquitin-like protein is Atg8 whereas the mammalian Atg8-like proteins include both the LC3 and GABARAP subfamilies.

The processing of these ubiquitin-like proteins is highly similar across the different species but will be described using LC3 as an example. Initially the C-terminus of LC3 is proteolytically cleaved by ATG4, forming LC3-I and subsequently activated by ATG7 (an E1-like enzyme)[14]. The activated LC3-I is then conjugated to the lipid phosphatidylethanolamine (PE) in a ATG3 (E2-like enzyme) and ATG12–ATG5–ATG16L (E3-like enzyme) dependent manner forming LC3-II[14,15]. The lipid modification anchors LC3-II to the autophagosomal membrane[16]. The lipidation of LC3 is reversible through the action of ATG4, freeing it from its membrane bound state. In yeast, the delipidation of Atg8 is thought to be essential for the normal formation of autophagosomes, potentially due to the removal of lipidated Atg8 from other membrane locations[17,18]. Comparatively, the delipidation of GABARAP/LC3 does not

seem to be necessary for standard autophagic flux in mammalian cells[19].

While the exact method behind the membrane elongation of mammalian autophagosomes remains to be determined, some human and yeast data suggests that it may occur through ATG2 and ATG9[20]. ATG2 and ATG9 localize to the expanding end of the phagophore. ATG2 is known to be able to transfer lipids and ATG9 is the sole transmembrane protein known to be involved in the formation of autophagosomes. An ATG9 homotrimer was demonstrated to form a pore from the outer to inner layer, and mutations within the pore impaired expansion. This led to the proposed mechanism that suggests that ATG2 transfers lipids from the ER to the phagophore, where ATG9 translocates the phospholipids from the outer to the inner membrane[20].

#### *1.1.3.3 Sealing of the autophagosome*

The eventual closure of the autophagosome is dependent on a large swath of proteins, including many of those involved in the membrane elongation, such as ATG2 and ATG5[21,22]. Additionally, Endosomal sorting complexes required for transport (ESCRT) and SNARE machinery play roles in the closure of autophagosomes, wherein the absence of these proteins leads to accumulation of unsealed phagophores[23–25] (reviewed in Jiang et al. 2021[26]).

#### *1.1.3.4 Fusion of the autophagosome with the lysosome*

Eventually, the outer membrane of the autophagosome fuses with the lysosomal membrane, resulting in a single-membrane vesicle within the lysosome – this structure is called an autolysosome. The fusion of these two organelles is influenced by numerous proteins. One significant group of players are SNARE proteins, which mediate the fusion process through lysosomal and autophagosomal localized proteins. STX17 is required for the fusion process, and is recruited to the mature autophagosomal membrane[27]. STX17 then interacts with lysosomal SNARE proteins,

potentially VAMP7 or VAMP8, through the intermediate SNAP29[27,28]. The final step of all forms of autophagy is, of course, that the hydrolases within the lysosome degrade the cargo allowing for various building blocks to be recycled[7].

#### *1.1.3.5 Forms of macroautophagy*

Macroautophagy can engage in both specific and bulk degradation. With each form of selective macroautophagy comes a new term such as mitophagy (degradation of mitochondria), ERphagy (degradation of the ER), ribophagy (degradation of ribosomes) and granulophagy (degradation of stress granules), amongst many others. These selective processes demonstrate how the targets of autophagy can change dramatically based on what the cell is experiencing. For example, exposure to hydrogen peroxide has been shown to increase mitophagy but not impact non-selective macroautophagy, whereas starvation increases mitophagy to a lesser degree but does induce non-selective autophagy[29]. Ribophagy is similarly impacted by the stress condition the cell is under. While starvation, sodium arsenite and chromosome mis-segregation induced ribophagy, neither inhibition of translation elongation, proteasome inhibition nor hydrogen peroxide treatment significantly increased ribophagy[30]. These results highlight just how particular the substrates of autophagy can be, as both hydrogen peroxide and sodium arsenite induce oxidative stress.

Selective macroautophagy makes use of receptor proteins to transport the target to the autophagosome. The receptor is dependent on the intended target, for example SQSTM1/p62 is a selective macroautophagy receptor that canonically targets ubiquitinated proteins and NUFIP1 is a receptor that targets ribosomes. These selective receptors do typically have one primary thing in common: either the ability to self-oligomerize, or a high concentration of the protein on the target's surface[31]. The receptors will also contain a LC3- interacting region, and/or a FIP200-interacting region[32–35]. This permits the recruitment of macroautophagic machinery to the site

of the target allowing the autophagosomal formation to begin. The LC3-interacting region ties the target to the growing autophagosomal membrane to cause its eventual degradation. The FIP200-interacting region recruits FIP200, a member of the ULK1/2 complex to the region which is essential for autophagosome formation.

Ubiquitination is frequently used as a cellular signal to target a substrate for degradation, either by autophagy or the proteasome. In selective macroautophagy there are both ubiquitin dependent, and independent pathways for cargo recognition (reviewed in Khaminets et al. 2016[36]). For example, some forms of mitophagy are modulated by a ubiquitin dependent system. In this case, when mitochondria are damaged the ubiquitin ligase PARKIN is localized to the outer membrane where it ubiquitinates mitochondrial surface proteins[37]. These ubiquitinated proteins can then be identified by autophagy receptors with ubiquitin binding domains, such as optineurin (OPTN) and NDP52[37–39]. These receptors can then induce autophagosome formation via their LC3-interacting regions. Intriguingly, mitophagy can also be induced by ubiquitin independent systems. One example of this is that hypoxia dephosphorylates an outer mitochondrial membrane receptor, FUNDC1[40]. This dephosphorylation results in increased binding between FUNDC1 and LC3, resulting in increased mitophagy.

Selective macroautophagy mechanisms are also not necessarily specific to each organelle, for example the homodimerization of Bnip3 in yeast was shown to be a ubiquitin independent signal for both ERphagy and mitophagy.

The process to recruit targets for selective macroautophagy can also be quite complex and involve a cascade of proteins. For example, granulophagy has been reported to be dependent on a classic selective macroautophagy receptor – SQSTM1/p62. While this receptor is typically reported as a ubiquitin receptor, in this case it acts in a ubiquitin independent fashion. This research demonstrates that symmetrically methylated arginines in FUS are recognized by an SQSTM1/p62 and C9ORF72

complex[41]. The interaction between FUS and the complex is mediated by SMN. Ultimately, the LC3-interacting region of SQSTM1/p62 recruits autophagic machinery and begins the degradation of stress granules.

These examples demonstrate the immense diversity, and complexity, in targeting mechanisms for selective macroautophagy. Additionally, they also provide further context as to how a cell's autophagy targets can change depending upon the environmental conditions.

### 1.1.1 Chaperone-Mediated Autophagy

Originally considered to be a process primarily concentrated on protein quality control, CMA has continued to demonstrate its importance in critical processes, including responses to stress and neurodegenerative disease[42–47]. In CMA an amino acid motif is used to identify targets which are then transported to and across the lysosomal membrane by chaperones[7,48,49]. A pentapeptide recognition motif, Lysine-Phenylalanine-Glutamate-Arginine-Glutamine (KFERQ) – or a KFERQ-like motif, is used to identify targets for CMA[50]. This motif is bound by cytoplasmic HSC70 and transported to the lysosomal membrane where the substrate and HSC70 associate with LAMP2A. This association forms the LAMP2A complex that is then stabilized by HSP90. Before the substrate can be translocated it needs to be unfolded by HSC70 and other chaperones. HSC70 plays a crucial role in both the translocation process and in the subsequent monomerization of LAMP2A to prepare for the next substrate[7]. LAMP2A represents the rate limiting factor of this process. The translocation of the target also relies upon lysosomal HSC70, localized in the lysosomal lumen[42]. Based on sequence alone, up to 45% of proteins may contain the canonical KFERQ-like motif, however because the KFERQ-like motif must be accessible by HSC70 a more restricted set of proteins are actually targeted by CMA[51]. The availability of this motif is heavily dependent on the tertiary structure of the protein, as well as post-translational modifications[52–54]. This is demonstrated by experiments that have generated

antibodies against the motif and pulled down approximately 30% of cytosolic proteins[55]. Due to this dependency on structure, disease-specific modifications, protein misfolding or protein damage can impact the availability of specific substrates to CMA. Despite the high percentage of proteins with a KFERQ-like motif, exceedingly few have been experimentally confirmed as CMA substrates indicating the potential for many more proteins to be validated[51].

Despite being termed a KFERQ-like motif, the actual peptide motif recognized by HSC70 may be quite different than the originally described sequence. While ribonuclease A (RNase A), the first protein identified as a CMA substrate, contained the KFERQ sequence, it was later determined that the canonical motif is more reliant on the physical properties of each residue rather than the specific KFERQ sequence[51,55]. The properties that must be present are the following, and in order: one or two positively charged peptides (Lysine/Arginine), one or two hydrophobic peptides (Isoleucine, Leucine, Valine or Phenylalanine); one negatively charged peptide (Aspartic acid/Glutamic acid) and one Glutamine on either side of the motif[55]. To further complicate matters, post-translational modifications can modify existing motifs to act as KFERQ-like motifs. Notably, phosphorylated residues can replace negatively charged peptides, and acetylated Lysine can replace Glutamine[51].

Due to these particularities in the way that KFERQ-like recognition occurs, the process is both flexible and specific. While it is specific degradation, the proteins with accessible and appropriate KFERQ-like motifs can change depending on cellular conditions and post-translational modifications. This allows for CMA to adapt to the cell's current state.

### 1.1.2 Microautophagy

Microautophagy involves the direct uptake of cargo into the lysosomes via invagination of the lysosomal membrane[7,56]. Comparatively little is known regarding microautophagy, including its regulation, involved proteins or its targets[7,48]. This is

especially true in mammalian cells, due to the small size of the lysosomes and lack of tools to study this phenomenon. Consequently, the majority of studies have been performed in yeast which contain one large vacuole, rather than numerous lysosomes. Notably however, there is some evidence that mammalian and yeast microautophagy may have distinct regulatory processes[57].

Despite its name, microautophagy is documented to be capable of degrading much larger components of the cell than soluble proteins. In yeast there is evidence of selective degradation of parts of the ER, peroxisomes, nucleus, mitochondria and lipid droplets (reviewed in Schuck 2020[58]), in addition to general non-specific microautophagy.

One related process is endosomal microautophagy wherein substrates are directly taken up into multivesicular bodies (MVBs) (late endosomes) which then fuse with lysosomes. This process utilizes essential proteins found in both autophagic and endosomal processes. ESCRT-I and III are used to bud vesicles into the endosomal lumen, and HSC70 mediates specific protein degradation through KFERQ-like motifs in mammalian cells[59]. While CMA and endosomal microautophagy share this requirement for HSC70 and KFERQ-like motifs, they can be functionally distinguished by the requirement of LAMP2A for CMA.

### 1.1.4 Differentiating autophagy types

The existence of three forms of autophagy complicates the study of these degradative processes, as more than one of these versions of autophagy may contribute to any phenomenon. To be able to differentiate microautophagy, macroautophagy and CMA a number of processes and techniques have been developed.

One classic example is the depletion of key proteins using siRNA or CRISPR. For example, it is possible to selectively block CMA by producing LAMP2A$^{-/-}$ organisms or cell lines, which lack the rate-limiting protein in CMA[60,61]. Similarly, there are many

key factors in macroautophagy that one can knockout to inhibit macroautophagy including ATG5, ATG7 and FIP200[62–64], with minimal or no impact on CMA or microautophagy. In macroautophagy it may be beneficial to perform experiments with knockouts targeting different stages of autophagosome formation in order to control for any potential compensatory mechanisms or off-target effects specific to the knockout of one protein. For example one could perform experiments in both an *ATG7*$^{-/-}$ (halts phagophore expansion) and a FIP200$^{-/-}$ (halts phagophore nucleation) cell line/organism. Endosomal microautophagy can be targeted by knocking out TSG101, a subunit of the ESCRT-I complex[65]. Unfortunately, depletion of TSG101 can have significant unintended consequences including impaired MVB formation, impaired receptor degradation and the formation of abnormal tubular structures stemming from the early endosome[66,67]. Furthermore, TSG101, as a subunit of the ESCRT-I complex, is also involved in exosome biogenesis[68]. Loss of TSG101 results in decreased exosome biogenesis, further highlighting its multifaceted role in the cell. The impact of TSG101 depletion on all these processes are major caveats to any results stemming from depletion of TSG101.

These modifications allow researchers to study what occurs to their target or mechanism of interest without specific types of autophagy. While these processes are not perfect, they do provide some additional confidence in the role of specific types of autophagy[69].

Measuring the flux of each type of autophagy frequently relies on measuring the levels of key proteins. For example, the level of CMA can be inferred by analyzing LAMP2A and lysosomal HSC70 levels, both of which are positively correlated with CMA[42,70]. Similarly, with macroautophagy it is possible to look at the ratio of LC3-I to LC3-II levels and levels of SQSTM1/p62, a known macroautophagic substrate/receptor to measure autophagosome formation and degradation[71]. Increased levels of LC3-II could be caused by increased formation of autophagosomes, impaired

ATG4, or impaired fusion with lysosome and degradation of autophagy substrates. Therefore, it is crucial to monitor both LC3-II and the levels of known substrates of macroautophagy, such as SQSTM1/p62 as their levels are indicative of the functioning of the entire macroautophagic process. For example, in macroautophagy knockout cells we expect to see an accumulation of SQSTM1/p62 and absent LC3-II – together these results support the depletion of autophagy.

While it is possible to study microautophagy, as previously mentioned it is more complicated due to a lack of effective tools. There does however exist a technique to differentiate between CMA and endosomal microautophagy activity by using a fluorescent tagged GAPDH system, and knocking out CMA or microautophagy[65]. GAPDH is a substrate of both autophagic processes, and its accumulation or lack thereof can be used as a measurement of autophagic flux through these pathways.

## 1.2 Regulation of Autophagy

Just as it is important to understand how autophagy occurs mechanistically, it is also important to understand what induces and inhibits these processes. Each autophagic process is regulated differently, however there are many common threads among the environmental factors that control them.

### 1.2.1 Regulation of macroautophagy

Macroautophagy occurs constitutively, and it can selectively degrade its targets, including ubiquitinated proteins, mitochondria and other damaged organelles[36]. However, under certain stress conditions bulk macroautophagy is performed engulfing cytosolic contents non-specifically[7]. This catabolic process is an important aspect of the cellular stress response and promotes cell survival by allowing building blocks to be redirected towards essential functions[7].

Macroautophagy is frequently controlled through upstream pathways impacting mechanistic target of rapamycin complex 1 (mTORC1). The mTORC1

complex is composed of mTOR, regulatory protein associated with mTOR (Raptor) and mammalian lethal with Sec13 protein 8 (mLST8)[72,73]. Notably, mTORC1 sits at the intersection between anabolism and catabolism – in addition to suppressing macroautophagy it promotes protein and nucleotide synthesis[74].

#### *1.2.1.1 Downstream interactions of mTORC1*

mTORC1 is a critical regulator of the macroautophagy pathway. This occurs through a few crucial downstream interactions. Under basal conditions, mTORC1 binds to the ULK1/2 complex and phosphorylates two of its components, ULK1/2 and ATG13[7]. This prevents the nucleation of the phagophore, and therefore halts autophagosome formation, and in turn limits macroautophagy. However, when mTORC1 is inactivated, which occurs through numerous stressed conditions, ULK1/2 and ATG13 are partially dephosphorylated thus promoting macroautophagy[7].

The second integral interaction is through transcription factor EB (TFEB), the identified master regulator of the Coordinated Lysosomal Expression and Regulation (CLEAR) gene network[75]. The transcription of numerous genes involved in autophagy and lysosome function is promoted by TFEB, leading to increased lysosomal biogenesis, autophagosome-lysosome fusion, autophagosomal biogenesis and autophagic flux[75,76]. Cells overexpressing TFEB have more autophagosomes, lysosomes and autophagolysosomes as well as enhanced degradation of proteins – and cells lacking TFEB experience the opposite. Importantly, mTORC1 regulates this transcriptional response by controlling the localization of TFEB. mTORC1 phosphorylates TFEB when active, retaining TFEB in the cytosol and on the lysosomal membrane[77,78]. However, when mTORC1 is inactivated, TFEB is dephosphorylated and translocates to the nucleus where it activates the CLEAR network inducing macroautophagy.

These downstream interactions of mTORC1 are critical to the cellular response to environmental conditions, as they relay the message to the lysosomal/autophagic

machinery. However, upstream of mTORC1 is what dictates how this central regulator will react – and in turn whether it will activate or inactivate TFEB, ULK1/2 or ATG13.

#### *1.2.1.2 Upstream regulators of mTORC1*

There are a plethora of environmental cues that trigger changes in mTORC1, as effective anabolism and catabolism are crucial for cell survival. The environmental cues that induce macroautophagy are frequently those that trigger a stress response, including hypoxia, starvation, ER stress, low growth factors and low ATP (reviewed in Parzych & Klionsky 2014[7]). A few environmental cues triggering macroautophagy will be explored below.

Two small guanosine triphosphatases (GTPases), Ras-related GTP-binding proteins (Rag family) and Ras homolog enriched in brain (RHEB), are integral for mTORC1 regulation and are frequently targeted to control macroautophagy[79]. The binding of both GTPases to mTORC1 are dependent on whether they are guanosine triphosphate (GTP) or guanosine diphosphate (GDP) bound[80–82]. Rag proteins are responsible for translocating mTORC1 to the lysosomal surface by interacting with the Raptor subunit, so that mTORC1 may then interact with RHEB, its activator[83–87]. The state of the Rag proteins is dependent on a large number of distinct molecules including the GTPase activating protein (GAP), the GATOR1 complex[80]. RHEB is under the control of its GAP, the TSC complex (TSC1, TSC2, TBC1D7) which promotes the maintenance of RHEB's GDP-bound state that is incompatible with mTORC1 interaction[82].

One well defined stressor that induces macroautophagy is starvation. This is imperative to cellular survival as macroautophagy can recycle cytosolic molecules into their base components allowing critical cell components to continue to be produced despite having no access to new nutrients. In amino acid starvation the cell has regulators that sense low levels of amino acids and respond by altering the guanine binding status of Rag proteins, producing conformations incompatible with being bound to mTORC1. Through this process, mTORC1 is inactivated, thus activating

macroautophagy. The exact process through which this occurs is dependent on the amino acid triggering the response, as well as the Rag protein being targeted[88–91]. Two amino acids with well-defined sensing pathways include leucine and arginine, both of which impact the GATOR1 factor.

A similar response is seen upon lack of nucleotides in the cell. Interestingly, this response is focused on purine nucleotide levels, adenylates and guanylates, and pyrimidine levels do not impact mTORC1 signalling[79,92]. Low levels of adenylates block mTORC1 activity by inhibiting the TSC complex, in turn inhibiting RHEB[79,92]. Guanylates also impacted this mechanism, however their long-term absence was required to affect autophagy and resulted in lower levels of RHEB[79]. One potential explanation for this focus on purine nucleotides is that the production of both guanylates and pyrimidines is dependent on adenylates[79]. There are established mechanisms that measure cellular energy levels by tracking adenosine triphosphate (ATP) levels and impact mTORC1, however disruption of the purine synthesis pathway was notably different from these pathways. Therefore, it remains unclear how exactly purine nucleotide depletion activates autophagy.

### 1.2.2 Regulation of chaperone-mediated autophagy

As we observe with macroautophagy, CMA can be induced by numerous stressors. In CMA in particular, these stressors frequently cause protein damage that then requires them to be cleared from the cell, such as oxidative stress[42], prolonged starvation[93] and hypoxia[94] (reviewed in Cuervo & Wong 2014[49]). These stressors impact the levels of LAMP2A, the rate limiting factor of CMA, either through increased transcription, as in oxidative stress, or reduced degradation, as in starvation[42,95].

CMA is also well documented to be activated by lack of nutrients; however, it follows a different pattern and mechanism of activation than macroautophagy. In CMA the process is driven by alterations in LAMP2A availability. Macroautophagy functions primarily in the first few hours (4-6 hours), while CMA is activated after this

time period (8-10 hours) and can continue for a few days[93]. One proposed theory for this difference is that macroautophagy works to recycle macromolecules immediately, while CMA degrades proteins that were upregulated during starvation but are no longer required – or aid in long-term adaptation to the starvation conditions[49]. CMA can be used to adapt to this long-term stress by targeting proteins that impact the cellular proteome, such as transcription factor inhibitors[96]. This uptick in CMA upon prolonged nutrient starvation is regulated by decreased degradation of LAMP2A[95].

### 1.2.3 Regulation of microautophagy

While the regulation of mammalian microautophagy is poorly elucidated, studies in yeast suggest that it is controlled by similar conditions to CMA & macroautophagy – namely through energy sources and nutrient levels[48]. Mammalian endosomal microautophagy is induced by serum and amino acid starvation, but not by serum starvation alone[65,97]. Interestingly, both microautophagy in yeast, and endosomal microautophagy in Drosophila are regulated through mTORC1 homologs, suggesting this may be the case in mammals as well[98,99]. Supporting that possibility is the fact that mammalian endosomal microautophagy is induced by rapamycin, an inhibitor of mTORC1[57].

## 1.3 The substrates of autophagy can change depending on induction mechanism

Autophagy can be induced through numerous stressed conditions, and through a variety of mechanisms. This variety permits the cell to successfully survive in diverse stressed conditions, as autophagic catabolism works to maintain homeostasis. However, it is unlikely that the substrates of autophagy would remain consistent across diverse stresses and this has been demonstrated in the literature.

While many sensing mechanisms which regulate macroautophagy function, at least in part, through mTORC1, this does not necessarily indicate that they have identical targets. There is evidence that inducing autophagy with Torin1, an mTOR

inhibitor, and nutrient starvation result in distinct lysosomal proteomes[6,100]. While many of the more abundant, classic lysosomal markers were equally represented across both conditions, there were significant changes in a number of proteins[6]. The authors theorize that this is because nutrient starvation can also act through mTOR independent pathways, and because Torin1 is a more potent inhibitor. Alternatively, as mentioned previously, similar stressed conditions can result in different selective macroautophagy targets. For example, two inducers of oxidative stress, hydrogen peroxide and sodium arsenite induce different forms of selective autophagy. This presents the possibility that the substrates themselves may be targeted for autophagic degradation. This is further evidence of the cell adapting to changing environmental cues which could indicate that what is degraded under other stressors may also be unique. Identifying unique macroautophagy substrates under different stressed conditions may provide evidence for important cellular responses to each condition.

### 1.3.1 Determining the substrates of autophagy

There is increased interest in defining the lysosomal proteome across cell types, environmental conditions and disease models[101]. This task can be approached by performing liquid chromatography mass spectrometry (LC-MS) on lysosome enriched samples. What becomes more complicated is the existence of a multitude of ways to prepare samples enriched in lysosomes. Three common methods include density gradient centrifugation, use of superparamagnetic iron oxide nanoparticles (SPIONs), and lysosomal immunoprecipitation (LysoIP).

Density gradient centrifugation is a classic protocol to enrich lysosomes, however it presents some major drawbacks. While it is relatively fast and does not require advanced treatments or stable cell lines, it is not as specific as SPION or LysoIP protocols. Density gradient lysosomal fractions are frequently contaminated by mitochondria and peroxisomes[101,102]. Additionally, under conditions like one sees in lysosomal storage disorders (LSDs), where the lysosomal contents are abnormal, the

density of the lysosomes can change[102,103]. This results in the lysosomes localizing to a different fraction, or across multiple fractions.

The SPION technique is a modified pulse-chase experiment, wherein cultured cells are treated with SPIONs for 24hrs (pulse), and it is then removed from the media and cells are incubated for another 24hrs (chase)[102]. The SPIONs are taken up by the endocytic pathway of the cell, and eventually localize to the lysosome. Once the lysosomes contain the SPIONs, it is possible to isolate the lysosomes using magnetic columns. This results in a highly pure lysosomal enrichment and is reported to take approximately 2hrs.

LysoIP is a technique that uses a rapid isolation system for lysosomes in order to identify the contents of the lysosome itself[104]. The LysoIP method relies upon developing cells expressing transmembrane protein 192 (TMEM192) attached to three tandem hemagglutinin (HA) tags[104]. While TMEM192 is not a classic lysosomal marker, the developers of this system explain that this transmembrane protein retains its lysosomal localization when overexpressed better than other markers. The lysosomes themselves can then be isolated from whole cell lysates using anti-HA magnetic beads. The resulting lysosomal isolation does not contain measurable levels of markers for typical contaminants, such as mitochondria, ER, cytosol, Golgi or peroxisomes[104]. This method is the fastest of those described here, with samples being able to be collected in under an hour. This is an appealing method as it is fast and specific, making it ideal for analyzing lysosomal contents in different conditions. This method is illustrated in Figure 2.

An independent analysis of lysosomal proteomes prepared by these methods determined that the SPION and LysoIP techniques were superior to sucrose density gradient centrifugation and differential centrifugation[101]. Both techniques were more efficient, more specific, and more reproducible.

One of the benefits, and drawbacks, of all of these techniques is that they do

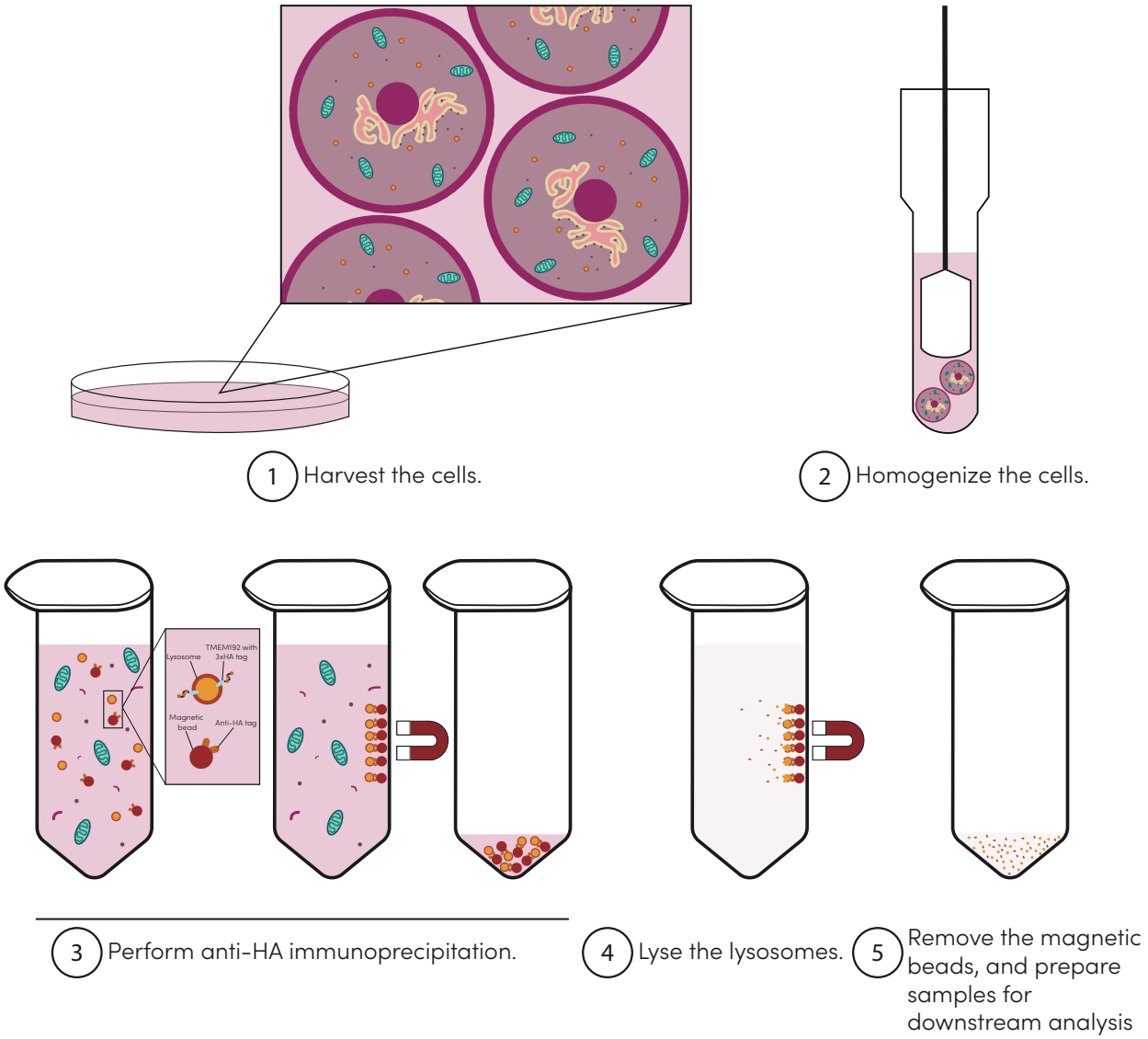


**Figure 2: Schematic illustrating the lysosomal immunoprecipitation (LysoIP) protocol.** This figure has been adapted from, and depicts a method initially described in Abu-Remaileh et al. 2017. The LysoIP protocol is a rapid isolation method for lysosomes. It makes use of cells expressing a TMEM192-3xHA construct, that then express TMEM192 with three tandem HA tags. As TMEM192 localizes to the lysosomal membrane, anti-HA magnetic beads be used to isolate a pure population of lysosomes. The control is executed on wild-type cells not expressing the construct. The first stage of the process is to harvest the cells by scraping them into phosphate buffered saline (PBS) and centrifuged to pellet the cells. The cells are then resuspended, and a portion is removed to analyze the whole-cell fraction later. The remaining suspension is then homogenized on ice before being centrifuged again. The supernatant, now containing the cellular organelles, is removed and incubated with prewashed anti-HA beads for 10 minutes at 4°C on a rotator. The mixture is placed on a magnetic rack and the suspension removed, and the beads washed with PBS three times. After the final wash is removed, the beads are resuspended in resuspension buffer (20mM HEPES, 1mM EDTA, 150mM NaCl, 1% TRITON-X, Phosphatase/proteinase inhibitor) in order to lyse the lysosomes. The beads are incubated with the resuspension buffer for 10 minutes at 4°C on a rotator. Finally, the suspension is placed on the magnetic rack once more and the supernatant iss removed and placed in a new tube. This suspension iss further processed for downstream analysis including western blot and mass spectrometry.

not distinguish between the different forms of autophagy as the samples are collected directly from the lysosome. While this is beneficial as it allows us to simultaneously analyze multiple processes, it also makes it difficult to know how a target was transported to the lysosome. Determining whether a particular substrate arrived in the lysosome due to macroautophagy, microautophagy or CMA requires additional experiments.

### 1.4 Stress granules

Stress granules form when translation initiation is halted due to stress, resulting in accumulations of RNA and RNA binding proteins (RBPs). These assemblies typically contain stalled translation initiation factors, mRNA and small ribosomal subunits[105]. As proteins continue to accumulate, additional proteins may either interact via Protein-RNA or Protein-Protein interactions which explains why approximately 50% of the stress granule core is composed of RBPs[106]. This assembly process occurs through liquid-liquid phase separation (LLPS) that relies on proteins with low complexity domains (LCDs)[107]. LLPS typically forms dynamic and reversible condensates. Appropriately, stress granules are dynamic structures, containing denser cores surrounded by a less concentrated shell[108].

Stress granules represent an important point of translational control under stress which helps promote cell survival. Under stressed conditions translation is stalled, allowing for post-transcriptional control over various proteins[109]. This halting permits the cell to focus on producing proteins that will enable cell survival and adaptation.

While stress granules themselves are not intrinsically harmful, some researchers have hypothesized that they may become persistent in neurodegenerative disease states leading to the classic aggregates we observe in ALS and potentially Alzheimer's disease and frontotemporal lobe dementia (FTLD)[110]. Therapeutics that target stress granule formation have shown positive effects in neurodegenerative disease models

of ALS and FTLD[111,112].

Importantly, studies have shown that the clearance of stress granules is heavily dependent on autophagy, thus drawing a link between potential disease causing mechanisms and autophagy[41,113].

LLPS is not limited to the formation of stress granules, in fact it is frequently used to explain the formation of other membraneless organelles such as Cajal bodies, nuclear speckles and synaptic densities (reviewed in Wang et al. 2021[114]). Frequently, the proposed benefit to these membraneless organelles is hypothesized to be that these condensates concentrate specific proteins allowing for increased rates of biochemical reactions, or opposingly to sequester certain molecules to prevent their activity[115–117]. Various metabolic enzymes have been shown to undergo LLPS, to both induce and inhibit enzymatic activity, forming metabolic enzyme condensates[115,118]. For example, CTP synthase is inhibited by CTP which induces the condensation of CTP synthase, forming an inactive polymer[119]. LLPS of metabolic enzymes is not limited to the formation of condensates solely containing metabolic enzymes, in fact in addition to the standard initiation factors, multiple metabolic enzymes have been found to localize to stress granules in yeast[118,120].

One particularly interesting subset of these metabolic enzymes within stress granules are three enzymes from the purine biosynthesis pathway. This includes paralogs Ade16p and Ade17p, whose mammalian homolog is 5-aminoimidazole-4-carboxamide ribonucleotide (AICAR) transformylase/inosine monophosphate (IMP) cyclohydrolase (ATIC) and Imd3p whose mammalian homolog is IMP dehydrogenase 1/2 (IMPDH1/IMPDH2)[118]. Mammalian IMPDH2 was also identified as being localized to stress granules, although this was only affirmed via one method of analyzing lysosomes and not the other within one study[108]. In mammalian cells, while ATIC is utilized to produce adenylates and guanylates, IMPDH1/IMPDH2 are the rate limiting enzymes for guanylate production. None of these proteins contain the LCDs typically

associated with stress granule recruitment, so their localization to stress granules remains unexplained.

Metabolic enzyme condensates are frequently assumed to play a role in metabolic regulation, although the regulatory components have not been well-defined for many of them[118]. The presence of metabolic enzymes within stress granules, especially rate-limiting ones, suggests that stress granule induction may help control metabolic pathways under stress. The interaction between metabolic enzymes, stress granules and autophagy presents a tempting hypothesis that the three compose a complex regulatory loop to regulate metabolism under stress.

### 1.5 Autophagy and Disease

Autophagy has a defined role in an extensive list of human diseases, making it an interesting and valuable area of study. Impairment of autophagy has been implicated in cancer, neurodegeneration, infection, autoimmune diseases and more[1]. Of particular interest to this project is its role in neurodegenerative disease. Some researchers hypothesize that macroautophagy helps clear the toxic aggregates, theorized to develop from persistent stress granules, that are found in so many of them. In murine central nervous system (CNS) macroautophagy knockouts, neurodegeneration and the accumulation of pathological inclusions in the brain is observed, which highlights how lack of autophagy can lead to a disease state[121]. Additionally, many neurodegenerative diseases, such as ALS and Alzheimer's disease, have genetic risk factors that impair macroautophagy[122]. For example, mutations which cause ALS occur in several genes, such as SQSTM1/p62, OPTN, TBK1 and C9ORF72, that have been implicated in macroautophagy, as discussed in more detail further on[122]. Some studies, although not all, have demonstrated that activation of autophagy in disease models of ALS improves pathology[122].

It is not solely macroautophagy that may play a role in disease states. While frequently overlooked in favour of its more researched compatriot, CMA has been

shown to degrade numerous disease-causing proteins including tau, a-synuclein and TAR DNA binding protein 43 kDa (TDP-43)[53,54,123]. Furthermore, the degradation of these proteins by CMA can be impaired by disease causing mutations or aggregates[53,54,123]. Targeting CMA has even been shown to improve behavioural and physical changes in a mouse model of Alzheimer's disease[124].

Based on this evidence, impairment of autophagy represents both a possible mechanism of disease, and a potential therapeutic target. It remains unclear how the cargo degraded by autophagy changes under pathological conditions as compared to other autophagy-inducing conditions.

### 1.6 Amyotrophic Lateral Sclerosis

ALS is a devastating and fatal neurodegenerative disease that targets the upper and lower motor neurons[125]. This leads to increasingly severe motor symptoms that can either begin with symptoms in the extremities (spinal onset) or with speech and/or swallowing symptoms (bulbar onset)[125]. Eventually, breathing and swallowing impairment leads to the death of patients – typically 2-5 years after diagnosis[125]. The disease is characterized by aggregates of RBPs, such as TDP-43 aggregates[126]. Some current models assert that disease pathology occurs when persistent stress granules accumulate, either through increased stability, increased formation, or impaired clearance of the granules. Unfortunately, there are only a few therapeutic options for ALS patients – and those that do exist are not curative and are unable to prolong life expectancy by more than a few months.

The mechanism behind the neuronal death observed in ALS is currently unknown, and the search for the mechanism is complicated by the extreme heterogeneity in ALS patients. It seems likely that there will be a spectrum of mechanisms dependent on the cause of the disease in each individual. This cause, however, is frequently unknown, and the vast majority of ALS patients present with sporadic illness[127]. Only about 10% of patients have a family history of the disease,

and of this 10% about 70% of the cases can be narrowed down to a genetic cause[127]. There is an extensive list of ALS-linked genes, many of which are associated with RBPs, autophagy and clearance of stress granules[127].

ALS pathology is characterized, in part, by cytoplasmic inclusions in affected motor neurons[128–130]. These aggregations frequently contain causative ALS proteins such as TDP-43, SOD1 and FUS, even in cases without pathological mutations in these proteins. Although the mechanism is not yet fully elucidated, these inclusions are frequently hypothesized to derive from aberrant stress granules (reviewed by Baradaren-Heravi et al. 2020[131] and Zhang et al. 2021[132]).

One difficulty with ALS research is that it remains difficult to model, however many models focus on the characteristic inclusions present in ALS patients and thus focus on producing stress granules. Sodium arsenite treatment is frequently used to induce stress granule formation as an indirect representation of the disease[133]. In addition to producing cytoplasmic inclusions, sodium arsenite replicates another key feature of the disease, impaired nucleocytoplasmic transport[133]. While sodium arsenite remains an imperfect model for the disease, it is useful for early stage research.

### 1.6.1 Autophagy in ALS

A number of genes linked to ALS are involved in autophagy, including OPTN, TBK1, SQSTM1/p62, C9ORF72 and SMN – and mutations in these genes can prevent the elimination of stress granules[41,134,135]. This highlights the strong link between stress granules and ALS, and therapeutics that target stress granule formation have shown positive effects in neurodegenerative disease models of ALS[99].

Our lab has demonstrated that SQSTM1/p62 works in conjunction with two other ALS-related genes, C9ORF72 and SMN, to degrade stress granules by autophagy[41]. It is possible that defects in one or more of these genes may impair the pathway and lead to increased stability of the stress granules. Another interesting role for C9ORF72 repeats, the most common genetic cause of ALS, is that they promote

phase separation and stress granule formation[136]. Based on these results, it is tempting to hypothesize that C9ORF72 repeats play a two-pronged role in disease pathology – by limiting autophagic degradation of stress granules and favouring stress granule formation.

TBK1 has been linked with two other ALS genes, SQSTM1/p62 and OPTN. TBK1 works to phosphorylate OPTN, which induces autophagic degradation of damaged mitochondria, and SQSTM1/p62 which promotes the maturation of autophagosomes[1,122]. Mutations to TBK1 have been shown to reduce OPTN phosphorylation and decrease mitochondrial clearance[122]. In addition, mutations to SQSTM1/p62 or OPTN themselves can also impair autophagy. Particularly interesting, is a study that showed that mutant SQSTM1/p62 led to reduced levels of mutant SOD1 in autolysosomes, suggesting that it disrupted the autophagic clearance of the protein[137].

Furthermore, studies have shown that inhibiting autophagy can worsen pathology in models of ALS, whereas activating autophagy can lessen degeneration[1,122]. This evidence points towards an important role for autophagy in ALS and highlights it as a potential therapeutic target.

Describing what is being degraded in cells where stress granules are present has the potential to give us a better understanding of the role of autophagy in stress granule degradation, and in turn its role in numerous neurodegenerative diseases such as ALS and FTLD[110]. Not only would this enable us to better understand stress granule degradation by autophagy, but it would allow us to discover novel autophagy targets beyond stress granules that may be important for disease pathology. It would be important to look at stress granule components being degraded by autophagy, in addition to the contents of whole stress granules, because evidence suggests that this degradation occurs in a piecemeal fashion[138]. This would provide us with information as to what parts of the stress granules are being degraded first.

## 1.7 Summary

In summary, autophagy can be induced through various mechanisms under various conditions, and these can result in a unique lysosomal proteome. Additionally, the role of autophagy in clearing deleterious aggregates and proteins, including stress granules, is theorized to play an important role in ALS. An analysis of the lysosomal proteome after stress granule induction as compared to during nutrient starvation induction would provide us with an opportunity to further describe what is being degraded under these conditions and how they differ. This could be beneficial as it may demonstrate key differences between the two conditions, and show important substrates only targeted to lysosomes in certain situations.

## 1.8 Hypothesis

The lysosomal proteome will change depending on the autophagy-inducing condition.

# Chapter 2: Methods

## 2.1 Cell Lines

1. HEK293T (ATCC)

2. HEK293T cells, *ATG7*$^{-/-}$. The procedure to develop these cells is described in greater detail below. In brief, a CRISPR-Cas9 system was used to knockout ATG7 using two different small guide RNAs (sgRNAs). Multiple colonies were collected from each guide. Absence of ATG7 expression was confirmed via Western blot.

3. HEK293T cells expressing TMEM192-3XHA (HEK293 LysoIP). The procedure to develop these cells is described in greater detail below. In brief, a pLJC5-Tmem192-3xHA plasmid (Addgene plasmid #102930; http://n2t.net/addgene:102930 ; RRID:Addgene_102930), PMD2.G and psPAX2 were transfected into HEK293T cells. The lentiviral particles released by the cells were collected, isolated, and subsequently used to infect HEK293T cells. The cells were put under puromycin selection to produce a pure population of LysoIP cells. Expression was confirmed via Western blot.

4. HEK293T *ATG7*$^{-/-}$ cells expressing Tmem192-3XHA (*ATG7*$^{-/-}$ LysoIP). *ATG7*$^{-/-}$ cells were prepared as described in (2), and then infected with lentivirus as described in (3).

## 2.2 Cell Culture

Cells were cultured in 10% fetal bovine serum (FBS) (ThermoFisher, 12483020) and 1% Penicillin-Streptomycin (Wisent Bioproducts, 450-201-EL) supplemented DMEM (Wisent Bioproducts, 319-015-CL). All cells were maintained in incubators at 37°C, 5%

$CO_2$. When confluent, cells were dissociated from the plate using Trypsin/EDTA (Wisent Bioproducts, 325-043-EL), and which was then neutralized using an equal volume of supplemented media. The concentration of the cell suspension was determined using a hemacytometer.

## 2.3 Production of LysoIP Cells

In order to produce the LysoIP cells, we made use of the pLJC5-Tmem192-3xHA plasmid, pLJC5-Tmem192-3xHA was a gift from David Sabatini (Addgene plasmid #102930; http://n2t.net/addgene:102930 ; RRID:Addgene_102930)[104].

### 2.3.1 Lentivirus Production

Cells were plated in 5x15cm plates, they were 70-90% confluent on the day of the initial transfection. Two hours before the transfection the media was replaced, existing media was replaced with 20 mL of fresh media. The following reagents were mixed and incubated for 5 minutes at room temperature – these amounts are for one 15 cm plate.

- 7.2 µg of PMD2.G
- 10.8 µg of psPAX2
- 6 µg of pLJC5-Tmem192-3xHA

*In 1200 µL of DMEM*

Then, 96 µL (per plate) of polyethylenimine (PEI) was added and incubated for 20 minutes at room temperature. 1300 µL of transfection mix was added to each plate.

24 hours later the media was removed and replaced with 15 mL of fresh media. 48 hours after transfection the media was collected and replaced. The collected media was spun for 5 minutes at 2000 rpm. Supernatant was removed and stored at 4°C. 72 hours after the transfection, media was once again collected and spun at 2000 rpm. The two media collections were filtered through a 0.45 µm filter. Then, the collections were concentrated by ultracentrifugation at 20,000 rpm for 2 hours at 6°C

in a Beckman SW28 Ti swinging rotor.

After ultracentrifugation the supernatant was discarded. The pellet was resuspended in 200-400 µL in 1xPBS. Virus was either used immediately, or flash frozen in liquid nitrogen and stored at -80°C. If frozen, virus was thawed on ice before use.

#### 2.3.2 Infection & Selection

Cells were plated the day before into a 6 or 24 well plate, and cells were ~50% confluent on the day of infection. On the day of infection, new media with 10 µg/mL of polybrene was added. A serial dilution was performed with the lentivirus to expose seeded cells to various concentrations. After 3 days the media was changed to selection media, using puromycin. In HEK293 WT cells 2 µg/mL was used, whereas for the *ATG7*$^{-/-}$ cells 1 µg/mL was used. This selection continued until all the control cells had died, approximately 3 days. Expression of the construct was confirmed via Western blot.

## 2.4 Production of *ATG7*$^{-/-}$ cells

#### 2.4.1 Bacterial Transformation

Competent E. coli cells were thawed on ice. 1 mL of plasmid was mixed with 30 mL of E. coli cells and incubated on ice for 20 minutes. Cells were subjected to heat shock at 42C for 45 seconds. Cells were plated on LB Agar plates containing 100 µg/mL of ampicillin.

#### 2.4.2 Developing CRISPR-Cas9 Plasmid

In order to develop *ATG7*$^{-/-}$ cells, the protocol described in Ann Ran et al. 2013 was used and is briefly described below[139]. The sgRNA sequences were obtained from Integrated DNA Technologies, and modified to contain the appropriate end caps to be inserted into the Bbs1 cut site in the pSpCas9(BB)-2A-Puro plasmid (Figure 2A).

pSpCas9(BB)-2A-Puro (PX459) V2.0 was a gift from Feng Zhang (Addgene plasmid #62988 http://n2t.net/addgene:62988 ;RRID:Addgene_62988). The top strand of each sgRNA contained the 5'-CACCG addition, and the bottom strand contained 5'-AAAC and C-3' additions, the whole sequences can be found in Figure 2B.

The top and bottom strands of each sgRNA were resuspended to a concentration of 100 µM. In order to anneal and phosphorylate the oligonucleotides, the following solution was prepared and placed in a thermocycler (37°C for 30 min, 95°C for 5 min, ramp down to 25°C at 5°C/min):

| Component | Amount (µL) |
|---|---|
| sgRNA top (100 µM) | 1 |
| sgRNA bottom (100 µM) | 1 |
| T4 ligation buffer (10X) | 1 |
| T4 PNK | 1 |
| $ddH_2O$ | 6 |
| Total | 10 |

The phosphorylated and annealed oligonucleotides were diluted 1:200 and referred to as diluted oligonucleotide duplexes. In order to cut the pSpCas9(BB)-2A-Puro plasmid at the insertion site the following reaction was incubated at 37°C for 1 hour.

| Component | Amount (µL) |
|---|---|
| pSpCas9(BB)-2A-Puro plasmid miniprep (500 ng) | - |
| CutSmart buffer | 2 |
| Bbs1 enzyme | 0.5 |
| $ddH_2O$ | Up to 20 µL |
| Total | 20 |

To clone the sgRNA into pSpCas9(BB)-2A-Puro a ligation reaction was set up as follows. The control was a no insert (no oligonucleotide) reaction. This reaction was

performed to ligate the annealed sgRNA into the Cas9 plasmid at the Bbs1 cut site. The reaction was incubated in a thermocycler as follows: 6x 37°C for 5 min, 21°C for 5 minutes (total of 1 hour).

| Components | Amount (µL) |
|---|---|
| pSpCas9(BB)-2A-Puro cut by Bbs1: 50 ng | - |
| Diluted oligonucleotide duplexes | 1 |
| T4 ligase | 0.5 |
| T4 ligase buffer | 1 |
| $ddH_2O$ | Up to 10 µL |
| Total | 10 |

The plasmid was transformed into competent E. coli cells and plated on an ampicillin (100 µg/mL) LB agar plate and incubated overnight at 37°C. The following day a few colonies were picked and individually inoculated in ampicillin LB Broth (100 µg/mL), they were incubated at 37°C overnight. Plasmid DNA was isolated using the QIAprep Spin Miniprep kit (Qiagen, 27104) according to manufacturer instructions.

Finally, the sequence of each plasmid was verified by sequencing with the U6-Fwd primer, performed by StemCore Laboratories at the Ottawa Hospital.

### 2.4.3 Transfection

Plasmid DNA was isolated using the QIAGEN Plasmid Plus Midi Kit (Qiagen, 12945) as per manufacturer instructions.

HEK293T cells were ~50% confluent. For one well of a 6 well plate 1 µg of plasmid DNA was pipetted up and down with 200 µL of OPTIMEM (ThermoFisher, 31985-070) and 4 µL of PEI, then incubated for 20 minutes at room temperature. Meanwhile, cells were washed 1X with PBS, changing the media to 2 mL of full media. DNA/PEI mix was added to each well of cells, ensuring at least one well remained free of the DNA/PEI mix. The cells were incubated overnight at 37°C.

The following day the media was changed in the morning, and cells were washed 1X with PBS. The media was replaced with full media supplemented with 2 µg/mL of puromycin. Selection was performed for 3 days.

Surviving cells were then single-cell seeded by serial dilution in order to isolate clonal populations. Following growth of individual colonies, colonies were screened for *ATG7*, LC3B and p62 to assess their knockout status. Colonies selected for use based on these tests were also tested for puromycin sensitivity to ensure that the Cas9 plasmid did not permanently integrate into the genome.

**2.5 Lysosomal Immunoprecipitation (LysoIP)**

Initially, the protocol was pulled from the paper that first described the LysoIP method[104]. The following steps were performed to complete the pilot testing of the method, as well as the first samples sent to mass spectrometry. Cells were plated two days before to reach about 80% confluency. There were three treatment conditions. The sodium arsenite treatment condition consisted of: 1 hour sodium arsenite (250 µM), followed by 1 hour bafilomycin $A_1$ (400 nM). The HBSS condition consisted of: 1 hour HBSS, followed by 1 hour bafilomycin $A_1$ (400 nM) in HBSS. The control condition, or bafilomycin $A_1$ condition, consisted of 1 hour of new media, followed by 1 hour bafilomycin $A_1$ (400 nM). After the first hour's treatment the cells were washed 2X with PBS. Pierce Anti-HA Magnetic Beads (ThermoFisher, 88836) were pre-washed 3x 1 mL with chilled KPBS (136 mM KCl, 10 mM KH2PO4, pH 7.25 was adjusted with KOH), 50 L of beads were used for one 10 cm plate. Cells were washed two times with PBS before being scraped into 1 mL KPBS. Samples were centrifuged at 1000 x g for 2 minutes at 4°C. Supernatant was removed, and the pellet was resuspended in 1 mL of KPBS, 100 µL was removed for whole cell analysis. This sample was subjected to a typical protein isolation protocol as described below before being used. The remaining 900 µL was gently homogenized for 30 strokes with a 2 mL homogenizer on ice. Homogenate was centrifuged at 1000 x g for 2 minutes at 4°C. Supernatant was collected and incubated

with pre-washed beads on a gentle rotor for 3 minutes at room temperature. The beads/bound lysosomes were washed with 1 mL KPBS three times. The last wash was removed, and the beads were resuspended in 100 µL of resuspension buffer (20 mM HEPES, 1 mM EDTA, 150 mM NaCl, 1% TRITON-X, Phosphatase/proteinase inhibitor)[140] and incubated for 5 minutes on ice. Samples were placed on a magnetic rack and supernatant was collected for further analysis.

While this was the original protocol that was followed, a few changes were made. First, after the initial test the number of strokes with the homogenizer was increased from 30 to 90 strokes. After observing the cells under the microscope, it was determined that 30 strokes did not sufficiently homogenize the cells. After sending samples up to mass spectrometry for analysis and having yield issues with some of the samples, we sought to improve the output of the protocol. This was done in a few ways and pulled from a few different papers that made modifications including: using PBS instead of KPBS, incubating the samples with the beads for 10 minutes on the rotator at 4°C and incubating the beads in resuspension buffer for 10 minutes on the rotator at 4°C[6,141].

This method is briefly illustrated in Figure 2.

## 2.6 Silver staining and Western blotting

### 2.6.1 Sample preparation and electrophoresis

Samples analyzed by western blot or silver stain were either pulldown samples or whole cell lysates from the same samples. Pulldown samples were not modified after the LysoIP protocol, 5% of the samples were run. For the whole cell lysate fraction removed during the LysoIP protocol the following was performed.

The solution was centrifuged at 1000 x g for 2 minutes, and the supernatant removed. The pellet was resuspended in 100 µL cell lysis buffer (0.1 M Tris (pH 7.4), 5 M

NaCl, 0.5 M EDTA, 1% Triton-X 100, protease inhibitor tablet). The solution was frozen at -80°C for 20 minutes, then thawed on ice. The sample was then centrifuged at 1000 x g for 5 minutes at 4°C, the supernatant removed and the pellet resuspended in PBS. 10% of this solution was run, this corresponds to 1% of the total cell lysate.

To prepare the samples for electrophoresis they were mixed with 4X Laemmli Sample Buffer (BioRad, 1610747), diluting the Laemmli buffer to 1X, and incubated for 10 minutes at 95°C to denature the proteins. The samples were run on a 10% polyacrylamide gel at 150 V for ~1 hour.

### 2.6.2 Western blotting

A transfer was performed to a polyvinylidene fluoride (PVDF) membrane for 1.5 hours at 100 V.

Membranes were then blocked for 1 hour in 5% milk in 1% TBST (10 mM Tris-HCl (pH 8), 150 mM NaCl, 0.05% Tween 20). They were probed with primary antibodies in 1% TBST overnight at 4°C, and the following morning were washed 3x with 1% TBST. All antibodies used are described in Table 1. The membranes were then probed with the corresponding secondary antibody for 1 hour in 5% milk in 1% TBST. Finally, they were washed three times again with 1% TBST.

Visualization was performed using Luminata Crescendo Western HRP substrate (Millipore Sigma, WBLUR0100) on the ImageQuant LAS 4000. Quantitative analysis was performed using Image Studio Lite as per manufacturer instructions, band intensity was normalized to the indicated controls.

**Table 1: Antibodies**

| Target | Manufacturer | Application |
|---|---|---|
| **ATG7** | Cell Signalling Technology<br>Polyclonal Rabbit<br>2631S | Western Blot |
| **Calnexin** | Cell Signalling Technology<br>Monoclonal Rabbit<br>2679S | Western Blot |
| **G3BP** | Abcam<br>Monoclonal Rabbit<br>ab181149 | Immunofluorescence |
| **GAPDH** | Santa Cruz Biotechnology<br>Monoclonal Mouse<br>sc-32233 | Western Blot |
| **HA** | Millipore Sigma<br>Monoclonal Mouse<br>05-904 | Western Blot,<br>Immunofluorescence |
| **IMPDH2** | Proteintech<br>Polyclonal Rabbit<br>12948-1-AP | Western Blot |
| **LAMP1** | Cell Signalling Technology<br>Monoclonal Rabbit<br>9091T | Western Blot,<br>Immunofluorescence |
| **LC3B** | Sigma Aldrich<br>Polyclonal Rabbit<br>L7543 | Western Blot |
| **P62** | Sigma Aldrich<br>Polyclonal Rabbit<br>P0067 | Western Blot |
| **PPAT** | Proteintech<br>Polyclonal Rabbit<br>15401-1-AP | Western Blot |
| **SOD1** | Abcam<br>Polyclonal Rabbit<br>ab52950 | Western Blot |
| **TOMM20** | Invitrogen<br>Polyclonal Rabbit<br>PA5-39247 | Western Blot |
| **Vinculin** | Abcam<br>Monoclonal Rabbit<br>ab129002 | Western Blot |

### 2.6.3 Silver staining

Silver staining was performed using the PlusOne™ Silver Staining Kit, Protein (GE Life Sciences, 17-1150-01). The method was performed as instructed by the manufacturer, and is briefly described below. First, the solutions were prepared as described in Table 2.

**Table 2: Silver staining solutions.**

| Solution Name | Component |
|---|---|
| **Fixing Solution (40% ethanol)** | 100 mL Ethanol<br>25 mL Glacial acetic acid<br>Water to 250 mL |
| **Sensitizing solution** | 75 mL Ethanol<br>10 mL Sodium thiosulfate (5% w/v)<br>17 g Sodium acetate<br>Water to 250 mL<br><br>Before use add 1.25 mL glutardialdehyde (25% w/v) |
| **Silver solution** | 25 mL silver nitrate solution (2.5% w/v)<br>Water to 250 mL |
| **Developing solution** | 6.25 g sodium carbonate<br>Water to 250 mL, stir until sodium carbonate is dissolved<br><br>Before use: Add 0.2 mL formaldehyde (37% w/v) |
| **Stop solution** | 3.65 g EDTA-$Na_2$-$H_2O$<br>Water to 250mL |
| **Washing solution** | Water |

After performing electrophoresis, the gel was removed from its cast and placed in a tray containing the fixing solution on a shaker. Left it in the fixing solution for 30 minutes. Removed the fixing solution and replaced with sensitizing solution and shook the gel for 30 minutes. Washed the gel with water 3x for 5 minutes each. Removed the last wash and added the silver solution, letting the gel shake for 20 minutes. Washed again 3x for 5 minutes each. Replaced the water with the developing solution and left

shaking until the bands reached the desired intensity (2 to 5 minutes) then transferred the gel immediately to the stopping solution. Left in the stopping solution on the shaker for 10 minutes. Washed three times for 5 minutes each. Imaged the gel using the Gel Doc XR+ System (BioRad).

## 2.7 Immunocytochemistry

Cells were treated as described in the figure captions. In Figure 3A cells were plated on coverslips, in Figures 6 & 7 cells were plated in 384-well plates. Cells were washed 1x with PBS and fixed with 4% paraformaldehyde for 10 minutes. This was followed by 3x washes with PBS, before permeabilizing the cells with permeabilization buffer (0.2% Triton-X-100, 20 mM $NH_4Cl$, in PBS) for 10 minutes. Cells were washed 3x with PBS. Cells were blocked for 1 hour in 5% goat serum in PBS. Primary antibodies were diluted in 5% goat serum in PBS and incubated at 4°C overnight. The following day cells were washed with PBS 3x, and secondary antibody was added in 5% goat serum in PBS. This was incubated for 1 hour at room temperature. Cells were washed 3X with PBS, and mounted with DAPI mounting medium or kept in PBS if in the 384-well plate.

Figure 3A was imaged by Dr. Alexandre Savard on the Zeiss AxioImager M2 at 63x. Figures 6 & 7 were imaged by Dr. Stephen Baird on the Opera Phenix at 40x.

## 2.8 Mass Spectrometry

### 2.8.1 Preparation of samples

This protocol was adapted from Wyant et al. 2018. 45-80% of the pulldown was used, and resuspension buffer was added to the pulldown solution to end up with a total volume of 200 µL. 20% SDS was added to a final concentration of 2%. The samples were sonicated for 10 seconds. The samples were then spun down at 20,800 x g for 1 minute at 4C and the supernatant was transferred to a new tube. Dithiothreitol

(DTT) was added to a final concentration of 5 mM, and samples were incubated for 15 minutes at 45°C. Iodoacetamide (IAA) was added to a final concentration of 10 mM. IAA is light sensitive, and therefore from this point on the solutions were protected from light. Samples were incubated in the dark for 30 minutes at room temperature. Proteins were then precipitated with 4 volumes of ice cold acetone to 1 volume sample and incubated overnight at -20°C.

The following day, samples were centrifuged at 20,800 x g for 30 minutes at 4°C. Supernatant was removed. Precipitates were washed with 500 µL of ice-cold acetone two times. After each wash pellets were air dried. After the second wash & dry, the pellet was dissolved in 100 µL of 75 mM Tris-HCL (pH 7.8). 1.5 µL of SOLu-Trypsin (Sigma, EMS0004-100UG) was added to the solution, and samples were incubated for 16 hours at 37°C.

The following day acetic acid was added to a final concentration of 0.5%. The pH of the samples was tested with a pH strip to ensure that the pH was acidic. In order to desalt the samples, Sep-Pak tC18 (1cc, 50mg) cartridges were used (Waters, WAT054960). The remaining steps were adapted from the Waters manual, and all steps were done by gravity. Each component was added immediately as the previous component was completely in the bed of the column. The cartridge was washed and conditioned with 900 µL of acetonitrile (ACN) followed by 300 µL of 50% ACN, 0.5% glacial acetic acid (HOAc). Cartridges were equilibrated with 900 µL of 0.1% trifluoroacetic acid (TFA). Samples were loaded in 0.4% TFA. Columns were then washed/desalted with 900 µL of 0.1% TFA. Column was washed again with 0.5% HOAc. Samples were eluted with 500 µL of 50% ACN, 0.5% HOAc and eluate was collected in a tube before being sent to the proteomics core. Dr. Zhibin Ning of the proteomics core then prepared the samples for, and ran them through, LC-MS.

### 2.8.2 Data Processing

Raw data from mass spectrometry was processed and analyzed using MaxQuant[142] on UseGalaxy.org[143] to determine label-free quantification (LFQ) intensities for identified proteins. The raw files were processed against the UniProt human protein database. The parameters for the analysis were determined by the tutorial written by Föll & Fahrner (2021) for Galaxy[144]. These parameters are briefly described below.

At least one minimum unique peptide was required, with a minimum length of 7 amino acids. Trypsin was selected as the digestion enzyme and one missed cleavage was permitted. The fixed modification 'Cysteine carbamidomethylation' was selected, no variable modifications were selected. Razor and unique peptides were used, and the protein false discovery rate (FDR) was set to 0.01. The selected quantitation method was 'label-free quantification'. Match between runs was not used. Contaminants and reverse sequences were identified by MaxQuant but were not used in downstream analysis.

## 2.9 Bioinformatic analysis identifying enriched proteins

Two different methods were used to identify enriched proteins across the different treatment conditions. The first was using the ***proteus*** package (Version 1.0.0) in R, which enables the visualization of differentially enriched proteins[145]. The second was a computational tool, Mass Spectrometry interaction Statistics (MIST) that assigns scores to each protein, analyzing the affinity of the protein for each condition[146]. While the *proteus* package was beneficial for visualizing differential expression, MIST was used for further analysis due to its design for immunoprecipitation.

### 2.9.1 *proteus* in R

Despite its usefulness for immunoprecipitation, the MIST score does not provide any statistical analysis. The package ***proteus*** was used to analyze the differential

expression of various proteins of interest and assess their statistical significance, or lack thereof, by looking at the LFQ intensities directly. The evidence file from MaxQuant was used as the original input file, and UniProt identifiers were used to annotate each protein. All commands are described in the package tutorial available on GitHub (https://github.com/bartongroup/proteus).

#### 2.9.2 Mass Spectrometry interaction Statistics (MIST)

The MIST tool assigns a quantitative score to each protein for all the inputted conditions, and scores how unique the protein is to each condition. The score is a weighted sum based on three criteria: abundance, reproducibility, and specificity. This system allowed for two different MIST set ups to accomplish different goals. Inputting data for one treatment condition from the HEK293T cells (*ATG7*$^{-/-}$ or wild-type) and the corresponding LysoIP cells permitted the identification of *lysosomal hits* within said condition. Comparatively, inputting the data for all treatment conditions and all cell types identifies proteins unique to the LysoIP cells under each condition – *treatment specific hits*.

For both input types, the same parameters were followed. The tool was accessed online (https://modbase.compbio.ucsf.edu/mist/). The data was prepared as described, and LFQ intensity was used as the quantitation measure. The HIV Trained Mode was selected, and Singleton Filtering was turned on.

### 2.10 Ingenuity Pathway Analysis (IPA)

#### 2.10.1 Differential enrichment of canonical pathways

To identify differentially enriched pathways, the *lysosomal hits* MIST scores were used and compared to a baseline. For the treatment analyses a log2 fold change was calculated, both sodium arsenite and HBSS scores were compared to bafilomycin $A_1$, and in the *ATG7*$^{-/-}$ analyses the *ATG7*$^{-/-}$ sample was compared to the wild-type.

Due to the nature of the data from immunoprecipitation, some scores were 0 in the bafilomycin/wild-type conditions, to evade any issues a value of 0.0001 was added to all MIST scores at the suggestion of Qiagen IPA trainers.

Using the log2 fold change values, it was possible to perform a Core Analysis followed by a Comparison Analysis to visualize the changes in pathway expression. Only pathways that had absolute z-scores greater than 2 and were statistically significant ($p < 0.05$) were shown. Fisher's Exact test was used to calculate significance.

Using the Pathway Overlay tool, it was possible to observe the actual and predicted effects of these changes on individual pathways.

#### 2.10.2 Linking proteins of interest to ALS and stress granule formation

It is possible through IPA to create your own networks through the Path Explorer function. To explore the potential relationship between the purine biosynthesis pathway and both ALS and stress granule formation, all the molecules that take part in, or are produced by, the pathway are placed in the network. Then, the Path Explorer is used to draw links between the disease/function of interest and the molecules. The links are pulled from the Ingenuity Knowledge Base and include links such as correlations, causations, reactions and interactions.

For the figures, specific links were chosen based on relevance to other findings within the thesis, or potential interest. This was done for ease of interpretation of the figure. Many more potential relationships existed, and could be explored at a later date.

### 2.11 Bioinformatic identification of protein-protein interactions

Proteins identified by MIST as *treatment specific hits* were entered into the Cytoscape application and analyzed using the ***StringApp*** and ***clusterMaker2***[147–149]. Sodium arsenite specific hits and bafilomycin $A_1$ specific hits were analyzed individually.

*StringApp* was used to identify protein-protein interactions across these hits, and *clusterMaker2* identified the top nodes within the network through clustering algorithms. It was then possible to determine the top enrichments within each cluster through the Cytoscape application. These steps were achieved by following the StringApp tutorial identified here: https://apps.cytoscape.org/apps/stringapp.

## 2.12 Bioinformatic analysis of cellular component enrichment

This analysis was performed in two ways. The first was through the Cytoscape application, which performed a COMPARTMENTS analysis as described by Binder et al. 2014[150]. This was useful to see what cellular compartments were enriched in the treatment specific networks generated within Cytoscape. This analysis assigns a score between 1-5 stars, only 5 star hits were visualized on the figures.

The second computational tool was WEB-based Gene SeT AnaLysis Toolkit (WebGestalt, http://www.webgestalt.org), which identified enriched gene ontology terms within *lysosomal hits*[151]. The top 10 hits for each analysis were displayed. The method of interest was 'Over-Representation Analysis', and the functional database was 'Gene ontology – Cellular Component'.

## 2.13 Bioinformatic identification of regions of interest

### 2.13.1 Identifying low-complexity domains

To identify potential low-complexity domains (LCDs) within proteins of interest, Platform of Tools for Low Complexity (PlaToLoCo, https://platoloco.aei.polsl.pl/#!/query) was used[152]. This tool uses five different LCD-identifying algorithms. The amino acid sequence for each protein was accessed through the NCBI database and inputted to PlaToLoCo. All methods were selected for analysis.

### 2.13.2 Identifying KFERQ-like motifs

To identify KFERQ-like motifs within genes of interest, the KFERQ finder (V0.8, https://rshine.einsteinmed.edu) was used[51]. This computational tool searches a genetic sequence and identifies any classical KFERQ motif, or motifs identified to behave as such. All standard and advanced motifs were selected as output options.

## 2.14 Statistical Analysis

Statistical analysis for western blot quantification was performed using the GraphPad Prism 9 software. Normal distribution was assumed for all tests. Two-way ANOVA tests were performed followed by a Tukey's multiple comparison test. The Tukey's multiple comparison test was used when comparing every mean with every other mean. Statistical significance is represented as follows: * = $p < 0.05$, ** = $p < 0.01$, *** = $p < 0.001$.

# Chapter 3: Results

## 3.1 Cells expressing TMEM192-3xHA maintain their response to stress and LAMP1 abundance.

### 3.1.1 Production and validation of wild-type HEK293 LysoIP cells.

The lysosomal immunoprecipitation system (LysoIP), originally described in Abu-Remaileh et al. 2017, relies upon cellular expression of TMEM192 fused to three tandem human influenza hemagglutinin (HA) epitope tags (TMEM192-3xHA)[104]. The expression of this fusion allows for whole lysosomes to be rapidly immunoprecipitated from Dounce homogenized cell lysates using anti-HA magnetic beads, and subsequently lysed for proteomic analysis of the cargo (Figure 2)[6]. The speed, efficiency and specificity of this process has been demonstrated in numerous publications which have performed LC-MS in order to identify lysosomal proteins[141,153–155]. There is interest in understanding how autophagy targets change depending on the cellular conditions, and previous publications indicate that these targets can change significantly even under conditions operating through the same regulator, mTORC1[6]. As discussed above, one clinically relevant condition is sodium arsenite induced oxidative stress. Sodium arsenite induced stress is widely used to simulate ALS-like conditions through its production of stress granules. While this stressor does not directly relate to the clinical condition it functions as a tractable model[41,133,140,156]. The LysoIP system presents an intriguing opportunity to identify autophagy targets specific to stress granule inducing conditions. In order to complete these experiments, it was first necessary to produce cells expressing the LysoIP construct.

Therefore, the pLJC5-Tmem192-3xHA (Plasmid #102930) plasmid was ordered from Addgene, and a lentivirus was produced to infect HEK293 cells. Following transduction and selection, immunocytochemistry and western blotting techniques

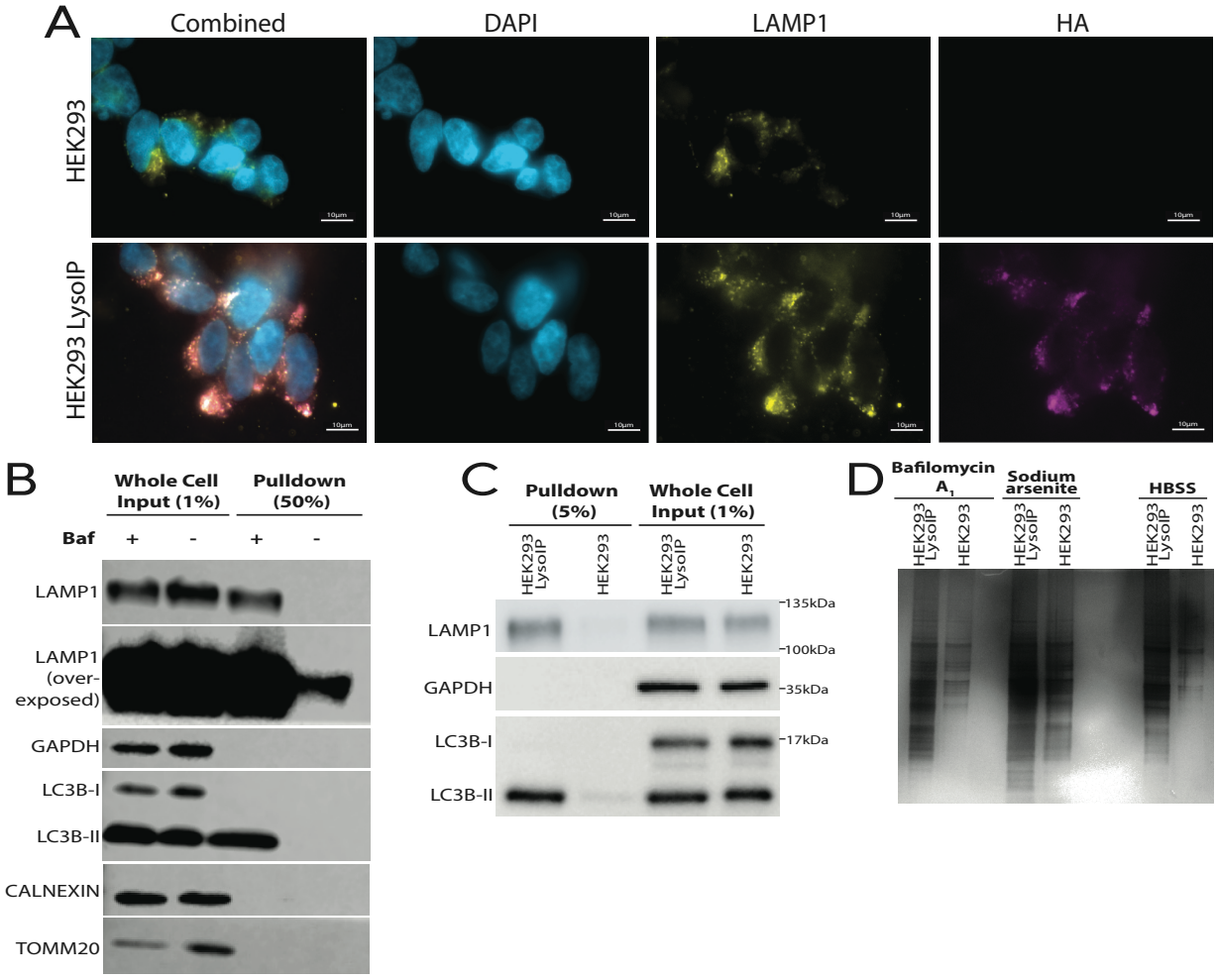


**Figure 3: Validation of HEK293 LysoIP cells and demonstration of effective pulldown. A)** Immunofluorescence demonstrating the expression of the LysoIP (TMEM192-3xHA) contruct in HEK293 LysoIP cells but not wild-type. This is visualized through the HA tag. These images also demonstrate the co-localization of the HA tag with LAMP1. Images acquired by Dr. Alexandre Savard at 63x on the Zeiss AxioImager M2. **B)** Western blot confirming that the LysoIP pulldown is efficient and specific, treatment groups include +/- 5h 400nM bafilomycin $A_1$ treatment. Lysosomal markers are present in the pulldowns (LAMP1, LC3B-II) and whole cell input, while non-lysosomal markers are not present in the pulldowns but are present in the whole cell input (GAPDH, LC3B-I, Calnexin, TOMM20). Calnexin is an endoplasmic reticulum (ER) marker, TOMM20 a mitochondrial marker, GAPDH and LC3B-I are both cytoplasmic markers. Importantly, we do not see a significant LAMP1 signal without the bafilomycin treatment. 50% of the total pulldown was loaded compared to 1% of the whole cell input. **C)** Western blot demonstrating the improved pulldown protocol. Changes in the protocol between B & C include using PBS instead of KPBS, incubating the beads and sample for 10min at 4°C on a rotator and incubating the samples with resuspension buffer for 10min at 4°C on a rotator. Lysosomal markers are present at a higher concentration than previously illustrated (LAMP1 & LC3B-II) while maintaining the absence of GAPDH. 5% of the pulldown was loaded compared to 1% of the whole cell input. **D)** A silver stain protocol was performed to look at the total protein pulldown under three treatment conditions, and compare the HEK293 to LysoIP cells. There is a visibly higher signal in the LysoIP group in each treatment condition, demonstrating that the pulldown is effective.

were employed to demonstrate the expression of the HA tag that is absent in wild-type cells (Figure 3A & Figure 4E). Due to the desire to isolate lysosomes, it was important to ensure that the HA tag is expressed at the proper subcellular location. Immunofluorescent microscopy of the HA tag and LAMP1, a classic lysosomal marker, confirmed that the two co-localize, thus demonstrating that the construct is correctly located (Figure 3A). These techniques allowed for visual confirmation that the TMEM192-3xHA construct is expressed in these cells, which will henceforth be referred to as LysoIP cells.

Following the confirmation that LysoIP cells were successfully produced it was essential to demonstrate the efficiency and specificity of the pulldown. LysoIP cells were cultured to ~80% confluency and incubated +/- bafilomycin $A_1$ (400 nM for 5 hours). Bafilomycin $A_1$ inhibits the acidification of lysosomes, allowing cargo to accumulate and therefore increasing the yield of the immunoprecipitation[157]. Lysosomal markers were observed (LAMP1, LC3B-II) in the whole cell fractions and the LysoIP pulldowns (Figure 3B). Despite approximately equal expression in the whole cell fractions, the signals of LAMP1 and LC3B-II were drastically increased in the pulldowns treated with bafilomycin $A_1$. Various non-lysosomal markers were blotted to assess the purity of LysoIP pulldowns. Mitochondrial (TOMM20), ER (Calnexin), and cytoplasmic (GAPDH, LC3B-I) markers were notably absent from the pulldown samples but present in the whole cell fractions (Figure 3B). These results are consistent with previous publications[104].

Despite the success of these initial experiments, we estimated that only about 2% of cellular TMEM192-3xHA was pulled down in our LysoIPs when treated with bafilomycin $A_1$. This resulted in the exploration of methodological changes to increase the yield. Three primary changes were made to the initial method. First, for all wash and resuspension steps KPBS (136 mM KCl, 10 mM KH2PO4, pH 7.25 was adjusted with KOH) was initially used – this was changed to standard PBS. Secondly,

originally the lysosomal samples were incubated with the magnetic beads for 3 minutes at room temperature. This was changed to 10 minutes at 4°C on a rotator[141]. Finally, in order to lyse the lysosomes to release the internal contents, they were initially incubated in resuspension buffer (20 mM HEPES, 1 mM EDTA, 150 mM NaCl, 1% TRITON-X, Phosphatase/proteinase inhibitor) for 5 minutes on ice[140]. This was modified to incubation for 10 minutes at 4C on a rotator to ensure complete lysis. These modifications improved yield approximately 10-fold (Figure 3C). Whereas the initial protocol required 50% of the total pulldown to obtain approximately equal LAMP1 signals to 1% of the whole cell fraction, the new protocol requires solely 5% of the pulldown.

Due to the difficulty in obtaining sufficient material from untreated LysoIP immunoprecipitations (Figure 3B), it was decided that all treatment conditions would contain bafilomycin $A_1$. To test the hypothesis that sodium arsenite conditions would result in a distinct lysosomal proteome from starvation, it was necessary to test three conditions[2,6,97,158]. Sodium arsenite treatment induces stress granule formation, and upon removal, the stress granules are removed in part by autophagy. To study this process and compare it to the other conditions, the sodium arsenite treatment condition was explored as follows: sodium arsenite (250 μM, 1 hour) followed by bafilomycin $A_1$ in complete media (400 nM, 1 hour). Comparatively, starvation conditions were set up as follows: complete media was replaced with Hank's Balanced Salt Solution (HBSS) for 1 hour and then bafilomycin $A_1$ in HBSS (400 nM, 1 hour). Finally, as a control a bafilomycin $A_1$ only condition was used: complete media was added (1 hour) followed by bafilomycin $A_1$ in complete media (400 nM, 1 hour). From this point, these will be referred to as the sodium arsenite, HBSS and bafilomycin $A_1$ treatment conditions respectively unless otherwise indicated.

It was confirmed that these three treatment conditions were all able to be used successfully within the LysoIP paradigm, strongly enriching lysosome proteins including

LAMP1 and LC3-II (Figure 3D). Silver staining was performed on 5% of the pulldown for HEK293 and LysoIP cells in all conditions, showing that there is substantially more protein present in the LysoIP samples than in the HEK (Figure 3D).

### 3.1.2 Production and validation of *ATG7*$^{-/-}$ LysoIP cells.

After successfully producing LysoIP cells, it became necessary to produce *ATG7*$^{-/-}$ LysoIP cells. Using these cells makes it possible to determine whether specific proteins are dependent upon macroautophagy to accumulate within lysosomes, or if another process is involved.

It was first necessary to develop an *ATG7*$^{-/-}$ HEK293 cell population. This was pursued by following a CRISPR-Cas9 knockout protocol as described in Ran et al. 2013[139]. Using the cloning construct pSpCas9(BB)-2A-Puro (Figure 4A) and two pre-designed sgRNA sequences from Integrated DNA Technologies (IDT) (Figure 4B), two separate expression plasmids were generated. Plasmid DNA was transfected into wild-type HEK293 cells, and clonal populations were generated (Figure 4C & D). With the exception of sgRNA1/Clone 1, numerous populations were confirmed to have the expected differential expressions of certain proteins, an absence of ATG7 and LC3B-II, and an increase in SQSTM1/p62 expression (Figure 4C & D). LC3-II is decreased because ATG7 is a critical enzyme in the lipidation of LC3, therefore an absence of ATG7 results in the absence of LC3-II.[159]. SQSTM1/p62 is a macroautophagic target, therefore in the absence of macroautophagy it accumulates as we observe in our results (Figure 4D)[160,161].

Following the confirmation of successful ATG7 knockout, a few colonies of these cells were infected by the TMEM192-3xHA lentivirus. Expression of the construct was confirmed by probing for HA by western blot (Figure 4E). Despite lower levels of HA than in the HEK293 LysoIP cells, all *ATG7*$^{-/-}$ colonies infected by the virus expressed HA, at the appropriate weight for TMEM-3xHA, as well.

sgRNA1/Colony 2 *ATG7*$^{-/-}$ and sgRNA1/Colony 2 LysoIP cells were used for downstream experiments due to the complete absence of an ATG7 signal and increased HA abundance. From this point forward these will now be referred to as *ATG7*$^{-/-}$ and *ATG7*$^{-/-}$ LysoIP cells respectively. Both colonies were confirmed to be sensitive to puromycin, suggesting that the CRISPR-Cas9 plasmid was transiently

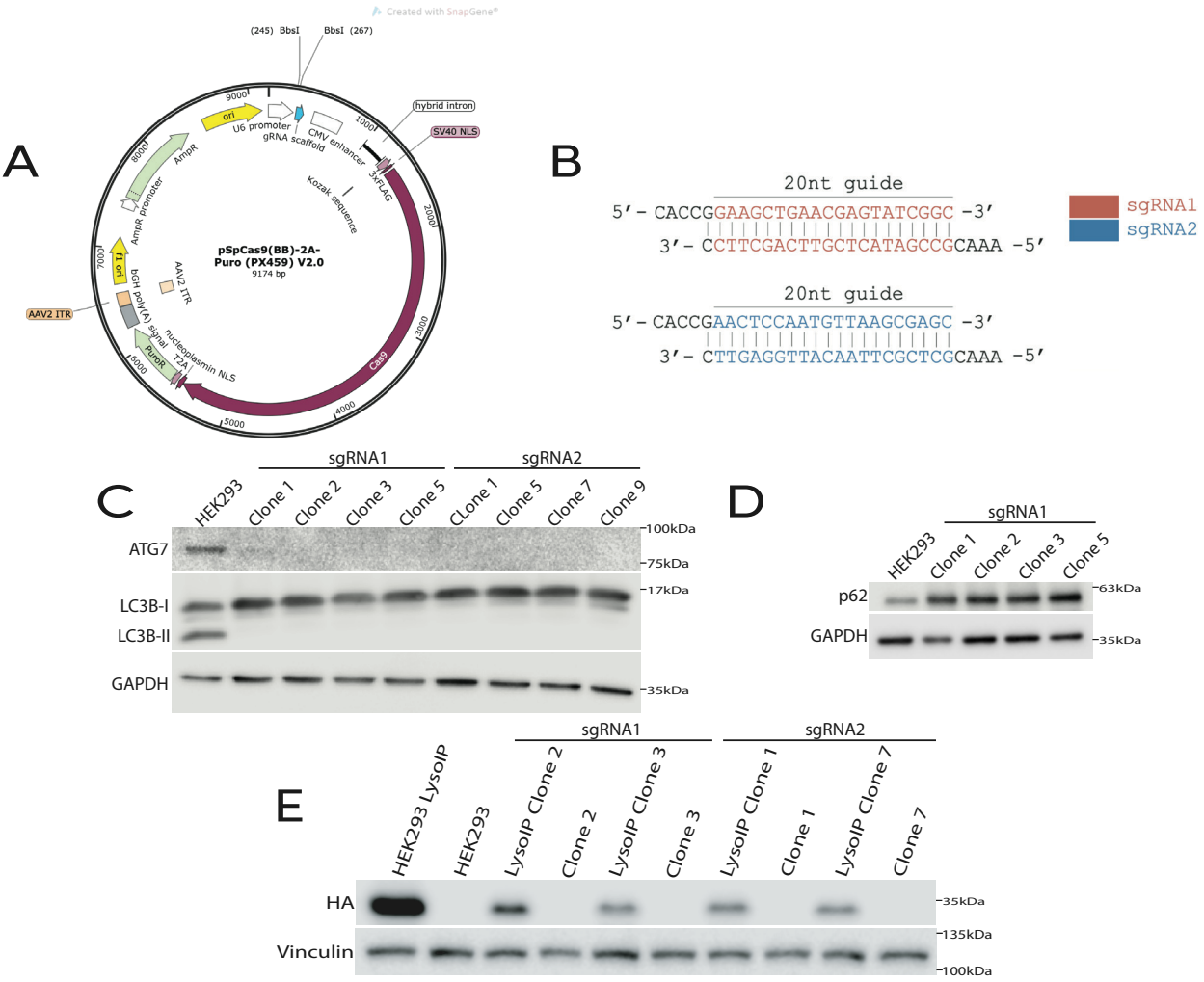


**Figure 4: Developing *ATG7*$^{-/-}$ HEK293 cells and *ATG7*$^{-/-}$ LysoIP cells. A)** A visual representation of the pSpCas9(BB)-2A-Puro plasmid used for the CRISPR knockout. Image retrieved from SnapGene. **B)** The sequences used for the CRISPR knockout. In colour are the sequences obtained from Integrated DNA Technologies (IDT), in black are the modifications required to insert the sequences into the plasmid. **C)** Western blot demonstrating the absence of ATG7 in *ATG7*$^{-/-}$ and the absence of LC3B-II. Cells were treated with 1h bafilomycin (400nM). Clonal populations were isolated from single-cell seeded wells. sgRNA1 Clone 1 appears to have remaining ATG7 expression, and was therefore excluded from further use. **D)** Western blot demonstrating an increase in p62 levels in *ATG7*$^{-/-}$ cells. Cells were untreated. **E)** Western blot confirming expression of the LysoIP construct in the LysoIP *ATG7*$^{-/-}$ cells. These include sgRNA1/Clone 2, sgRNA1/Clone 3, sgRNA2/Clone 1 and sgRNA2/Clone 7. Anti-HA antibody was used to confirm expression of the construct. In the proceeding experiments cells sgRNA1/Clone 2 expressing LysoIP and sgRNA1/Clone2 were used and referred to as *ATG7*$^{-/-}$ LysoIP and *ATG7*$^{-/-}$ respectively.

expressed. In the future to further validate the absence of the plasmid's expression, genotyping could be performed.

### 3.1.3 Major properties are not significantly impacted by the modifications.

In order to make the assertion that LysoIP lysosomes are adequately representing wild-type conditions, it was important to validate a few key properties. First, the levels of LAMP1 were checked by western blot in all four cell types (HEK293, *ATG7*$^{-/-}$, HEK293 LysoIP and *ATG7*$^{-/-}$ LysoIP). These cell types were treated under the previously described conditions: bafilomycin $A_1$, sodium arsenite and HBSS. All cell types retained equal levels of LAMP1 across all three treatment groups (Figure 5), providing justification that neither the construct expression nor the ATG7 knockout has a large impact on levels of a common lysosome marker. This is important as substantially different lysosome presentations could impact the quantitative measurement of the proteome, or the targets of autophagy itself.

It was also important to observe the reactions of the cell lines to the treatment conditions, specifically to assess their stress granule production. HEK293 and HEK293 LysoIP cells were stained for G3BP and HA (TMEM192-3xHA) after undergoing the following treatments: untreated, sodium arsenite (250 µM, 1 h), bafilomycin $A_1$ (400 nM, 1 h) or HBSS (1 h). There was not a significant difference in G3BP behaviour between the two cell types. The G3BP localization was diffuse in the untreated, bafilomycin $A_1$ and HBSS treated cells, however it formed puncta consistent with stress granules under the sodium arsenite condition (Figure 6 & Figure 7). The number of G3BP positive puncta was consistent across HEK293 and HEK293 LysoIP cells as well. While this does not guarantee that the contents of stress granules remain similar between the two cell types, it is nevertheless a positive indication that the stress response has not been severely changed upon the expression of the LysoIP construct.

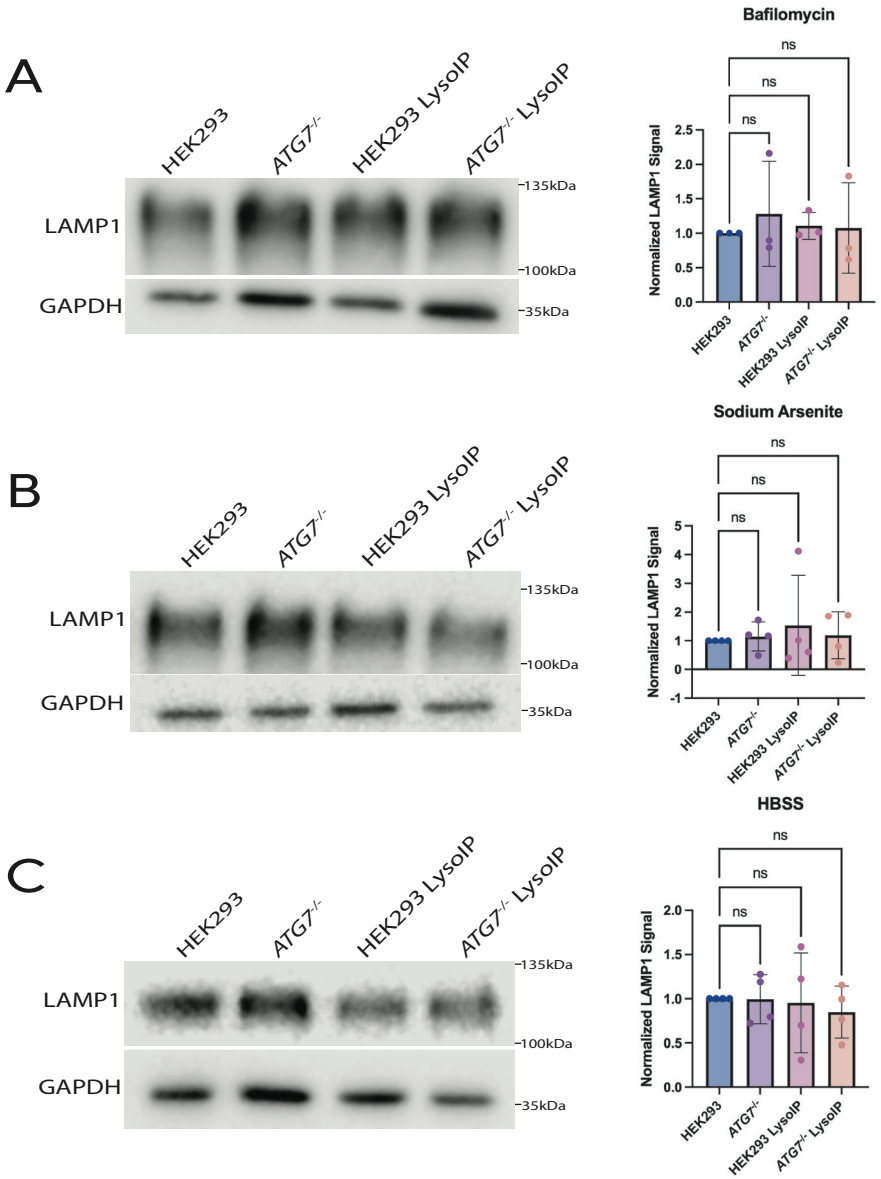


**Figure 5: Expression of the LysoIP or *ATG7*$^{-/-}$ construct does not significantly impact the expression of LAMP1 across three treatment groups.** When defining significance as $p < 0.05$, LAMP1 expression does not change significantly across the four cell types (HEK293, *ATG7*$^{-/-}$, HEK293 LysoIP or *ATG7*$^{-/-}$ LysoIP) when treated with bafilomycin $A_1$ (A, 400nM), sodium arsenite (B, 250µM ) or Hank's Balanced Salt Solution (HBSS) (C). All signals were normalized to the expression of LAMP1 in HEK293 cells. **A)** The mean with standard deviation (SD) is graphed for n=3 per cell type. **B & C)** The mean with standard deviation is graphed for n=4. Ordinary one-way ANOVAs were performed with Tukey's multiple comparison test.

## 3.2 Comparing the lysosomal proteome of cells exposed to starvation vs. oxidative stress.

### 3.2.1 Verifying the enrichment of lysosomes within samples.

It was important to ensure that the lysosomal immunoprecipitation was

successful before any samples underwent LC-MS. Western blot probing was performed on all samples prior to LC-MS preparation, and representative images of the three treatment conditions are shown in Figure 8. Samples were probed for two lysosomal markers, LAMP1 & LC3B-II, and two cytoplasmic markers, GAPDH & LC3B-I.

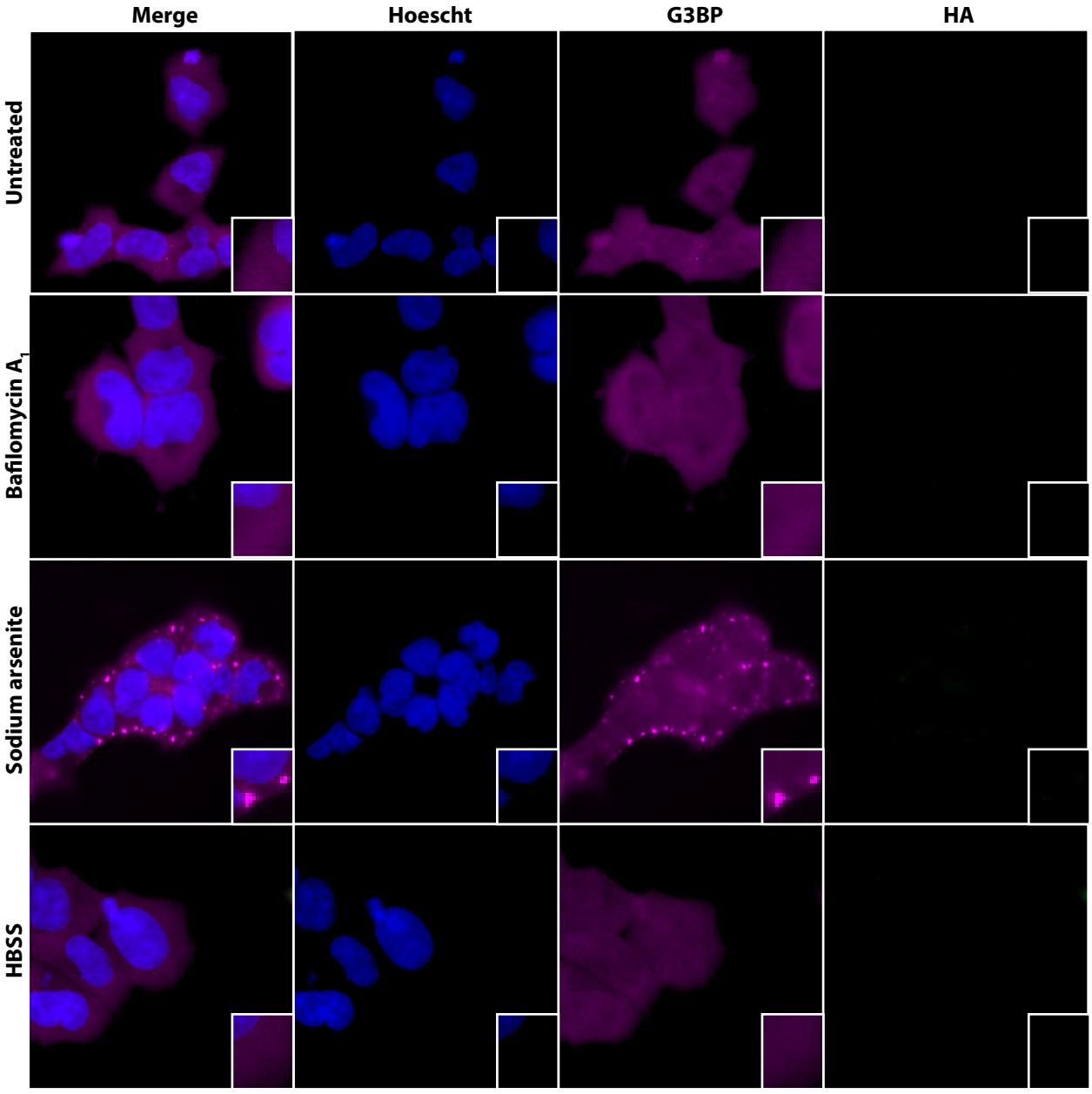


**Figure 6: Immunofluorescence of G3BP and HA in wild-type HEK293 cells under different conditions.** These images demonstrate the absence of HA expression in wild-type cells, across four conditions; untreated, bafilomycin $A_1$ (1h, 400nM), sodium arsenite (1h, 250μM) and HBSS (1h). Additionally, they show that when treated with sodium arsenite G3BP forms puncta consistent with stress granules. Comparing these results to Figure 7 demonstrates that stress granule formation is seemingly not significantly impacted by the expression of the LysoIP construct.

As expected, HEK293 & *ATG7*$^{-/-}$ cells do not demonstrate any successful pulldown. Additionally, the *ATG7*$^{-/-}$ and *ATG7*$^{-/-}$ LysoIP samples do not express LC3B-II, validating that standard macroautophagy contents are not localized to the lysosome in *ATG7*$^{-/-}$ cells as expected.

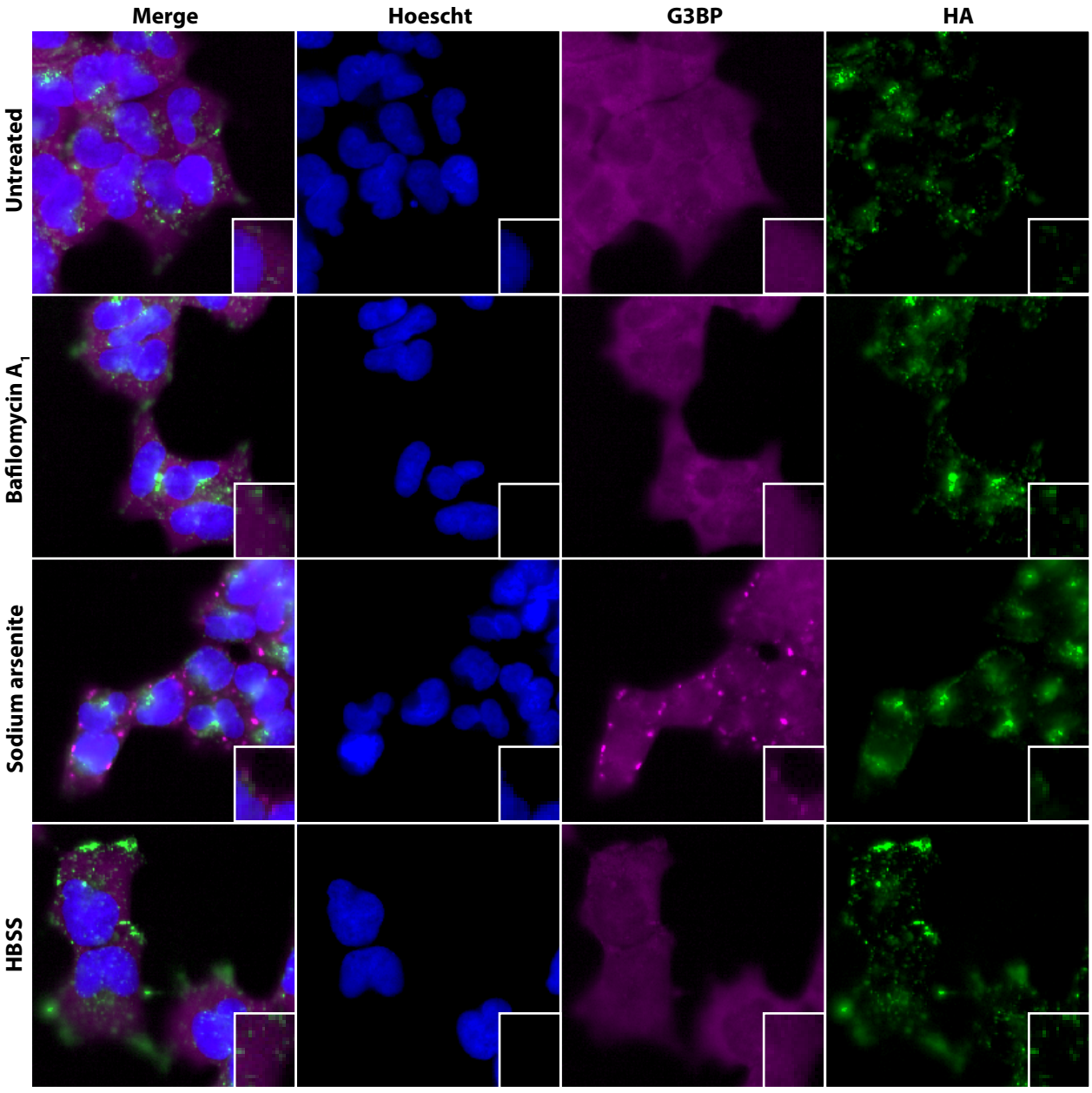


**Figure 7: Immunofluorescence of G3BP and HA in HEK293 LysoIP cells under different conditions.** These images demonstrate the expression of HA in the HEK293 LysoIP cells, due to the expression of the TMEM192-3xHA construct. The images were taken after exposure to four treatment groups; untreated, bafilomycin $A_1$ (1h, 400nM), sodium arsenite (1h, 250μM) and HBSS (1h). Additionally, after exposure to sodium arsenite G3BP forms puncta consistent with stress granules. This is comparatively similar to the reponse of HEK wild type cells to the same conditions as demonstrated in Figure 6.

Following these tests samples were prepared for LC-MS. There were three treatment conditions analyzed: bafilomycin $A_1$, sodium arsenite and HBSS. Bafilomycin $A_1$ represents the control, as only an extremely limited amount of lysosomes was recovered from untreated cells (Figure 3B). Furthermore, bafilomycin $A_1$ treatment is a better control for both the sodium arsenite & HBSS treatments which also include bafilomycin $A_1$. For the initial round of testing only two cell types were analyzed per condition – HEK293 and HEK293 LysoIP cells. The pulldown protocol was performed on both cell types, and it was these pulldowns that were used for downstream analysis. LC-MS analysis produced 3831 unique protein identifications after the elimination of contaminants and reverse sequences.

Initial analyses were performed using the proteus package in R. Comparing the LFQ values from the HEK293 cells to the HEK293 LysoIP cells demonstrated a significant enrichment of lysosomal markers in the LysoIP samples in both the sodium arsenite treatment group (Figure 9A) and the HBSS treatment group (Figure 9B). These results are summarized by volcano plots plotting the log2 Fold Change by the -log10 P-value. While it would be valuable to plot TMEM192 on this plot, seeing as it is the protein attached to the HA tag in LysoIP samples, its enrichment cannot be plotted on the volcano plot due to it being entirely absent from the HEK293 cell pulldowns (Figure 9C). Individual intensities per replicate are visualized for four lysosomal markers, TMEM192, CD63, LAMP1 and LAMP2 in Figure 9C.

These results indicate the success of the lysosomal pulldowns as both the western blots and the LC-MS analysis show an enrichment of lysosomal proteins in the LysoIP group across treatment conditions. Knowing this, it is now possible to explore the differences in lysosome contents between sodium arsenite and starvation (HBSS) treatments.

### 3.2.2 Understanding the difference in lysosomal proteins between starvation and sodium arsenite treated cells.

In order to be able to properly analyze these treatment conditions, an analysis software designed for immunoprecipitation data was used – Mass spectrometry Interaction STatistics (MIST)[146]. This software works by comparing input samples and looks for proteins unique to each condition by looking at three qualities: reproducibility (variability across replicates), abundance (peak intensity value), and specificity (uniqueness of the interaction). This amasses into one MIST score that can range from 0-1, the higher the score the more likely it is to be a hit. The value of this scoring platform is that it will enable the calculation of *lysosomal hits* and *treatment specific hits*. Because the formula attempts to find hits unique to each inputted group, if one inputs solely the LysoIP and HEK293 samples for **one** condition it is possible to identify hits specific to the LysoIP sample within said condition – i.e. *lysosomal hits*. This analysis is the identification of proteins that are not found in the HEK293 sample, and are therefore specifically lysosomal.

If one inputs all samples for **all** conditions, it is possible to find hits unique to **one treatment**, for example, the sodium arsenite LysoIP group – i.e. *treatment specific hits*.

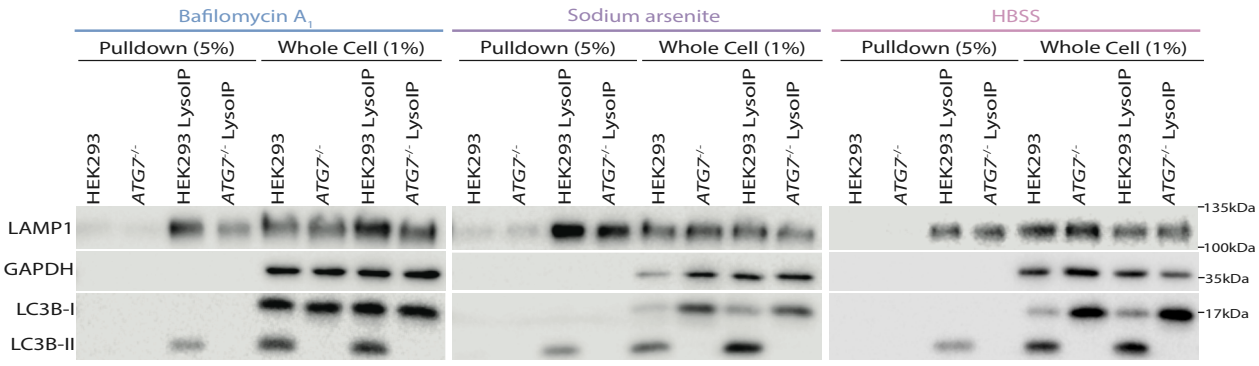


**Figure 8: Verification of lysosomal pulldown before preparation for mass spectrometry.** In advance of downstream analysis, each replicate was tested for efficiency and purity through western blot. The samples were probed for LAMP1 (lysosomal marker), GAPDH (cytoplasmic marker), LC3B-I (cytoplasmic marker) and LC3B-II (lysosomal marker). There were three treatment groups: bafilomycin $A_1$ (1h new media, 1h 400nM bafilomycin), sodium arsenite (1h 250μM arsenite, 1h 400nM bafilomycin) and HBSS (1h HBSS, 1h HBSS + 400nM bafilomycin). LAMP1 is present in all lysosomal pulldowns at approximately equal levels, while GAPDH and LC3B-I are present solely in the whole cell fraction. LC3B-II is present in the pulldown and whole cell fraction of LysoIP cells, but not in *ATG7*$^{-/-}$ or *ATG7*$^{-/-}$LysoIP cells.

The sodium arsenite LysoIP *treatment specific hits* are therefore proteins identified by MIST to be unique to sodium arsenite lysosomes and are not found in the bafilomycin $A_1$ or HBSS lysosomes. The sodium arsenite *lysosomal hits* are those that are identified as lysosomal, and may overlap with bafilomycin $A_1$ or HBSS *lysosomal hits* because each condition was analyzed independently.

The MIST score is arbitrary and is not related to a False-Discovery Rate (FDR) or

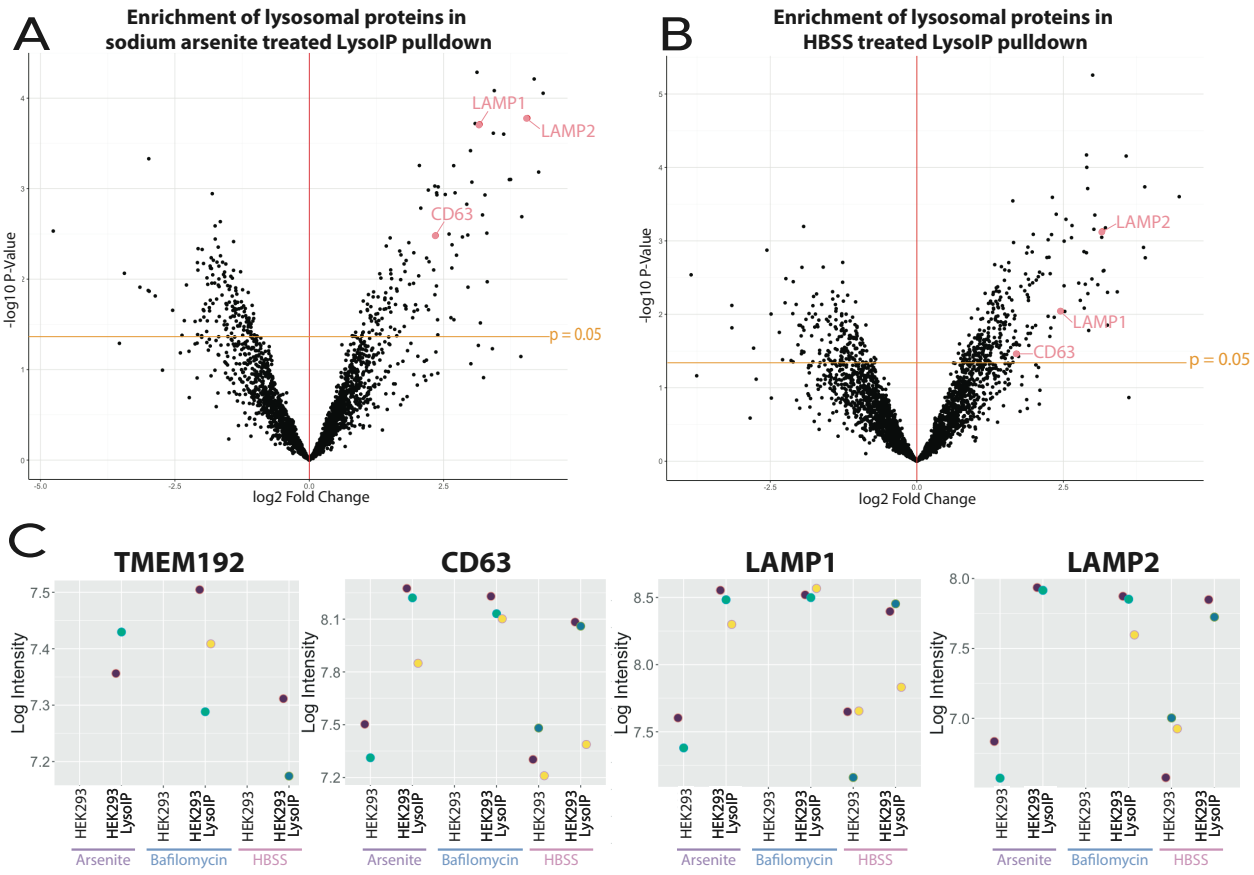


**Figure 9: Expression of lysosomal proteins as analyzed by mass spectrometry.** Raw mass spectrometry results were processed by MaxQuant on Galaxy.org, and further analyzed using the *proteus* package in R as per the instructions in the *proteus* reference manual. **A)** Analysis of the label-free quantification (LFQ) intensity of all protein hits between HEK293 LysoIP and HEK293 lysosomal pulldowns treated under the sodium arsenite condition (1h 250µM sodium arsenite, 1h 400nM bafilomycin $A_1$) demonstrates that LAMP1, LAMP2 and CD63 are all significantly enriched in the LysoIP group. This supports the assertion that the analyzed samples are highly enriched in lysosomes. **B)** Similarly, analysis of the LFQ intensity of all protein hits between HEK293 LysoIP and HEK293 lysosomal pulldowns treated under the HBSS condition (1h HBSS, 1h HBSS + 400nM bafilomycin $A_1$) demontrates significant enrichment of LAMP1, LAMP2 and CD63. **C)** Demonstrates the Log Intensity for each described protein, per replicate (n=3 for all conditions). The graphic demonstrating the intensity of TMEM192 expression explains why it is not present in the volcano plots of A & B, as there is no expression of this protein in any of the HEK groups.

p-values. For this reason, we opted to use a MIST score of 0.6 or above as a threshold to a hit in this analysis. The benchmark of 0.6 was identified by inspecting the data and assessing a score that demonstrated a high enrichment of lysosomal proteins as identified by gene ontology (Figure 10B & Figure 19).

Based on these definitions, one would expect lysosomal markers to be common in all three treatments: bafilomycin $A_1$, sodium arsenite and HBSS. However, each treated group of lysosomes will also contain its own unique treatment specific cargo. This is what is observed between the sodium arsenite and HBSS groups, which share 521 *lysosomal hits* as determined by MIST (Figure 10A). When analyzed for gene ontology cellular components, these overlapping genes are highly enriched in lysosomal terms (Figure 10B). This indicates that the primary components of the overlapping hits relate to the lysosome. However, the *lysosomal hits* that were only identified in the sodium arsenite condition present a very different cellular component profile as compared to those only identified in the HBSS condition (Figure 10C & D). The 616 *lysosomal hits* only identified in sodium arsenite show enrichment in secretory components and ficolin-1-rich granules, whereas the 178 unique HBSS hits are primarily enriched in mitochondrial proteins. These results demonstrate that the protein content the sodium arsenite and HBSS lysosomes have in common are primarily related to the lysosome itself, while their individual *lysosomal hits* are quite distinct from each other.

In a quest to further define the changes occurring between treatment groups, Ingenuity Pathway Analysis (IPA) software was used to identify any differentially enriched canonical pathways. To use this software, it was required to produce a log2(foldchange) for each condition. This was accomplished by using the LysoIP *lysosomal hits* MIST scores for sodium arsenite and HBSS and comparing each individually to the bafilomycin $A_1$ equivalent scores. Therefore, the initial fold changes were determined by comparing the treatment groups of interest (sodium arsenite

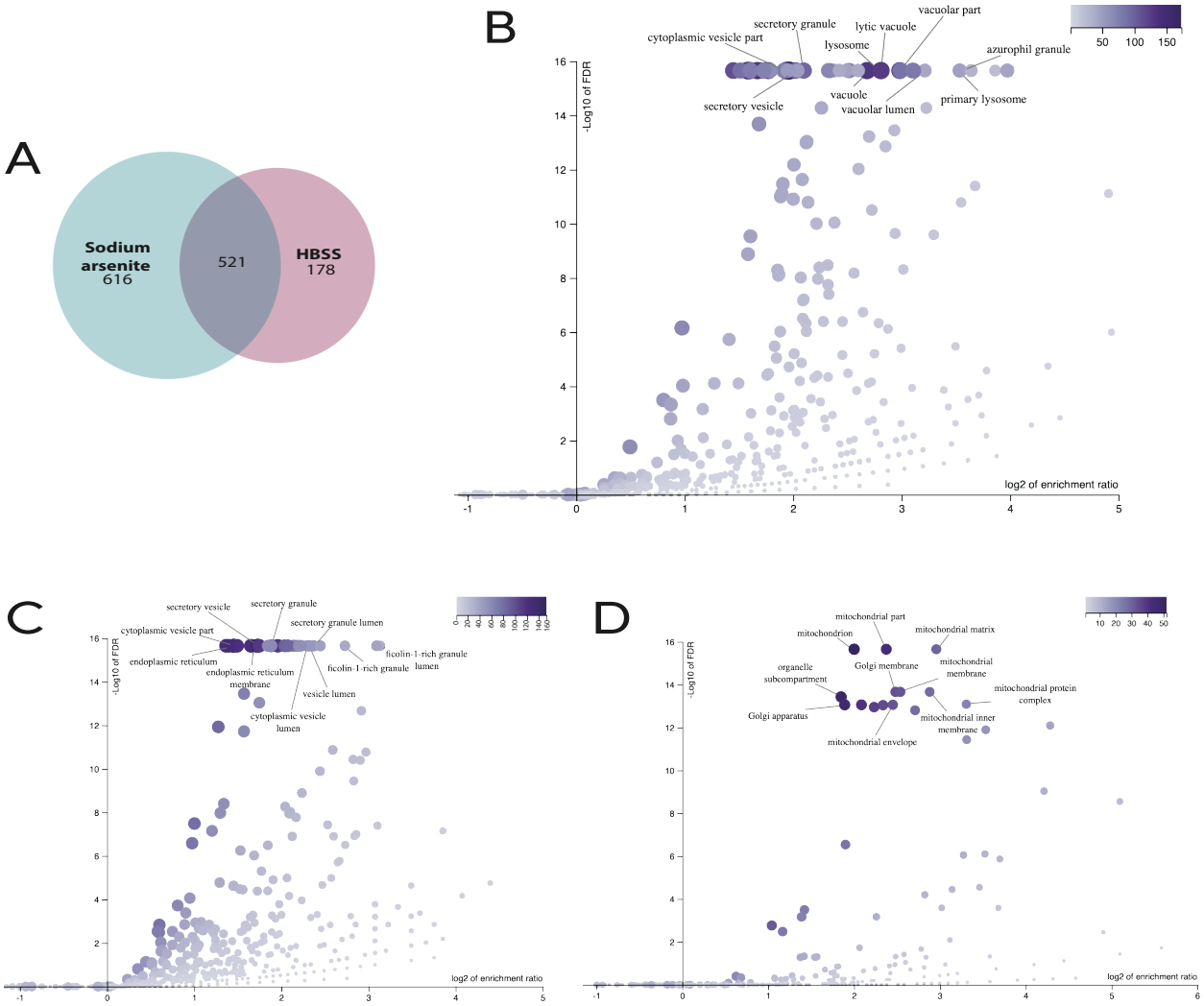


**Figure 10: Despite sharing many hits, lysosomes from sodium arsenite and HBSS treated cells contain distinct cellular component enrichments.** The mass spectrometry results were analyzed using Mass Spectrometry Interaction STatistics (MIST) as described in Jaeger et al. 2011. In order to describe lysosomal hits within each treatment group, the HEK293 LysoIP and HEK293 samples from each each treatment were analyzed using the software separately from other treatment groups. A protein was considered a lysosomal hit if the MIST score was 0.6 or above. **A)** The sodium arsenite treatment group contained 616 specific lysosomal hits, and 521 shared hits with the HBSS treatment group. The HBSS treatment group resulted in 178 individual lysosomal hits. **B)** The 521 shared lysosomal hits were put through an overrepresentation analysis using WebGestalt looking for Cellular Component geneontology enrichments. The colour and size of the dots scale up as the number of genes present in each category increases. The top 10 hits are labeled. The overlapped genes are significantly enriched for lysosomal and vacuolar geneontology terms. **C)** The 616 specific lysosomal hits to the sodium arsenite treatment group were analyzed as described in B), here we see enrichment in a number of components including various vesicles, ficolin-1 rich granules and the endoplasmic reticulum. **D)** The 178 specific lysosomal hits to the HBSS treatment group were analyzed as described in B), in this treatment we see significant enrichment in various mitochondrial components, in addition to the Golgi apparatus. The geneontology terms between C & D do not overlap, indicating specific enrichments within each treatment condition's lysosomes.

or HBSS) to the control (bafilomycin $A_1$). From there it was possible to compare the enrichment changes of sodium arsenite vs. HBSS in various pathways. There were numerous identified pathways with differential enrichments (Selected pathways: Figure 11A, all significant pathways with |z score| > 2: Figure S1), however we focused on those with the most drastic differences between sodium arsenite and HBSS as they are the most interesting to further analyze. It is also important to keep in mind that the changes in presence of pathways here, represent changes of abundance within the lysosome, a degradative organelle. Therefore, if proteins are enriched within the lysosome that indicates they are being degraded, and this may result in a decrease of its levels within the whole cell. This would not occur under these experimental conditions due to the presence of bafilomycin $A_1$ preventing degradation, however it would under homeostatic conditions. Notably nine of the ten proteins in the 'Purine Nucleotides De Novo Biosynthesis II' pathway were increased in the sodium arsenite treated samples (Figure 11B & Figure 15A). Comparatively, six proteins were decreased, two were increased and two were not identified in the HBSS treated samples. One of the proteins absent from the HBSS treatment condition was PPAT, which was highly enriched in the sodium arsenite treated samples. The only protein from this IPA pathway not identified by LC-MS in either sample was IMPDH1, which is an isoform of the IMPDH enzyme. The second isoform, IMPDH2 was however identified and was enriched in the sodium arsenite condition.

As sodium arsenite is a model of ALS-like conditions, one goal of the project was to determine if there were any ALS-linked proteins within the sodium arsenite lysosomal contents. Ten causative or ALS risk factor proteins (TMEM106B, SOD1, VAPB, DCTN1, PFN1, TUBA4A, SQSTM1/p62, VCP, CHMP2B & TARDBP) were identified as localizing to the sodium arsenite treated lysosomes by their MIST score (Table 3). Table 3 also demonstrates the MIST score of these proteins under the HBSS condition. Three proteins have MIST scores above 0.6 in both the HBSS and sodium arsenite treatment

groups: TMEM106B, SQSTM1/p62 and VAPB. However, the remaining seven only attain the MIST benchmark of 0.6 in the sodium arsenite lysosomes.

In addition to the lysosomal proteins discussed above, it is also possible to identify proteins that are purely unique to a single treatment, *treatment specific hits*. Instead of calculating a MIST score comparing only HEK293 and HEK293 LysoIP samples from a single treatment group, all three treatment groups (bafilomycin $A_1$,

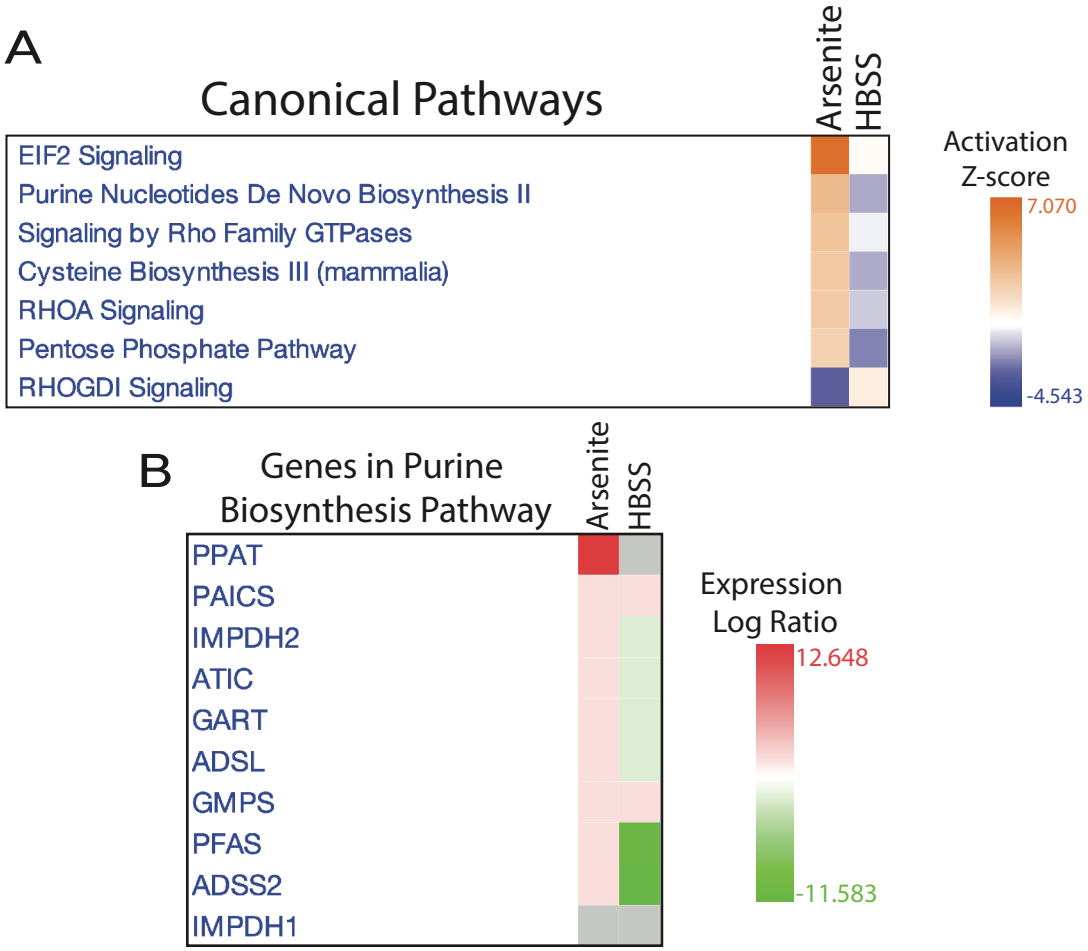


**Figure 11: Different pathways are enriched in lysosomal hits depending on the treatment condition.** The fold change of each protein detected by mass spectrometry was calculated by comparing the bafilomycin MIST score to either the sodium arsenite or HBSS MIST score. This allowed for two lists, demonstrating which proteins in sodium arsenite or HBSS were differentially expressed as compared to the bafilomycin treated samples. This data was transformed into a log2 fold change and inputted into Ingenuity Pathway Analysis (IPA), which enabled the calculation of pathway enrichment or lack thereof. **A)** This figure demonstrates a selection of differentially expressed pathways wherein the Z-score of the sodium arsenite vs. HBSS conditions were highly differentiated. It shows pathways where there was an upregulation in one treatment condition but a downregulation in the other. **B)** This figure demonstrates the expression fold change of each protein involved in the purine biosynthesis pathway - one of the pathways present in A. All of the proteins in the sodium arsenite treatment condition are enriched, or not present. Comparatively, the majority of the proteins in the HBSS condition are downregulated.

**Table 3: Certain ALS-linked proteins are enriched in lysosomes from sodium-arsenite treated cells but not from starvation or bafilomycin treated cells.** This table displays ALS-linked proteins that had a *lysosomal hits* MIST score greater than or equal to 0.6 in the sodium arsenite condition.

| Protein | Causative (C) or Modifier/Risk Factor (M) | Sodium arsenite MIST Score | HBSS MIST Score |
|---|---|---|---|
| TMEM106B | M | 0.97618 | 0.98112 |
| SOD1 | C | 0.86678 | 0.28609 |
| VAPB | C | 0.86286 | 0.78716 |
| DCTN1 | C | 0.84554 | 0.50734 |
| PFN1 | C | 0.78091 | 0.42616 |
| TUBA4A | C | 0.76078 | 0.56468 |
| SQSTM1 | C | 0.75545 | 0.71873 |
| VCP | C | 0.70894 | 0.59675 |
| CHMP2B | C | 0.70709 | 0.57533 |
| TARDBP | C | 0.62411 | 0.52669 |

sodium arsenite and HBSS) are input at the same time. This results in a more stringent scoring system as there is more inputted data. It is similar to looking at *lysosomal hits* unique to HBSS or sodium arsenite (Figure 10C & D), however it is a more stringent analysis and narrows down the results. The resulting hits could be indicative of proteins that may solely be targeted under one condition or provide hints as to targeted processes (Figure 12 & Figure 13). This therefore explains the absence of typical lysosomal markers, these would not be considered unique to a single treatment group as they are present in all LysoIP samples regardless of treatment. These *treatment specific hits* represent a very small fraction of the total number of identified proteins, the sodium arsenite *treatment specific hits* (47 proteins) represent just 1.2% of the total identified proteins, and the HBSS *treatment specific hits* (20 proteins) represent just 0.5%. Networks of sodium arsenite and HBSS-specific LysoIP contents were created using the stringApp in the Cytoscape program. Using the COMPARTMENTS scoring system, it was possible to identify proteins within each network that met the highest score for specific subcellular compartments[150]. One of the most obvious differences between the two is that the sodium arsenite *treatment specific hits* contains a high

percentage of nuclear proteins (14.9%) compared to the HBSS *treatment specific hits* which contain none, this aligns with the documented nuclear export of many proteins upon sodium arsenite treatment[162]. In contrast, HBSS *treatment specific hits* have more cytoskeletal (10%) and mitochondrial hits (20%) than seen in sodium arsenite (2.13% cytoskeletal, 2.13% mitochondrial). This is indicative of the two treatment conditions resulting in vastly different cargo.

Cytoscape clusterMaker2 was used to analyze each treatment specific network. HBSS *treatment specific hits* were enriched in mitochondrial categories, while the sodium arsenite *treatment specific hits* result in more varied clusters with categories ranging from carbon metabolism to purine biosynthesis (Figure 12 B & C, Figure 13 B & C). One enrichment category found in the sodium arsenite group is oxidation reduction (Figure 12B). This aligns with what we know about sodium arsenite treatment – seeing as sodium arsenite induces oxidative stress and within mammalian cells it is metabolized through reduction and oxidative methylation[163]. A few of the proteins identified to participate in the oxidation-reduction reaction have been linked directly to response to sodium arsenite, and TXNRD1 one of the clustered proteins has been identified as a modifier of familial ALS[164–166]. Two other enrichment categories in the sodium arsenite *treatment specific hits* are 'purine biosynthesis' and 'purine ribonucleoside monophosphate biosynthesis', these are particularly interesting as it replicates results seen from the IPA analysis (Figure 11). IPA and Cytoscape respectively show that enrichment of purine biosynthesis proteins are found in both sodium arsenite *lysosomal hits*, and in sodium arsenite *treatment specific hits*.

To investigate in more detail the enrichment of purine biosynthesis enzymes in LysoIP samples, a volcano plot of identified proteins in sodium arsenite HEK293 LysoIP vs. HBSS HEK293 LysoIP pulldowns, was generated (Figure 14). The majority of these purine biosynthesis proteins were enriched in the sodium arsenite-treated condition, and four of them significantly so (PFAS, IMPDH2, ADSS2 and PAICS). One of

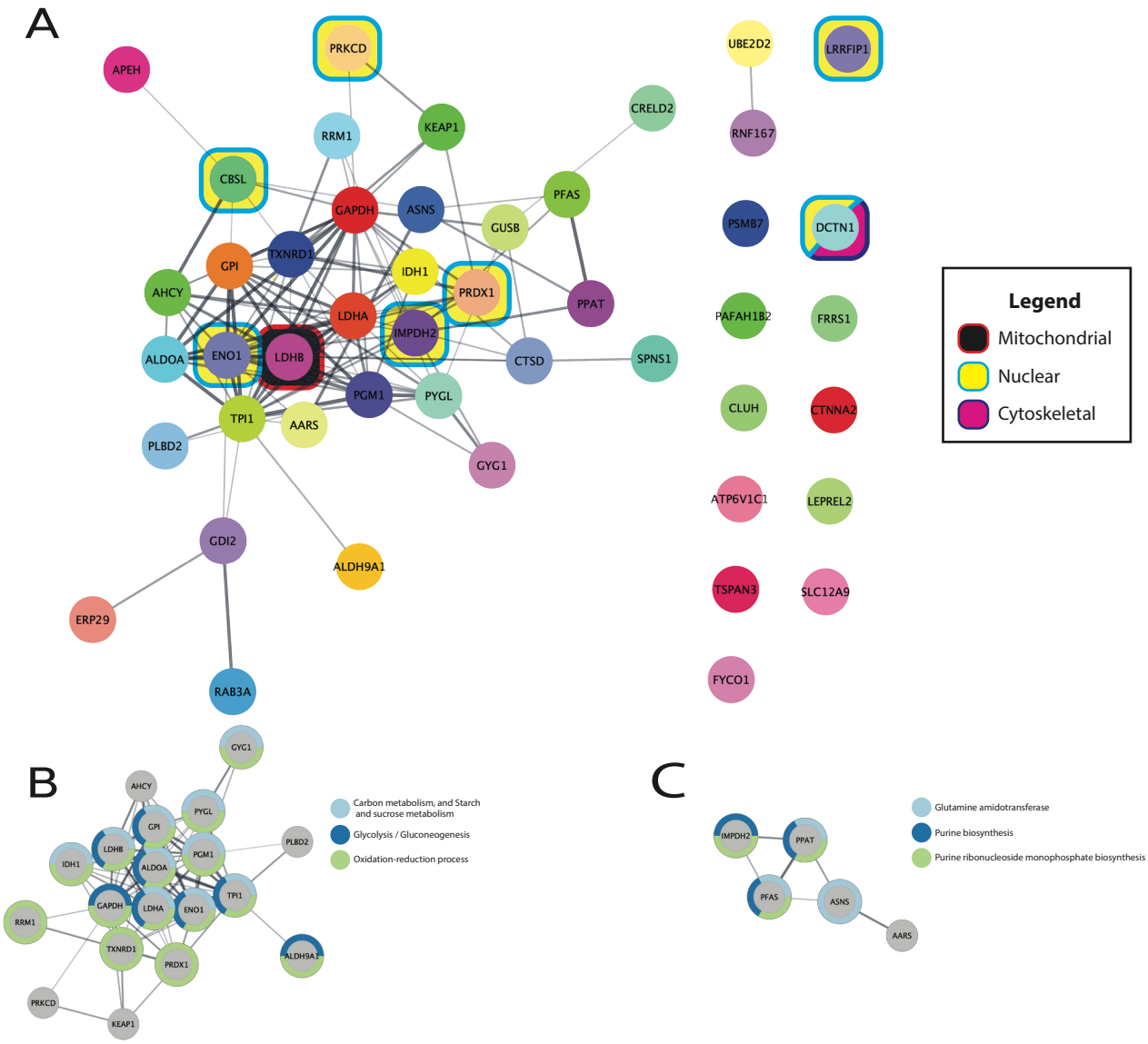


**Figure 12: Network of sodium arsenite specific hits reveals enrichment of certain subcellular compartments and pathways.** In order to calculate protein hits specific to each treatment condition, all of the LFQ intensity values for the bafilomycin, sodium arsenite and HBSS conditions were run through the MIST software simultaneously. This allowed the software to identify hits specific to each condition. Hits were determined to be proteins with scores at or above 0.6. **A)** This is a network of all the sodium arsenite hits, produced through the stringApp on the Cytoscape software. This software identifies functional and/or physical interactions between proteins. The width and transperency of the links between proteins is determined by the aggregate score, calculated by taking into account textmining, database information, experimental results, coexpression, cooccurence and fusion. The darker and wider the link, the stronger the confidence in the relationship. Various proteins within the network have been highlighted using COMPARTMENTS analysis as described in Binder et al. 2014. Briefly, a score of confidence is assigned towards the localization of a protein from one star (lowest confidence) to five stars (highest confidence). Only localizations with a score of five stars are highlighted here. 14.9% are nuclear, 2.13% are mitochondrial and 2.13% are cytoskeletal. **B & C)** Clustering analysis was performed through Cytoscape using the clusterMaker2 application. The top two identified clusters are shown in B & C. The top three enrichment categories are shown in varying colours, ranked by their false discovery rate (FDR). Individual proteins are highlighted according to their presence in the labeled categories.

them, PPAT, was not identified within the HBSS treatment condition, and is therefore not present on the volcano plot but does represent a protein of interest because of this. Also represented on this volcano plot are ALS-linked proteins and stress granule markers. Interestingly, none of the stress granule markers are significantly enriched in LysoIP samples in the sodium arsenite-treated condition (PABP, G3BP1, TIA1). This is interesting as previous research has indicated that stress granules are cleared by autophagy[41,167]. One ALS-linked protein of interest reached significance and is enriched within the arsenite treated condition – SOD1. There have been differing reports on whether or not wild-type SOD1 co-localizes to stress granules and it is not classically considered a stress granule marker, however the mutant protein is a causative ALS gene and widely reported to impact stress granule dynamics[168–170].

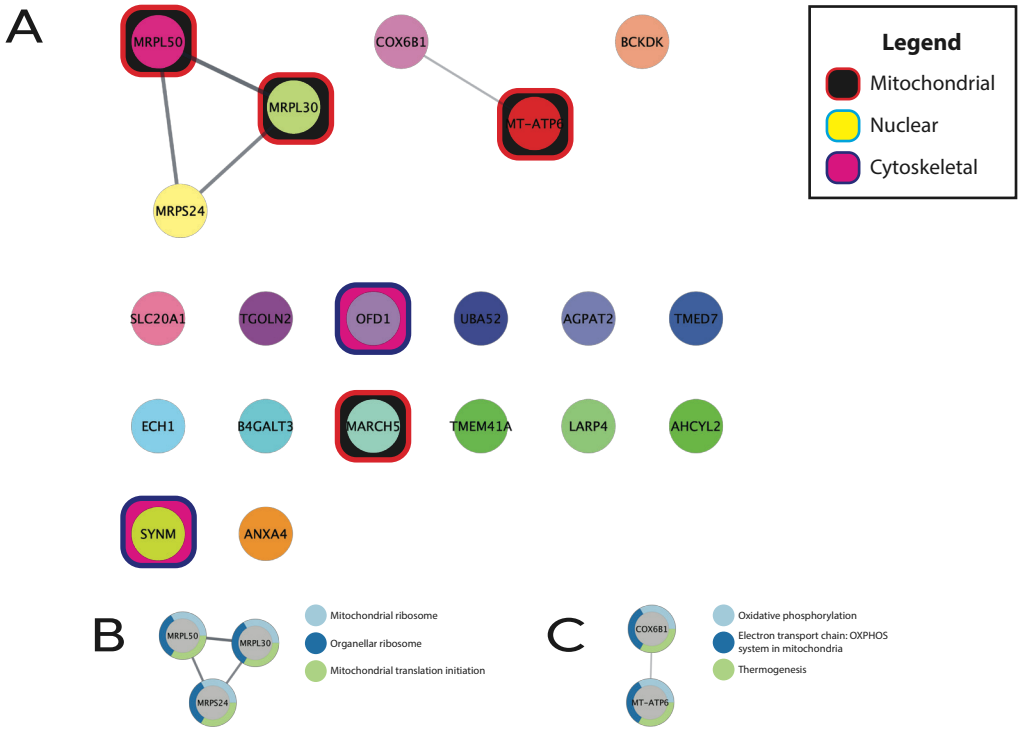


**Figure 13: Network of HBSS specific hits reveals enrichment of certain subcellular compartments and pathways.** The analysis was performed as described in Figure 12. **A)** This is a network of all HBSS specific hits, wherein proteins with five star localization scores are highlighted by their locale. 20% of the proteins are labeled as mitochondrial, and 10% as cytoskeletal according to the COMPARTMENT database. There are no nuclear proteins. **B & C)** The clusterMaker2 algorithm returned two clusters of significance from the HBSS network, and are shown here. The top three enriched categories, as determined by their FDR, are highlighted for each cluster. The individual proteins are coloured depending on their association with the categories. Amongst these two clusters is an enrichment in mitochondrial categories.

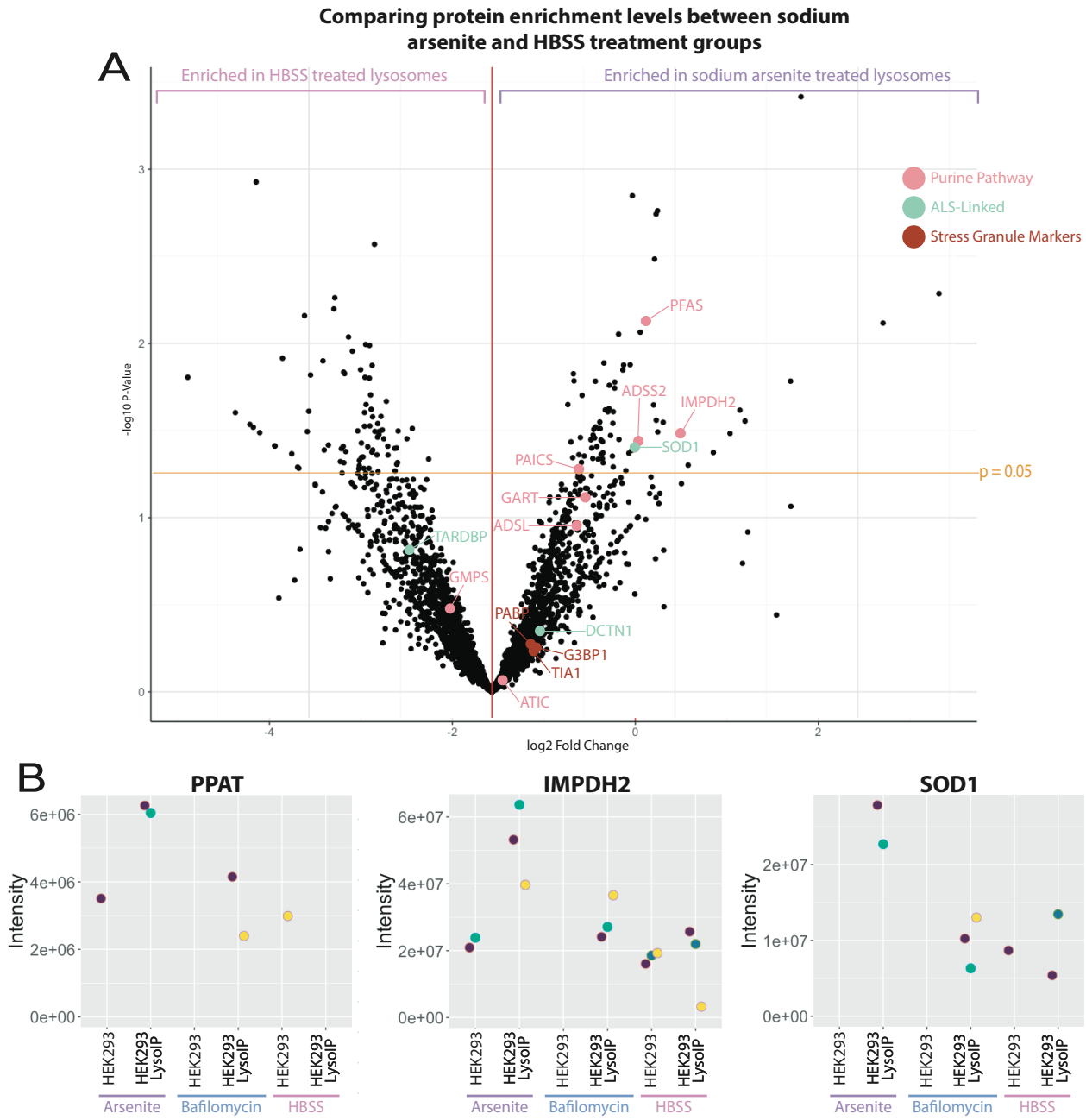


**Figure 14: Enrichment of proteins in lysosomes from sodium arsenite treated cells as compared to HBSS treated.** The following graphics were produced using the *proteus* package in R, and analyzed according to the recommended instructions described in the reference manual. **A)** The LFQ intensities of each protein were compared between the sodium arsenite and HBSS treated samples in order to calculate the fold-change and p-value. Highlighted on the graphic are various categories of interest including select ALS-linked proteins (turquoise), stress granule markers (brown) and all of the proteins present in the purine biosynthesis pathway (pink). One notable protein of the purine synthesis pathways excluded from the plot is phosphoribosyl pyrophosphate amidotransferase (PPAT), which was not isolated from the HBSS treated samples, and is therefore highly enriched in the sodium arsenite treated samples. **B)** These plots demonstrate the distribution of intensities for IMPDH2, SOD1 and PPAT - all proteins significantly enriched in the sodium arsenite treated condition. n=3 for all treatment conditions.

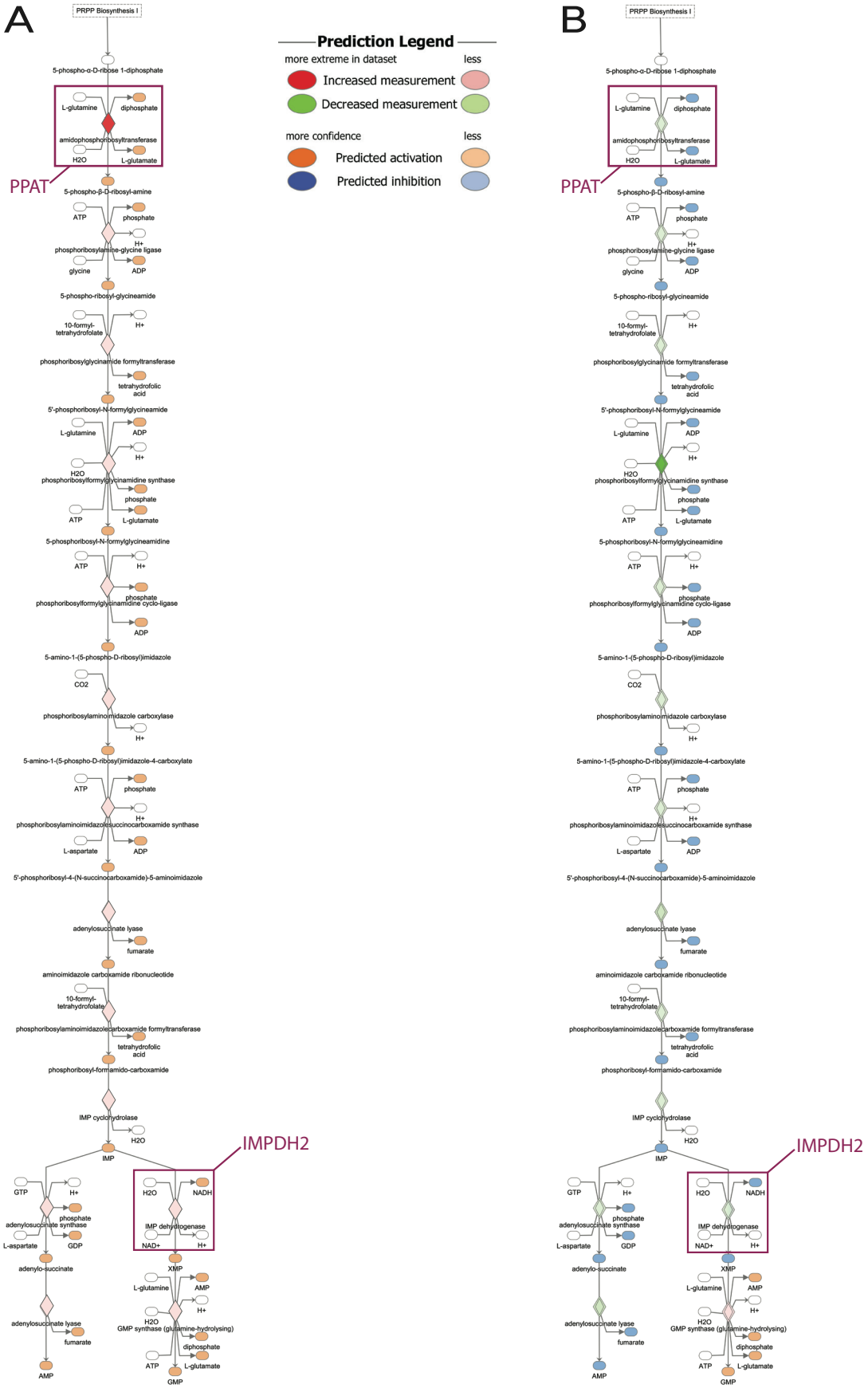
A
B
PRPP Biosynthesis I
5-phospho-α-D-ribose 1-diphosphate
L-glutamine
diphosphate
amidophosphoribosyltransferase
H2O
L-glutamate
PPAT
5-phospho-β-D-ribosyl-amine
ATP
phosphate
H+
phosphoribosylamine-glycine ligase
glycine
ADP
5-phospho-ribosyl-glycineamide
10-formyl-tetrahydrofolate
phosphoribosylglycinamide formyltransferase
tetrahydrofolic acid
5'-phosphoribosyl-N-formylglycineamide
phosphoribosylformylglycinamidine synthase
5-phosphoribosyl-N-formylglycineamidine
phosphoribosylformylglycinamidine cyclo-ligase
5-amino-1-(5-phospho-D-ribosyl)imidazole
CO2
phosphoribosylaminoimidazole carboxylase
5-amino-1-(5-phospho-D-ribosyl)imidazole-4-carboxylate
phosphoribosylaminoimidazolesuccinocarboxamide synthase
L-aspartate
5'-phosphoribosyl-4-(N-succinocarboxamide)-5-aminoimidazole
adenylosuccinate lyase
fumarate
aminoimidazole carboxamide ribonucleotide
phosphoribosylaminoimidazolecarboxamide formyltransferase
phosphoribosyl-formamido-carboxamide
IMP cyclohydrolase
IMP
IMPDH2
GTP
adenylosuccinate synthase
GDP
adenylo-succinate
AMP
NADH
IMP dehydrogenase
NAD+
XMP
L-glutamine
GMP synthase (glutamine-hydrolysing)
GMP
Prediction Legend
more extreme in dataset
less
Increased measurement
Decreased measurement
more confidence
Predicted activation
Predicted inhibition

**Figure 15: Changes in purine pathway protein expression levels depending on treatment and cell type.** The following graphics were made using IPA software. **A)** The overlay of the purine biosynthesis pathway here is using data measuring the change of protein enrichment in sodium arsenite treated samples as compared to bafilomycin $A_1$ treated samples. All of the involved proteins are upregulated in the sodium arsenite treated samples, in particular PPAT, which is highlighted on the graphic. Also highlighted is the rate limiting protein for guanosine monophosphate (GMP) synthesis, IMPDH2. **B)** The overlay of the purine biosynthesis pathway here is looking at the change in sodium arsenite treated wild type vs. *ATG7*$^{-/-}$cells. This demonstrates that the majority of the proteins of the pathway localize to the lysosomes at least partially in an ATG7 dependent fashion.

Due to the reoccurring presence of purine biosynthesis as a pathway hit, and many of its proteins being enriched in the sodium arsenite lysosomes, this encouraged a more thorough look at how the molecules that make up this pathway may be related to stress granule formation (Figure 16), and ALS in general (Figure 17). While neither stress granule or ALS related pathways were identified to be enriched by IPA, it is possible that some of the enrichments the analysis did identify are linked to these processes. It was of particular interest to look at the purine biosynthesis pathway because of its replicability. These networks were built using IPA by looking at any links between the purine biosynthesis pathway molecules - including involved proteins and molecular byproducts. While there were numerous interactions between purine biosynthesis molecules and both ALS and stress granules through intermediates, the lack of direct interactions makes it difficult to be sure of a true link. These interactions do however represent potential interactions to study more at a later date. The one interaction that exists purely between a purine biosynthesis pathway molecule and ALS is through L-glutamic acid (Figure 17). IPA classifies L-glutamic acid as a synonym for L-glutamate/glutamate, which can be seen as a by-product in a number of reactions along the pathway (Figure 15). Glutamate has widely been reported to be increased in the cerebrospinal fluid of ALS patients, in up to 40% of sporadic patients[171,172]. Not only that, but glutamate excitotoxicity  is a prevailing theory behind the cell death observed in ALS patients and is potentially the event targeted by Riluzole, an ALS drug[173]. While it is tempting to make a connection between the two, glutamate is involved in so many processes that it would require much more information about the role the purine

biosynthesis pathway plays in ALS to make any kind of reasonable determination. Furthermore, the excess glutamate present in many ALS-patients is typically explained by altered expression of the glutamate transporter, EAAT2[172].

These results beg the question, how would the absence of ATG7, and in turn macroautophagy itself, impact the presence of these proteins in sodium arsenite lysosomes. It would be beneficial to be able to determine if the proteins that are a part of this pathway are degraded by macroautophagy or not.

## 3.3 The absence of ATG7 impacts the degradation of purine biosynthesis pathway proteins.

In order to analyze the impact of *ATG7*$^{-/-}$ on sodium arsenite lysosome pulldowns, new pulldowns were performed from *ATG7*$^{-/-}$ cells and compared to the existing sodium arsenite-treated pulldowns. While this is not ideal, it became necessary, and the samples were prepared in identical fashions. We focused on the sodium arsenite condition for this analysis.

### 3.3.1 The lysosomal immunoprecipitations are enriched in lysosomal proteins.

As with the previous samples, it was important to ensure that the samples being analyzed were highly enriched with lysosomal proteins. Before LC-MS processing this was checked by western blot (Figure 8). Probing for lysosomal markers (LAMP1) and cytoplasmic markers (GAPDH, LC3B-I) ensured that these samples were indeed lysosomal immunoprecipitations. The absence of LC3B-II was continued evidence of the absence of ATG7 and macroautophagy in these cells.

After LC-MS, and raw data analysis by MaxQuant, the HEK293 LysoIP and *ATG7*$^{-/-}$ LysoIP cellular component enrichments of their respective *lysosomal hits* were compared. Not only were the vast majority of both of their hits lysosomal, but they both had the same top 10 hits (Figure 19). This demonstrates that lysosomal contents are only moderately affected by *ATG7*$^{-/-}$.

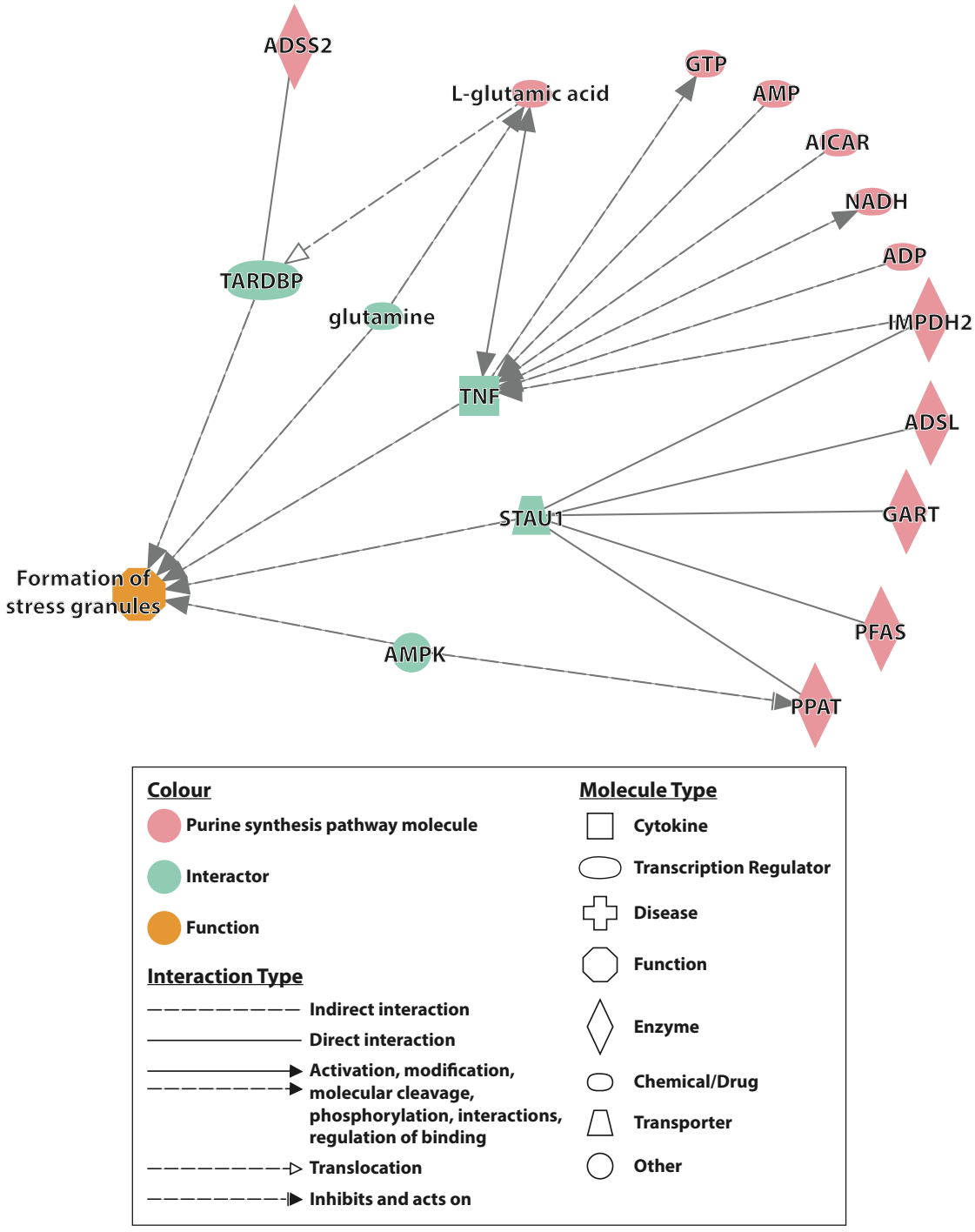


**Figure 16: Linking the purine synthesis pathway to stress granule formation.** The links in this network were constructed using IPA. This network demonstrates potential links between purine synthesis pathway molecules (pink) and the formation of stress granules through various intermediate proteins (blue). The links visualized here do not represent all possibilities, but were chosen either for the strength of the interaction or the perceived interest.

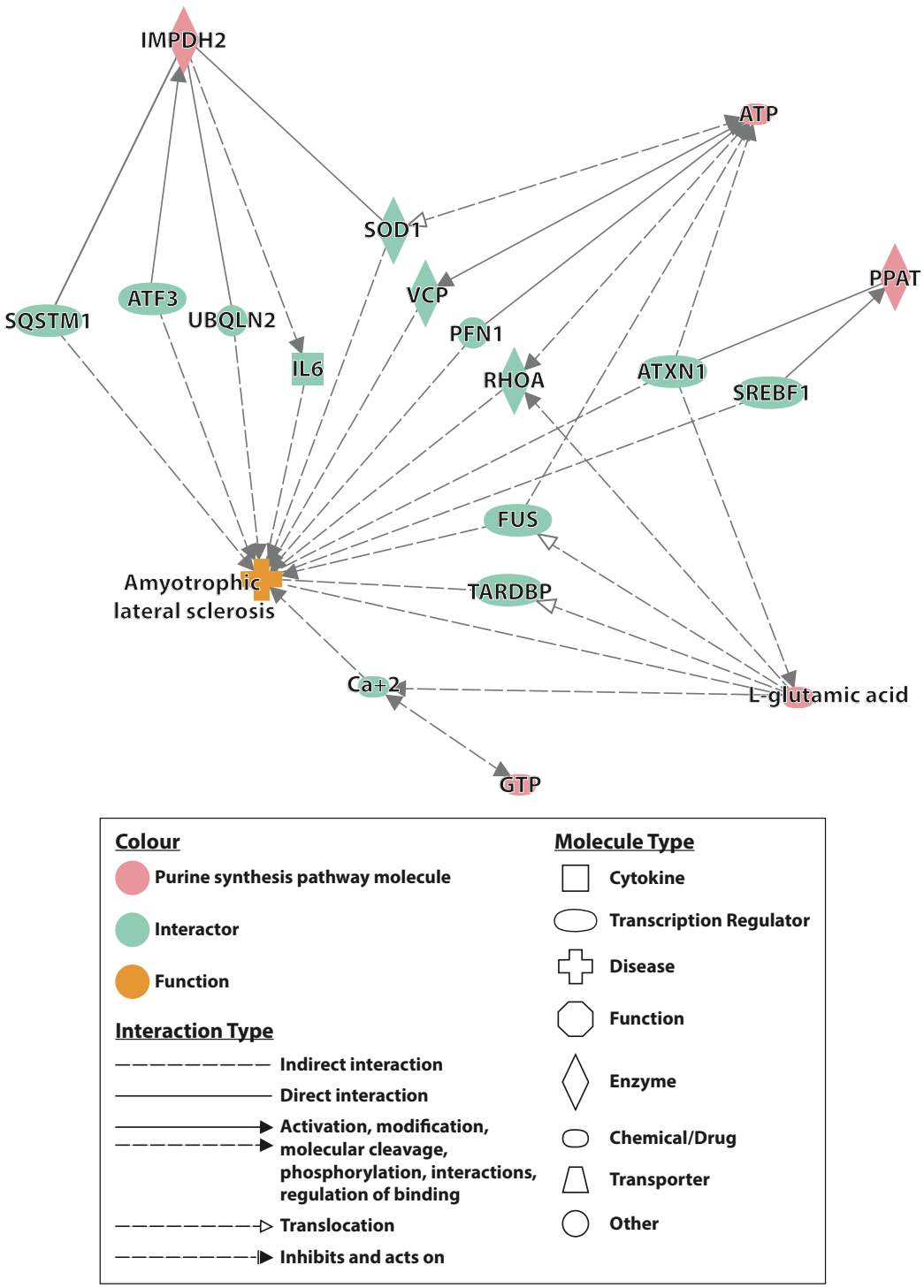


**Figure 17: Linking the purine synthesis pathway to amyotrophic lateral sclerosis (ALS).** The links in this network were constructed using IPA. This network demonstrates a selected number of connections between ALS and purine synthesis pathway molecules (pink) through interactors (blue). Only one purine synthesis pathway molecule is linked to ALS without an intermediate, L-glutamic acid. The links visualized here do not represent all possibilities, but were chosen either for the strength of the interaction or the perceived interest.

### 3.3.2 Various pathways are impacted by *ATG7*$^{-/-}$, including the purine biosynthesis pathway.

In order to compare the LysoIP pulldown to the *ATG7*$^{-/-}$ LysoIP pulldown, their respective MIST scores were used to calculate the fold change. IPA was used to analyze the changes to canonical pathways in the *ATG7*$^{-/-}$ LysoIP lysosomes (Figure 20A). Pathways with z-scores above an absolute value of 2 are shown on the graph in Figure 20A, as this corresponds to a p-value ≤ 0.05[174]. Pathways with negative z-scores were decreased in the *ATG7*$^{-/-}$ lysosomes, indicating they were reliant on macroautophagy to be targeted to the lysosome.

As expected, autophagy had a negative z-score, indicating that proteins involved in autophagy are decreased within the lysosome from *ATG7*$^{-/-}$ cells. One particular example has already been demonstrated, and that is LC3B-II.

Since proteins of the purine biosynthesis pathway were specifically found in HEK293 LysoIP samples from sodium arsenite-treated cells, we queried whether macroautophagy was required for their presence in lysosomes using samples from *ATG7*$^{-/-}$ LysoIP cells. Indeed, proteins involved in the purine biosynthesis pathway were decreased in LysoIP samples from *ATG7*$^{-/-}$ LysoIP cells with a strongly negative z-score (Figure 20A) and 73% (8/11) of its proteins decreased in *ATG7*$^{-/-}$ LysoIP samples (Figure 20B & Figure 15B).

After looking at the whole pathways, it was of interest to observe some of the relevant proteins individually. This was done through use of a volcano plot that shows the changes of protein expression from HEK293 LysoIP to *ATG7*$^{-/-}$ LysoIP samples (Figure 21). Various lysosomal proteins were observed, ideally the majority would not have changed significantly from one cell type to the other. This occurred for two of them, RAB9A and LAMP1. That LAMP1 remains essentially unchanged tracks with the initial western blots performed prior to LC-MS. However, two others were significantly reduced in the *ATG7*$^{-/-}$ LysoIP samples including TMEM192 – which is the protein attached to the HA tag. Due to these results, it will be important to consider

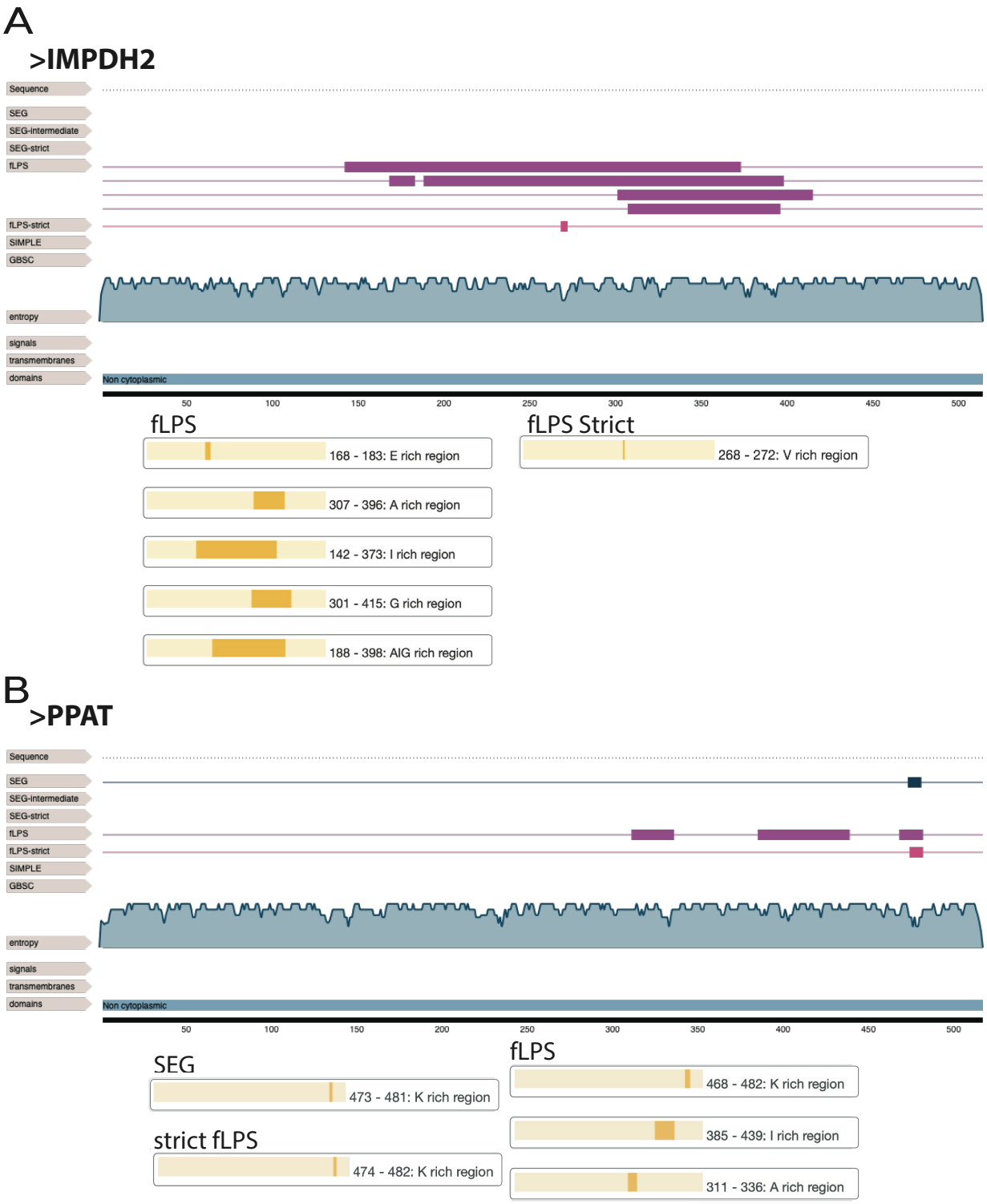


**Figure 18: IMPDH2 and PPAT contain may low complexity domains (LCDs).** The protein sequences of both IMPDH2 (A) and PPAT (B) were analyzed using PlaToLoCo, a web-based tool that combines five different tools aimed at discovering LCDs. PlaToLoCo was first described in Jarnot et al. 2020. The two figures show the localization of possible LCDs along the protein sequence, and underneath show the specific location and tool that was used to discover it. The use of multiple tools to find these LCD allows for the visualization of differences in biases, granularity and definitions of LCDs, and therefore provides a more accurate picture of what may indeed be a LCD in function.

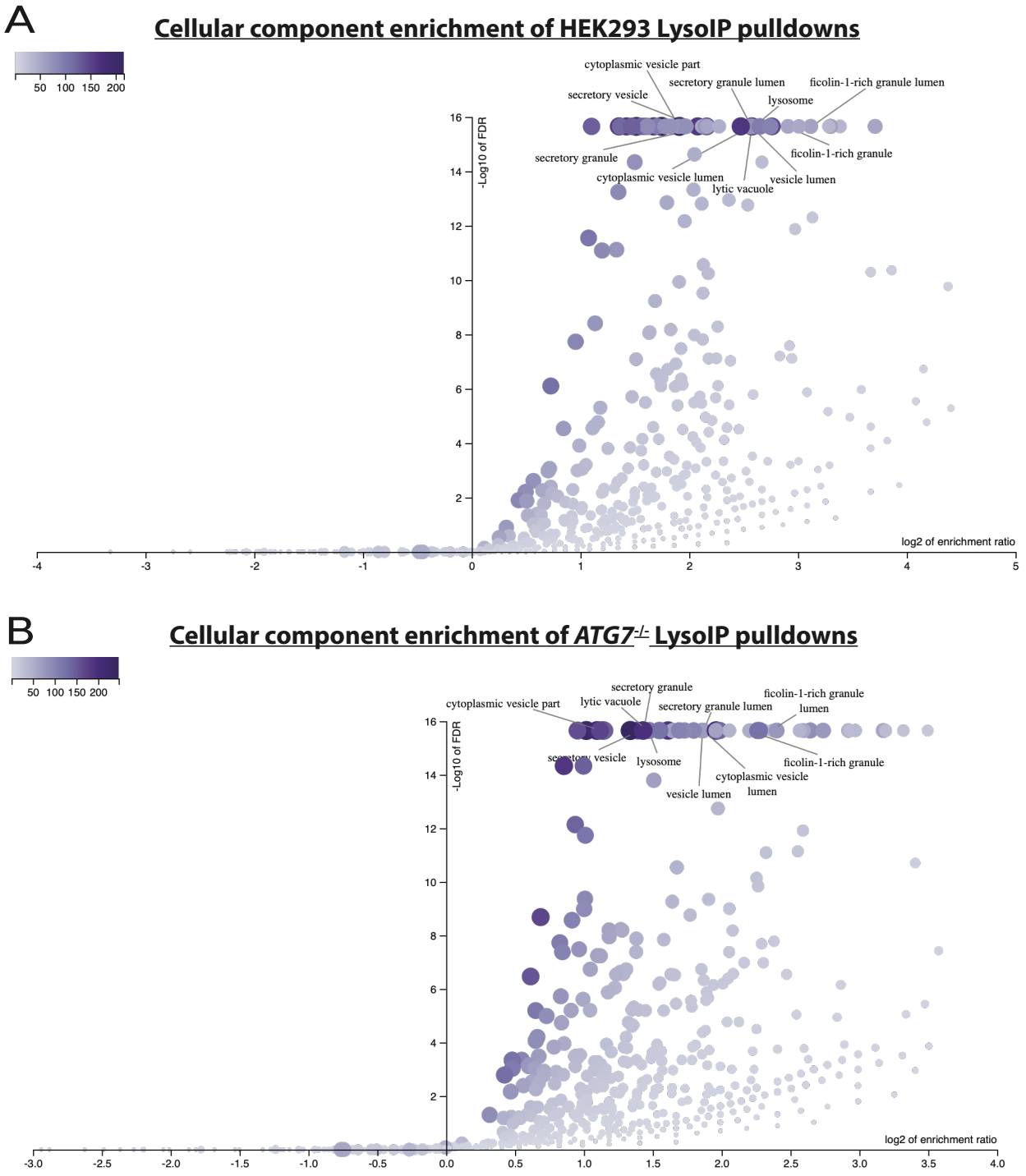


**Figure 19: Sodium arsenite treated *ATG7*$^{-/-}$ and wild type cell pulldowns are both enriched in lysosomal proteins.** Samples from HEK 293 LysoIP and ATG7-/- LysoIP pulldowns were prepared for mass spectrometry. These results were analyzed here for Cellular Component enrichment by WebGestalt. These graphs demonstrate that both HEK293 LysoIP (A) and ATG7-/- LysoIP (B) pulldowns are highly enriched in lysosomal proteins, indicating that the pulldown was efficient and specific in both cell lines - despite the knockout of ATG7.

that pulldown efficiency may have changed across the two cell types, even if that was not initially obvious from the original western blots (Figure 8). What was observed amongst the lysosomal proteins, and expected, is a highly significant decrease in LC3B expression due to the absence of LC3B-II.

The second group of analyzed proteins were ALS-linked proteins. TMEM106B was significantly reduced in *ATG7*$^{-/-}$ LysoIP samples suggesting it is dependent on macroautophagy in order to be degraded under these conditions. Intriguingly, FUS is more highly represented in the *ATG7*$^{-/-}$ lysosomes than in the wild-type. One notable

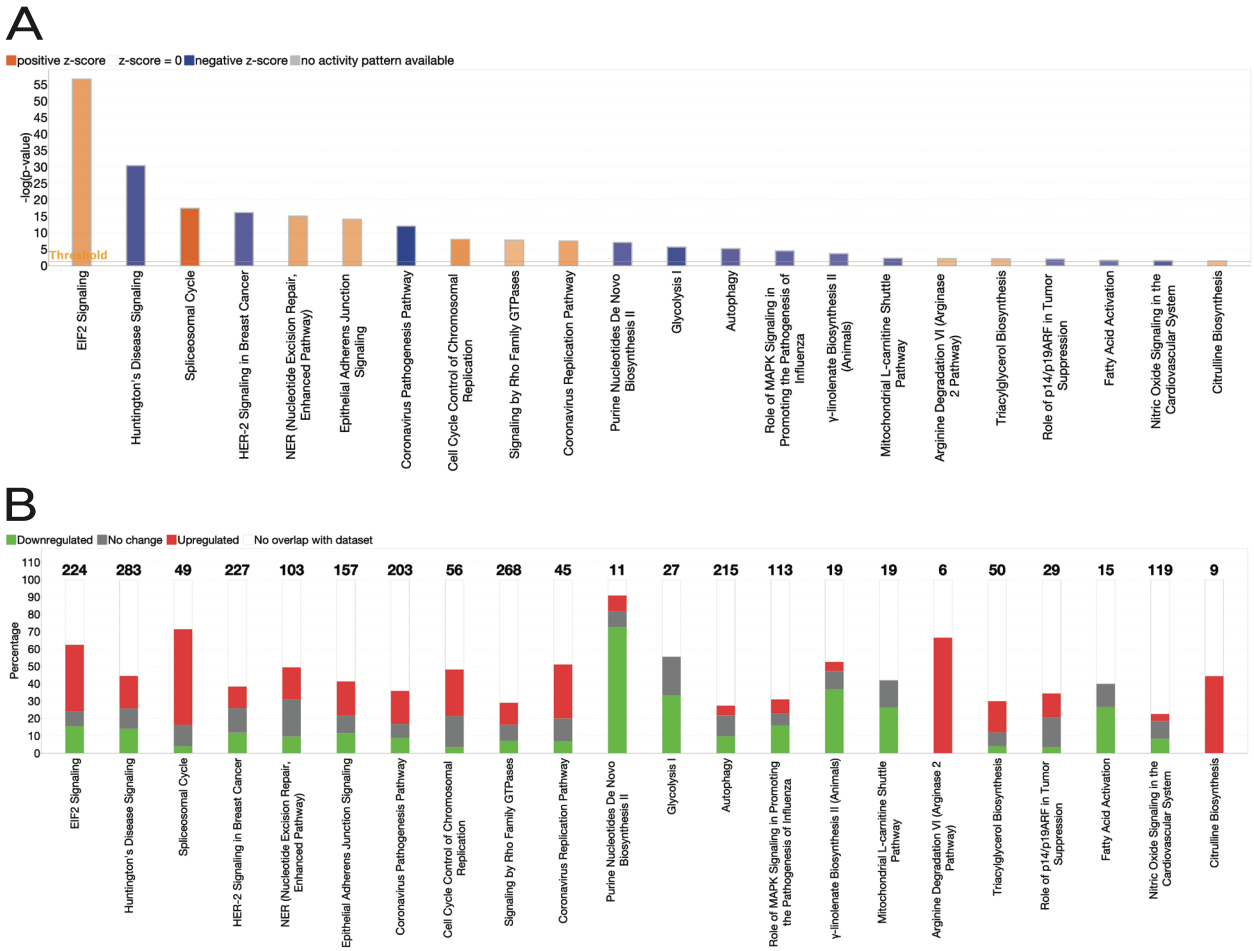


**Figure 20: Knockout of ATG7 results in significant changes to pathway enrichment in lysosomes from sodium arsenite treated cells.** The graphs were created using the IPA software, and demonstrate the change in pathways in *ATG7*$^{-/-}$ LysoIP lysosomes as compared to HEK293 LysoIP lysosomes. **A)** Highlights the pathways with z-scores with an absolute value ≥ 2, and a p-value < 0.05. The y-axis depicts the -log of the p-value, while the colour of the columns indicates the z-score. **B)** Using the same pathways as in A, this graphic depicts the percentage of proteins within each pathway that were up or downregulated. The numbers above each column indicate the total number of proteins within each pathway.

exception from the volcano plot is SOD1, it was not identified at all in the *ATG7*$^{-/-}$ LysoIP samples, and therefore represents a protein that is potentially highly dependent upon ATG7 for its localization to the lysosome.

Finally, all of the proteins within the purine biosynthesis pathway that were identified by LC-MS were plotted for their differences between wild-type and *ATG7*$^{-/-}$ LysoIP cells. IMPDH2 and GART were both significantly reduced in *ATG7*$^{-/-}$ lysosomes. On the other hand PPAT, which was highly enriched when comparing sodium arsenite to HBSS lysosomes, was not significantly impacted by *ATG7*$^{-/-}$.

## 3.4 Validation of altered protein expression across treatment groups and cell types.

### 3.4.1 Selecting proteins for further investigation.

Across all the analyses, the purine biosynthesis pathway kept showing up as being altered by both treatment conditions and macroautophagy. This pathway was enriched in sodium arsenite lysosomes and saw a significant decrease in *ATG7*$^{-/-}$ LysoIP samples. Due to this, two proteins from this pathway were chosen for further analysis: PPAT and IMPDH2. PPAT was the most highly enriched protein from the purine biosynthesis pathway (Figure 15A) and was not actually identified in the HBSS lysosomes (Figure 14B). This, in addition to the fact that it is the rate-limiting protein for the entire purine biosynthesis pathway, makes it an intriguing target to follow up on. IMPDH2 was also highly enriched when comparing sodium arsenite to HBSS treated lysosomes (Figure 14A & B), and was significantly reduced within lysosomes upon *ATG7*$^{-/-}$ (Figure 21). IMPDH2 is also the rate-limiting step to the GMP-producing branch of the synthesis pathway. Furthermore, both proteins were shown to be in the sodium arsenite *treatment specific hits* (Figure 12). This makes both proteins highly important to the synthesis of purines, and strong candidates for regulation by autophagy.

Notably, mammalian IMPDH2 and its yeast homolog were found to co-localize with stress granules along with other purine biosynthesis enzymes[118]. This suggests

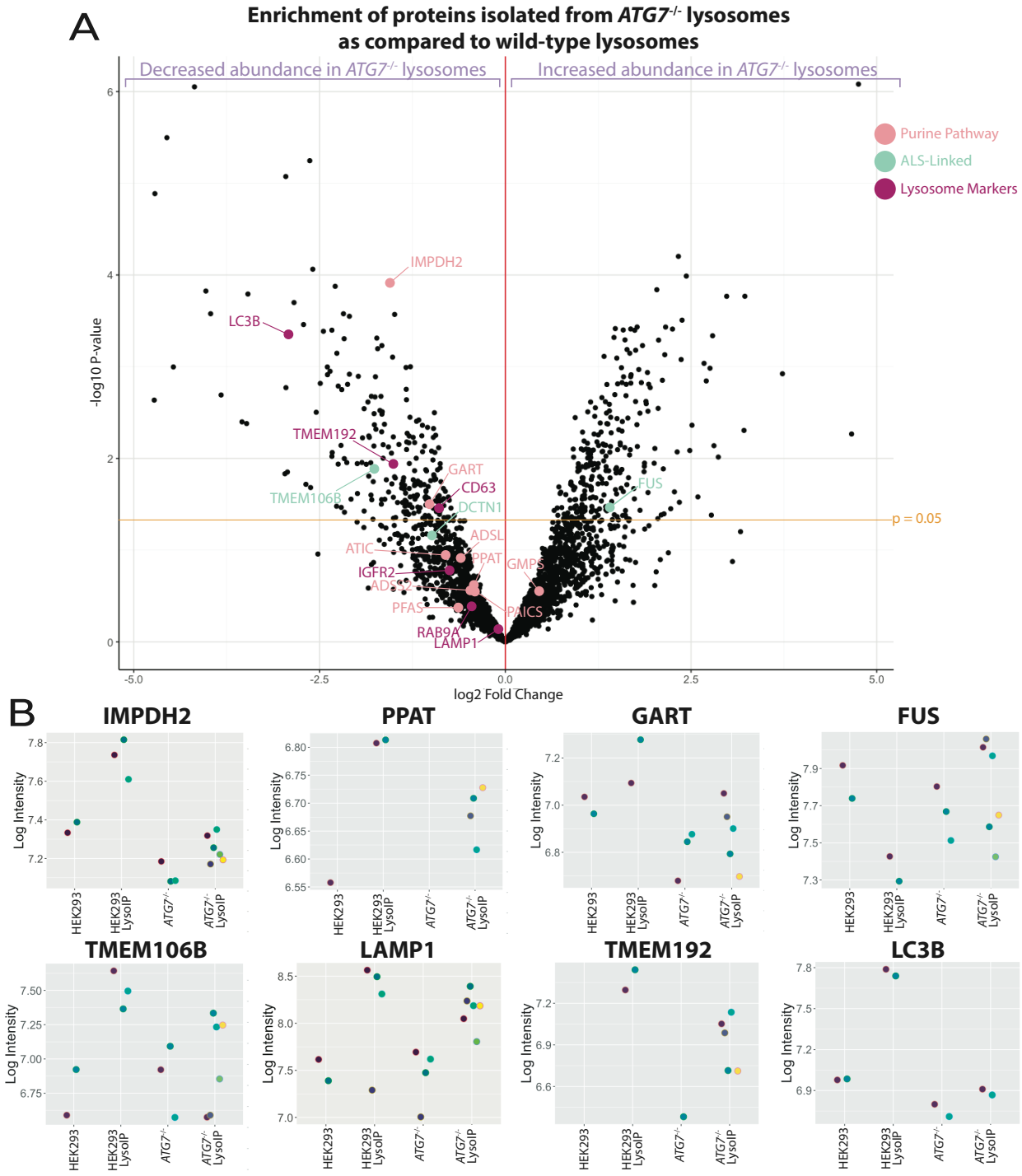


**Figure 21: Differential enrichment of proteins in lysosomes from sodium arsenite treated *ATG7*$^{-/-}$ cells as compared to sodium arsenite treated HEK293 cells.** These graphics were produced using the *proteus* package in R. **A)** Volcano plot depicting the differential enrichment of proteins in *ATG7*$^{-/-}$ lysosomes as compared to wild-type. Highlighted on the graph are select lysosomal markers (magenta), purine synthesis proteins (pink) and select ALS-Linked proteins (turquoise). **B)** The intensity data for eight proteins of interest are represented in these graphs, all of which have been treated with sodium arsenite. n = 3 for sodium arsenite treated HEK293, HEK293 LysoIP & ATG7$^{-/-}$; n = 6 for sodium arsenite treated ATG7$^{-/-}$ LysoIP.

these proteins could be degraded by autophagy as part of stress granules. Proteins that localize to stress granules frequently have low complexity domains (LCDs) or are RNA-binding proteins (RBPs). In an attempt to determine if either protein contained either property, two tools were used: PFAM domains[175] (RBPs) and PlaToLoCo[152] (LCDs). Neither IMPDH2 nor PPAT contained RNA-binding domains or RNA recognition motifs identified by PFAM. PlaToLoCo uses 5 separate LCD-identifying tools simultaneously, and while a few were identified in both proteins neither were wholly convincing when compared to TDP-43 that is known to contain LCDs (Figure 18 & Supplemental Figure 2). The LCDs in IMPDH2 were solely identified by one of the tools, and in PPAT by two of them (Figure 18). Comparatively, TDP-43 LCDs identified by four of the tools (Figure S2).

Another intriguing hit was SOD1 which has showed up consistently throughout experiments as localizing to sodium arsenite lysosomes. It was found to be significantly increased in sodium arsenite as compared to HBSS lysosomes (Table 3 & Figure 14), and it was not identified in *ATG7*$^{-/-}$ lysosomes (Figure 21). This makes it an intriguing protein to follow up on as well.

### 3.4.2 Lysosomal IMPDH2 levels drop in lysosomes from *ATG7*$^{-/-}$ cells, but whole cell levels are not impacted.

Western blots were performed across lysosomal pulldowns for all cell types and all treatment conditions. The IMPDH2 levels were normalized to LAMP1, as it is a lysosomal marker and typical housekeeping proteins are not applicable in this situation. The LAMP1 levels in *ATG7*$^{-/-}$ LysoIP pulldowns do appear to be less intense than in HEK293 LysoIP samples, which may help compensate if the pulldown efficiency was impacted (Figure 22A). Future work should attempt to use the HA signal from TMEM192-3xHA to normalize the IMPDH2 signal to confirm these results. In the sodium arsenite treatment condition, *ATG7*$^{-/-}$ significantly reduced lysosomal levels of IMPDH2 in LysoIP samples (Figure 22A). Furthermore, there was significantly increased IMPDH2

levels in the lysosomes treated with sodium arsenite as compared to the HBSS and bafilomycin $A_1$ treatments. These results indicate that IMPDH2 is at least partially dependent on macroautophagy for its localization to the lysosome, and this trafficking to the lysosome is increased in sodium arsenite conditions.

Despite its significant change in the lysosome, whole cell levels of IMPDH2 are not significantly impacted by sodium arsenite, or loss of ATG7 (Figure 22B). The lack of change due to *ATG7*$^{-/-}$ can likely be explained by the fact that the sodium arsenite treatment condition includes a treatment with bafilomycin, so while IMPDH2 may accumulate in the lysosomes it is not being degraded in either cell type thus maintaining an equal protein signal at the whole cell level. It would be beneficial to repeat these experiments without bafilomycin treatment to assess the response of whole cell IMPDH2 under sodium arsenite treatment in *ATG7*$^{-/-}$ cells.

Due to the fact that there is still IMPDH2 present in *ATG7*$^{-/-}$ lysosomes, albeit at a lower level, one tempting hypothesis is that this is due to an alternative form of autophagy. In a quest to determine whether IMPDH2 may be a target of CMA, the KFERQ finder web tool was used[51]. Nine KFERQ-like motifs were discovered in the IMPDH2 sequence (Figure 24). This certainly makes it feasible that this protein is a target for CMA, which may explain its continued presence in lysosomes. The presence of KFERQ-like motifs in IMPDH2 is comparable to known CMA substrates such as GAPDH (three KFERQ-like motifs) and ALIX (eleven KFERQ-like motifs). Supporting this theory is the demonstration that HSC70 is also identified as a lysosomal protein by MIST score.

### 3.4.3 The whole cell levels of SOD1 and PPAT are not impacted by cell type or treatment.

Due to a lack of sensitivity of both the PPAT and SOD1 antibodies, it was not possible to look at their lysosomal levels across treatment and cell types. However, it was possible to look at whole cell levels which remained essentially unchanged.

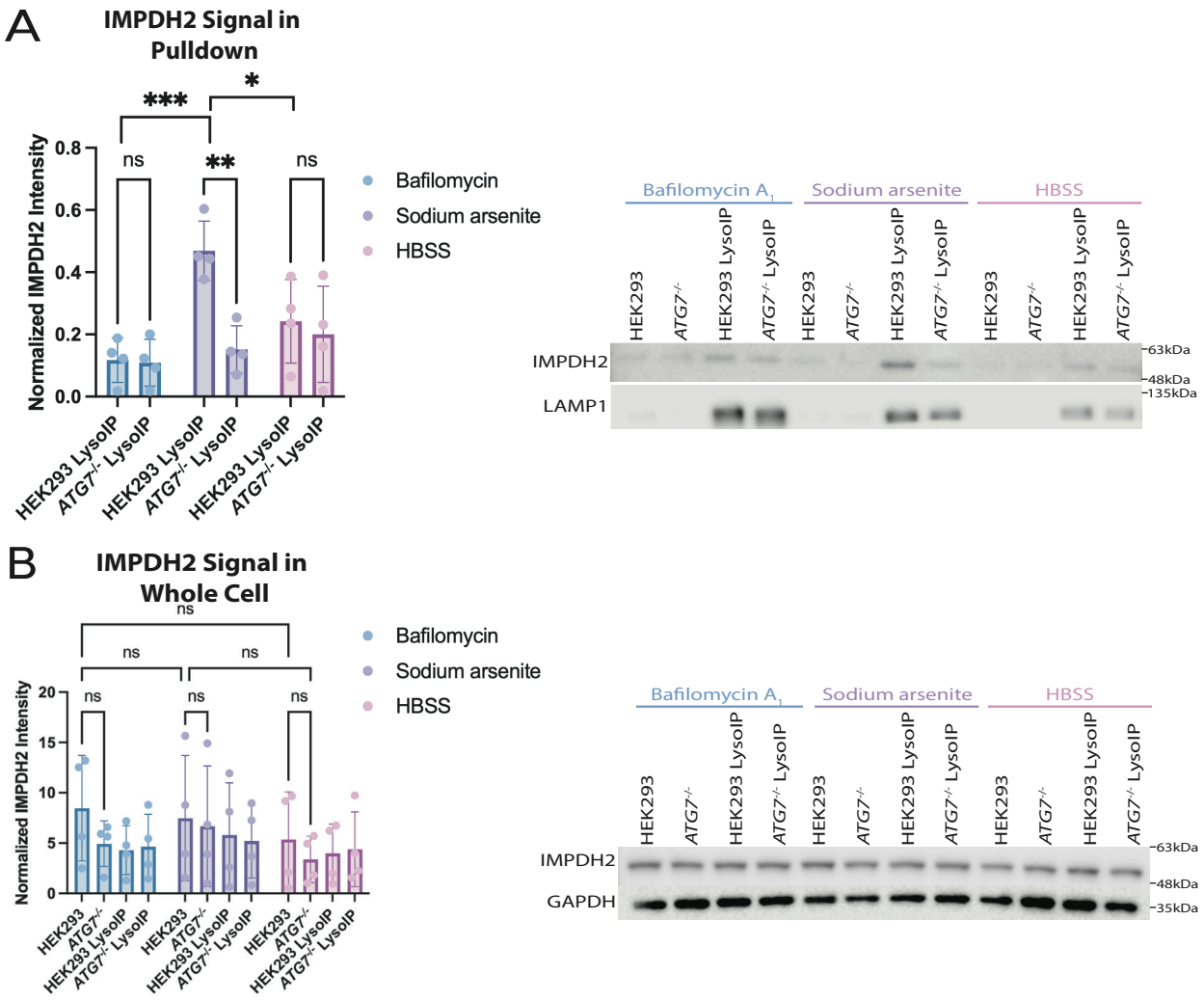


**Figure 22: The degradation of IMPDH2 by autophagy under sodium arsenite conditions is partially dependent on ATG7. A)** A graph quantifying the intensity of IMPDH2 in lysosomes under the different treatment conditions, the mean with SD is plotted here. The IMPDH2 signal within lysosomes is decreased significantly in *ATG7*$^{-/-}$ cells. There is also significantly higher IMPDH2 signal in the sodium arsenite treated LysoIP lysosomes as compared to the bafilomycin or HBSS treated LysoIP groups (n=4). However, there is still remaining IMPDH2 expression in the *ATG7*$^{-/-}$ LysoIP lysosomes. To the right is a representative western blot. The intensity of IMPDH2 was normalized to LAMP1. A two-way ANOVA was performed with Tukey's multiple comparison test. **B)** The IMPDH2 signal is not significantly changed between LysoIP or ATG7$^{-/-}$ LysoIP cells in whole cell fractions (n=4). The IMPDH2 signal was normalized to GAPDH. To the right is a representative western blot. A two-way ANOVA was performed with Tukey's multiple comparison test. $p < 0.05$ (*), $p < 0.01$ (**), $p < 0.001$ (***).

It was not possible to perform statistical analysis on the SOD1 levels due to a lack of replicates. PPAT remained statistically unchanged. Again, the lack of accumulation in *ATG7*$^{-/-}$ samples is likely due to the bafilomycin $A_1$ treatment that was necessary for previous experiments, future work will replicate these western blots without the bafilomycin $A_1$ treatment. However, as with IMPDH2, we did wonder whether

alternative forms of transport may be bringing these proteins to the lysosome. The sequences of these proteins were also put into the KFERQ motif finder. PPAT contained three KFERQ-like motifs, and SOD1 did not contain any motifs (Figure 24).

# Chapter 4: Discussion

Fundamental research demonstrates the importance of curiosity and determination time and time again. In fact, many medical treatments find their origins in basic science rather than in disease-centered research[176]. Indeed, arguably one of the most influential discoveries in recent years came about due to a curiosity about the bacterial viral response, leading of course to the powerful tool CRISPR/Cas9[177]. This is not to discount the value of targeted research on specific diseases, but rather to highlight the inherent value also present in aiming to find answers to questions just because they are of interest. At its core, that is the basis of this project. Although links can be drawn to ALS, the base desire was curiosity as to how proteins targeted to the lysosome change depending upon environmental cues.

The lysosome was originally discovered in 1955, a discovery that was later awarded a Nobel Prize, by Dr. Christian De Duve who named the degradation process autophagy, "self-eating"[178]. Much later, in 1992 Dr. Yoshinori Ohsumi published ground-breaking results, also earning him a Nobel Prize, further elucidating the process of autophagy and sparking interest in the process[179]. In the years since, the field has rapidly expanded, making discoveries about the mechanisms behind autophagy, defining LSDs, and highlighting it as a player in a great many diseases. This thesis attempts to expand this vast field of knowledge, by analyzing changes to the lysosomal proteome under different conditions. Previous work has demonstrated that while a key set of lysosomal proteins may remain the same, there are proteins differentially enriched within lysosomes depending on the cellular condition[6].

This thesis analyzed how the lysosomal proteome changes between cells undergoing nutrient starvation, and cells recovering from oxidative stress induced by sodium arsenite. Nutrient starvation was used as a condition due to its ubiquity in the autophagy field, and its extensive documentation as an autophagy inducer. Nutrient starvation was induced through treatment with HBSS. Treatment with sodium

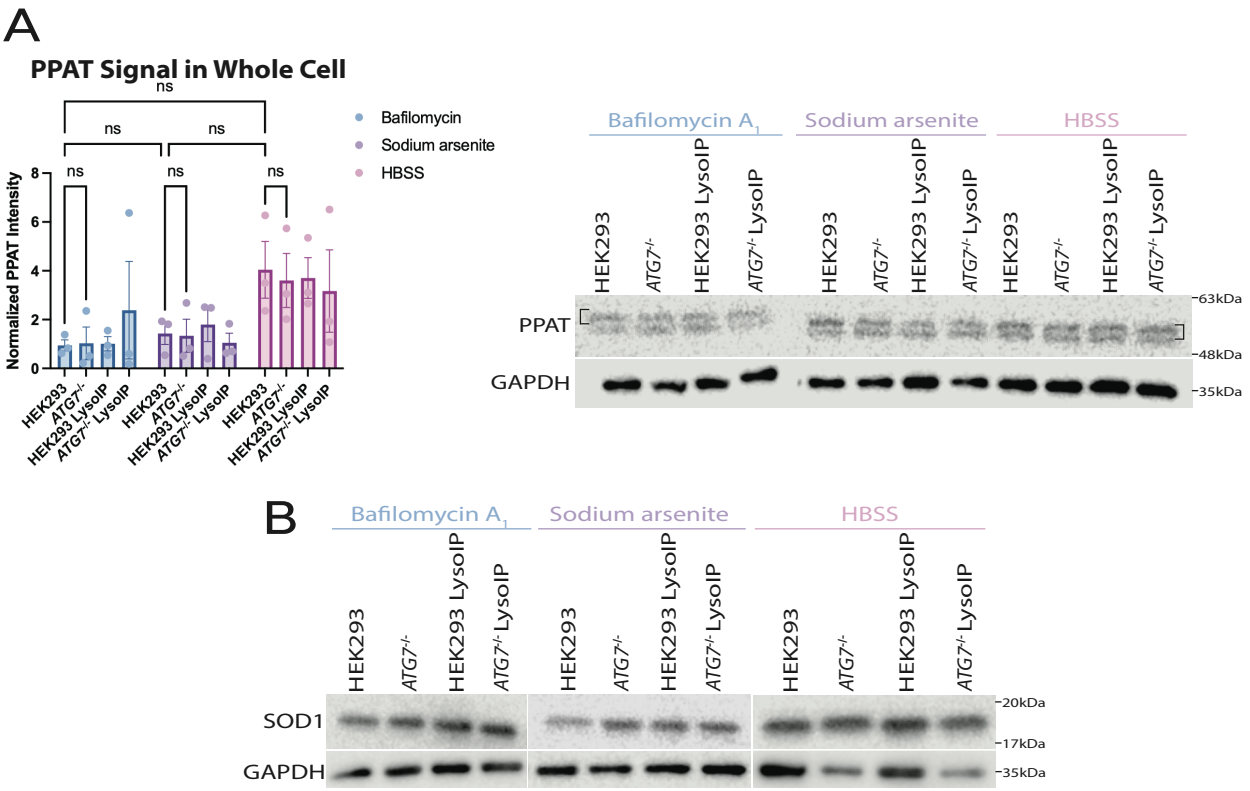


**Figure 23: Whole cell expression of PPAT and SOD1 are not impacted by *ATG7*$^{-/-}$. A)** The expression of PPAT is not significantly impacted by *ATG7*$^{-/-}$ in whole cell fractions (n=3). The PPAT signals were normalized to GAPDH. A one-way ANOVA was performed with Tukey's multiple comparison test, the mean with SD is plotted. To the right is a representative western blot, the top band is PPAT and is what was quantified. **B)** There is no obvious difference in SOD1 expression across the whole cell fractions (n=1). The GAPDH probing was performed on a separate membrane from SOD1.

arsenite was utilized to develop stress granules as a simple ALS model, sodium arsenite was then removed to induce granulophagy[113,180]. Bafilomycin $A_1$ was used either during (starvation) or after (sodium arsenite) to prevent lysosomal acidification and degradation to accumulate targeted substrates within the lysosome. The use of bafilomycin $A_1$ ensured that sufficient protein was collected from the lysosomes, as pulldown without this treatment was much less effective (Figure 3B).

From these pulldowns, LC-MS was performed, followed by several bioinformatic analyses to interpret the LC-MS data. One of the primary methods used was a scoring system, MIST, which assigns a score to each identified protein based on its abundance, reproducibility, and specificity[146]. In order to identify lysosomal proteins within each condition wild-type HEK293 pulldowns were compared to the

Acetylation and phosphorylation activated

Asparagine substitution

Acetylation activated

Phosphorylation activated

**> IMPDH2**

MADYLISGGTSYVPDDGLTAQQLFNCGDGLTYNDFLILPGYIDFTADQVDLTSALTKKITLKTPLVSSPMDTVTE

AGMAIAMALTGGIGFIHHNCTPEFQANEVRKVKKYEQGFITDPVVLSPKDRVRDVFEAKARHGFCGIPITDTGR

MGSRLVGIISSRDIDFLKEEEHDCFLEEIMTKREDLVVAPAGITLKEANEILQRSKKGKLPIVNEDDELVAIIART

KN

KVKKY

KITLK

DLK

RDYPLASKDAKKQLLCGAAIGTHEDDKYRLDLLAQAGVDVVVLDSSQGNSIFQINMIKYIKDKYPNLQVIGG

NVVTAAQAKNLIDAGVDALRVGMGSGSICITQEVLACGRPQATAVYKVSEYARRFGVPVIADGGIQNVGHIAKA

LALGASTVMMGSLLAATTEAPGEYFFSDGIRLKKYRGMGSLDAMDKHLSSQNRYFSEADKIKVAQGVSGAVQ

KFEKR

DKGSIHKFVPYLIAGIQHSCQDIGAKSLTQVRAMMYSGELKFEKRTSSAQVEGGVHSLHSYEKRLF

**> PPAT**

MELEELGIREECGVFGCIASGEWPTQLDVPHVITLGLVGLQHRGQESAGIVTSDGSSVPTFKSHKGMGLVNHVF

TEDNLKKLYVSNLGIGHTRYATTGKCELENCQPFVVETLHGKIAVAHNGELVNAARLRKKLLRHGIGLSTSSDSEM

ITQLLAYTPPQEQDDTPDWVARIKNLMKEAPTAYSLLIMHRDVIYAVRDPYGNRPLCIGRLIPVSDINDKEKKTSE

TEGWVVSSESCSFLSIGARYYREVLPGEIVEISRHNVQTLDIISRSEGNPVAFCIFEYVYFARPDSMFEDQMVYTV

RYRCGQQLAIEAPVDADLVSTVPESATPAALAYAGKCGLPYVEVLCKNRYVGRTFIQPNMRLRQLGVAKKFGVL

SDNFKGKRIVLVDDSIVRGNTISPIIKLLKESGAKEVHIRVASPPIKYPCFMGINIPTKEELIANKPEFDHLAEYLGAN

SVVYLSVEGLVSSVQEGIKFKKQKEKKHDIMIQENGNGLECFEKSGHCTACLTGKYPVELEW

**> SOD1**

MATKAVCVLKGDGPVQGIINFEQKESNGPVKVWGSIKGLTEGLHGFHVHEFGDNTAGCTSAGPHFNPLSRKH

GGPKDEERHVGDLGNVTADKDGVADVSIEDSVISLSGDHCIIGRTLVVHEKADDLGKGGNEESTKTGNAGSRLA

CGVIGIAQ

**Figure 24: There are KFERQ-like motifs present in IMPDH2 and PPAT, but not in SOD1.** Using the web-based KFERQ finder from Kirchner et al. 2019 it was possible to identify numerous KFERQ-like motifs in both PPAT and IMPDH2, and none in SOD1. These KFERQ-like motifs represent different variants on the canonical motif, however are still able to be targeted by the HSC-70 complex. These different kinds of motifs are colour-coded in the graphic according to the legend above. Acetylation and phosphorylation activated motifs are considered standard motifs, whereas asparagine substitution and acetylation + phosphorylation activation are considered advanced motifs as they require more modifications in order to be targeted. When multiple motifs exist at a single point along the sequence, the second motif is written underneath.

HEK293 LysoIP pulldowns, the proteins with scores over 0.6 in the LysoIP group were termed '*lysosomal hits*'. The caveat to this analysis is that LysoIP samples could be contaminated with other organelles if TMEM192 localizes to other cellular organelles like endosomes, or other sources of background binding. For simplicity's sake, and because the data supports a major enrichment of lysosomes and lack of other organelles (Figure 3B, Figure 10B & Figure 19), we will call proteins in LysoIP pulldowns lysosomal proteins.

The final results demonstrate that cells treated with HBSS as compared to sodium arsenite contain similar but distinct lysosomal proteomes. The sodium arsenite condition resulted in a lysosomal fraction highly enriched in proteins from the purine biosynthesis pathway, an enrichment that was in part dependent on ATG7. This indicates that the degradation of these proteins is reliant on macroautophagy. Three proteins enriched in lysosomes derived from cells treated with sodium arsenite, IMPDH2, PPAT and SOD1, were further analyzed. The lysosomal enrichment of IMPDH2 was at least partially dependent on ATG7, although some IMPDH2 was still identified in the lysosomes of *ATG7*$^{-/-}$ cells. This indicates that while IMPDH2 is likely degraded by macroautophagy, other autophagic processes such as CMA may also be at play. Whole cell levels of IMPDH2, PPAT and SOD1 did not differ in *ATG7*$^{-/-}$ cells which is likely due to all conditions including bafilomycin $A_1$ treatment preventing lysosomal cargo from being degraded. Further investigation using untreated cells will need to be performed to confirm this.

## 4.1 LysoIP is an efficient and specific isolation protocol to produce lysosome enriched samples

The pulldowns performed with LysoIP cells were highly enriched in lysosomal proteins across all conditions and lacked significant levels of markers for common contaminants often found in lysosomal enriched fractions (Figure 3B)[102]. Additionally, we were successful in improving the pulldown efficiency of the LysoIP protocol without

compromising the specificity of the process (Figure 3C). This was accomplished by increasing the length of time samples were isolated with the anti-HA magnetic beads, and increasing the length of time lysosomes were lysed using resuspension buffer[6,141]. These features were retained across both the HEK293 LysoIP and *ATG7*$^{-/-}$ LysoIP cells (Figure 8).

The specificity of the process was further demonstrated following LC-MS analysis wherein various lysosomal markers were individually enriched (Figure 9), and gene ontology analysis of MIST-identified *lysosomal hits* were highly enriched in lysosome-related identifiers (Figure 10B, Figure 19). These bolster the assumption that LysoIP pulldowns are highly enriched for lysosomes.

**4.2 Modified cells retain similar responses to stress as wild-type cells**

One concern for the use of the LysoIP cells is that the genetic modification may cause unknown effects, in this case the most significant concern being any changes to autophagy or the stress response.

Some of these concerns draw from necessities of the technique, because of the expression of TMEM192-3xHA there are higher levels of TMEM192 overall in the cell. It is unclear how this may impact cellular processes. Additionally, there is evidence that tags can influence the stability, function and level of the proteins they are attached to. A study in yeast actually demonstrated this through a well-documented 3xHA tag that was caused due to the spacer sequence between the protein and the tag[181]. This same spacer sequence is not present in the construct used for this study, however a similar situation could easily occur. This could at least in part be addressed by measuring levels of TMEM192 in the cell in later experiments.

Any significant changes induced to the lysosomes would of course be of concern for this project, and as TMEM192 localizes to the membrane it raises questions as to how other lysosomal proteins and the lysosome itself may react. One measurement we assessed was the level of LAMP1 in each cell type under each

condition, which did not change significantly across cell types in whole cell samples (Figure 5). While this is not a direct measurement of lysosome number, it does assuage concerns that the modifications may have impacted lysosomes to the extent that standard markers of lysosomes like LAMP1 were altered. In the original LysoIP paper, LAMP2 was used to estimate the percentage of lysosomes successfully purified[104]. This percentage was equal to other lysosomal measurements, including Cathepsin D and LysoTracker Red. This provides some validation that use of lysosomal membrane proteins can be an accurate measurement of lysosome numbers. However, future experiments could focus on further verifying that autophagy, including whole cell lysosome number, is not significantly impacted in LysoIP cells. In addition to the LysoIP construct itself, standard parts of the protocol such as media changes, presence of bafilomycin $A_1$, and removal from the incubator may have impacted autophagy. It may be of interest to perform experiments to assess the impact of these conditions on autophagy and the lysosomal proteome to understand how they may have impacted the results. This could be executed by measuring autophagic flux, and other lysosomal markers such as those mentioned above.

Furthermore, immunofluorescence demonstrated not only that HA is absent from HEK293 cells (Figure 3A & Figure 6), but also that stress granule formation is similar between wild-type HEK293 cells and LysoIP cells (Figure 6 & Figure 7). This was demonstrated through visualization of G3BP, a stress granule marker, which formed puncta only in the sodium arsenite condition[182]. While this is not a comprehensive assessment of stress granule formation, it is one positive indicator that the response is not significantly impaired. Further studies should quantify the number of stress granules between cell lines rather than relying on visual estimation.

### 4.3 Lysosomal components provide a snapshot into the cellular response to stress

We successfully demonstrated that while starvation and sodium arsenite treated cells contain lysosomes which retain a core group of proteins, many other

proteins isolated within lysosomes are unique to a single stressor (Figure 9 & Figure 10A). The shared proteins are primarily lysosomal (Figure 10B), and include well-documented lysosomal markers such as LAMP1, LAMP2 and CD63 (Figure 9). These three markers are also present at similar intensities across all treatment conditions (Figure 9C).

Comparatively, proteins unique to each condition display vastly different cellular component enrichments (Figure 10C & D) indicating that autophagic targets may differ between sodium arsenite and starvation treated cells.

This aligns with what was previously seen in a study comparing Torin1 autophagy activation to nutrient deprivation autophagy activation, wherein a core set of proteins remained consistent but with unmistakeable differences[6].

#### 4.3.1 Proteins enriched in the lysosome differ between starvation and sodium arsenite treatment conditions

Analyzing MIST-identified proteins unique to either sodium arsenite or HBSS treated cells displays a stark difference in cellular component enrichments within lysosomes. From proteins uniquely enriched in HBSS *lysosomal hits*, WebGestalt identified a significant presence of mitochondrial proteins (Figure 10D). This finding is in line with previous evidence that mitophagy is induced by starvation[183]. Comparatively, among *lysosomal hits* uniquely enriched in cells exposed to sodium arsenite WebGestalt identified proteins involved in secretory granules, ficolin-1-rich granules and the ER (Figure 10C).

Sodium arsenite has been documented to cause ER stress, thus explaining why ER-related proteins may be overly represented in the *lysosomal hits*[158,184]. Autophagy of the ER, or ER-phagy is frequently induced during and post-ER-stress. Macro-ERphagy is facilitated by several specific receptors, which are highly represented in the sodium arsenite *lysosomal hits.* There are six known mammalian receptors, of which four were found in the data and three of which had a MIST score over 0.6 (RTN3[185]: 0.65,

SEC62[186]: 0.87, TEX264[187]: 0.88, ATL3[188]: 0.59) (reviewed in Yang et al. 2021[189]). The presence of these receptors supports the idea that the ER was undergoing selective macroautophagy. Interestingly, SEC62 is involved in ER-phagy during recovery from stress which makes sense as sodium arsenite LysoIP samples were collected during a recovery period[186].

The presence of secretory and ficolin-1-rich granules is interesting. It is important to note that ficolin-1-rich granules are a subset of secretory granules[190]. Therefore, it is likely that they are both present not as two distinct enrichments, but rather due to the fact that they involve many of the same proteins. Ficolin-1 was additionally not detected by LC-MS, suggesting that a secretory granule other than ficolin-1-rich granules are truly enriched. However, HEK293 cells are not documented to produce secretory granules, which are typically produced in neuroendocrine, endocrine or exocrine cells[191,192]. One potential explanation could be due to the high number of proteasome subunit proteins, in the LysoIP samples and the secretory granule GO term. These proteasome proteins within our sample accounted for 18% of the whole 'secretory granule lumen' GO term. This may have led to the false identification of secretory and ficolin-1-rich granules. The proteosome complex itself was also significantly enriched in these LysoIP hits from sodium arsenite treated cells; while it did not reach the top 10 (which is what is mapped in Figure 10C) it has an FDR of 1.0073e-7 and a p-value of 5.2292e-9. Despite being a protein degradation system itself, the proteasome is also an autophagy substrate. This process is frequently termed proteaphagy[193]. Notably, while autophagy inducing conditions can have varying impacts on the proteasome itself and proteaphagy, many of them induce proteaphagy[193].

#### 4.3.2 Treatment conditions alter lysosomal protein contents

A core set of LysoIP proteins are unchanged by different stresses and likely represent constitutive lysosomal proteins. Another set of LysoIP proteins changed

depending on whether cells were exposed to starvation or sodium arsenite. One way to differentiate these groups is by using the MIST scoring system to look for hits unique to each cell treatment, *treatment specific hits*. These unique proteins were then analyzed through networks generated by Cytoscape, which demonstrated their interactions between themselves as well as cellular localization and GO term enrichment. A unique network was generated from the unique proteins identified for both sodium arsenite and starvation (Figure 12A & Figure 13A). Subsequently, a Markov clustering algorithm was performed, through ClusterMaker2, on each individual network– allowing the visualization of sub-networks (clusters) representing strong protein-protein interactions and proteins of similar functions (Figure 12B & C and Figure 13B & C)[149]. This was utilized here to identify proteins that are densely interconnected.

#### *4.3.2.1 Protein interaction networks display changes in cellular component enrichment*

The COMPARTMENT scoring system was used to identify proteins that localized to various cellular components. One of the prominent differences is the abundance of nuclear proteins in LysoIP samples from sodium arsenite treated cells (14.9% of identified proteins), whereas no nuclear proteins were identified in LysoIP samples from starved cells by the COMPARTMENT scoring system (Figure 12A & Figure 13A). This is of particular interest as nucleocytoplasmic transport is known to be disrupted in both ALS and stress granule inducing conditions[162,194–196]. Notably, in sodium arsenite treated cells many proteins exit the nucleus and accumulate in the cytoplasm in stress granules. Mutant TDP-43 is shown to mislocalize to the cytoplasm from the nucleus, in fact there is a mouse model which replicates the pathology of ALS by expressing TDP-43 with a defective nuclear localization signal[197]. Upon suppressing the expression of this mutant TDP-43, it is rapidly cleared from the cytoplasm which leads to functional recovery. The authors hypothesize that this process occurs through autophagy.

A few well-documented proteins involved in nucleocytoplasmic transport include Importin-α, Importin-β (karyopherin-β1) and Transportin-1 (karyopherin-β2). Classically, Importin-β and Importin-α proteins work in conjunction, with Importin-α binding cargo containing an appropriate nuclear localization signal and Importin-β facilitating the transport through the nuclear pore[198]. Transportin-1 on the other hand binds its cargo and facilitates translocation alone[199]. Notably, Importin-α subunit 2 and Importin-β had MIST scores over 0.6 in the lysosomal analysis from sodium arsenite-treated cells indicating they were present in the lysosomes. Other Importin-α subunits and Transportin-1 were present in the lysosomal samples from sodium arsenite treated cells but did not attain the MIST score cut off.

This nucleocytoplasmic transport system has been documented to impact two common ALS-linked proteins, FUS and TDP-43[196,200]. TDP-43 has a MIST score over 0.6 in sodium arsenite lysosomal fractions, and FUS is present but did not have a score above the threshold. Mutant FUS has been shown to mislocalize to the cytoplasm[196]. Both Transportin-1 and Importin-β have been shown to interact with a juvenile ALS FUS mutation and this interaction prevents the liquid LLPS of mutant FUS. This suggests that in the presence of these nucleocytoplasmic transporters stress granule formation may be limited. The nucleocytoplasmic transport of TDP-43 on the other hand is mediated by Importin-β and Importin-α[200]. TDP-43 was shown to bind multiple Importin-α subunits, and its localization to the nucleus was dependent on Importin-β. TDP-43 localization to the nucleus is theorized to be based on active import and passive export, therefore the functionality of these nucleocytoplasmic transporters is critical[201]. Unfortunately, like FUS and TDP-43, Transportin-1, Importin-β and Importin-α are all recruited to stress granules, thus sequestering them[162,202]. The presence of these nucleocytoplasmic transport factors in addition to TDP-43 and FUS supports the presumption that autophagy is degrading stress granules after the removal of the stressor.

Comparatively, the starvation specific hits were enriched in proteins localized to the mitochondrial compartment according to the COMPARTMENT scoring system which aligns with what was previously observed through WebGestalt (Figure 13).

#### *4.3.2.2 Markov clustering reveals differential enrichment of GO terms*

Clusters resulting from Markov clustering algorithms of the *treatment specific hits* of starvation LysoIP proteins demonstrated substantial enrichment in mitochondrial related terms. It is possible to be confident in the assertion that proteins associated with the mitochondria are enriched in the lysosomes of starved cells due to this finding being replicated through various analysis pathways, including GO term enrichment and COMPARTMENT scoring.

Markov clustering was also performed on the *treatment specific hits* of the sodium arsenite condition, and resulted in further insights (Figure 12B & C). When observing the sodium arsenite clusters, it is tempting to hypothesize that they demonstrate the activation and subsequent degradation by autophagy of the KEAP1-NRF2 pathway, a critical pathway in the cellular response to cytotoxic conditions[203]. Under homeostatic conditions NRF2, a transcription factor, is negatively regulated by KEAP1, which it escapes when exposed to certain cytotoxic conditions such as oxidative stress induced by arsenic[203]. NRF2 then induces the transcription of cytoprotective proteins.

NRF2 was not detected by LC-MS, however KEAP1 and some downstream proteins were identified as proteins uniquely localized to the lysosomal fraction collected from sodium arsenite treated cells. However, this is not unusual as NRF2 has been shown to be degraded by the proteasome, and KEAP1 has been shown to be a target of selective autophagy through p62 interaction[204,205]. In practice, NRF2 can induce the expression of glycolysis enzymes (GPI, ALDOA, ENO1 identified as unique sodium arsenite LysoIP proteins)[206], antioxidant related proteins (TXNRD1[207], PRDX1[208] identified as unique sodium arsenite LysoIP proteins) and carbon metabolism

proteins[209]. These three processes, glycolysis, antioxidant activity and carbon metabolism were all identified by GO term analysis as being enriched within the a cluster of unique sodium arsenite LysoIP proteins (Figure 12B).

PRDX1, a unique sodium arsenite lysosomal protein and a protein induced by NRF2 action, has actually been identified as a core stress granule protein in neural progenitor cells[210]. Additionally, NRF2 is known to induce purine biosynthesis and directly regulates PPAT levels, however it does not impact pyrimidine synthesis (Figure 12C)[211]. As the lysosomes from sodium arsenite treated cells were collected after a period of recovery, it makes sense that proteins that were upregulated in a stress response are beginning to be degraded. Interestingly, NRF2 activity is itself linked to ALS; decreased activity is associated with the disease and is considered by some to be a potential therapeutic target[212]. Genetic mutations of KEAP1 and NRF2 have additionally been found to modify sporadic ALS risk and age of onset[213]. Edaravone, an ALS medication that attenuates disease, is a free radical scavenger that has also been shown to increase the expression of NRF2[214]. These results support the idea that these proteins were expressed due to oxidative stress, and then degraded by autophagy during the recovery period. Additionally, that the enrichment of these proteins is unique to sodium arsenite treated lysosomes indicates that this response is unique to this condition.

Overall, these results suggest that the lysosomal proteome is, at least in part, a representation of the cell's response to individual stresses. From these results we can hypothesize what may be happening, or what may have happened, in the whole cell during the stressed condition. Autophagy is functioning as we would expect in these cells by degrading damaged cellular components, responsive proteins that are no longer needed after the stressor has been removed, and in the case of sodium arsenite, stress granule associated proteins. It is particularly interesting how dominant NRF2 related proteins and processes are in the sodium arsenite condition.

## 4.4 The purine biosynthesis pathway is solely enriched in sodium-arsenite treated lysosomes.

The significant enrichment of purine biosynthesis pathway proteins in the lysosomes from sodium arsenite treated cells quickly drew interest due to its reproducibility across samples and analyses. Enrichment of this pathway was identified by looking at canonical pathway enrichment by IPA (Figure 11A), through GO term enrichment in sodium arenite specific clusters (Figure 13C), and in the analysis of LC-MS intensity values comparing the sodium arsenite to the starvation condition (Figure 14). The variety of methods, techniques and algorithms utilized to generate this conclusion adds strength to the argument that this set of proteins is highly enriched in sodium arsenite lysosomes. Furthermore, when looking at each protein involved in the purine biosynthesis pathway, every one presents with increased levels in sodium arsenite lysosomes as compared to in bafilomycin $A_1$ lysosomes (Figure 11B & Figure 15A). Comparatively, in the starvation condition most of the proteins are present at lower levels in the lysosome than in the bafilomycin condition (Figure 11B).

Additionally, the enrichment of the purine biosynthesis pathway proteins in lysosomes after sodium arsenite treatment is intriguing. Mechanistically, this enrichment makes sense. Under oxidative stress we expect the activity of NRF2 to increase, and therefore induce the purine biosynthesis pathway, potentially by mediating the transcription of rate-limiting protein, PPAT[211]. The absence of purine nucleotides also induces macroautophagy through indirect inhibition of mTORC1, and therefore the proteins involved in their synthesis being autophagy substrates is interesting. It may indicate that after production of sufficient purines to re-activate mTORC1 the synthesis proteins are subsequently degraded to maintain homeostasis.

### 4.4.1 Purine synthesis is linked to ALS and stress granule formation

While no pathways for ALS disease progression or stress granule formation were determined to be significantly enriched through the IPA software, there are

existing links between these categories and purine biosynthesis pathway molecules (Figure 16 & Figure 17).

#### *4.4.1.1 Stress granule formation*

In yeast a portion of the purine synthesis enzymes localized to stress granules. These enzymes are homologs for the human ATIC and IMPDH1/2 proteins[118]. Mammalian IMPDH2 has also been identified as a stress granule component by LC-MS[106]. While there is not strong evidence of LCDs in IMPDH2 (Figure 18A), IMPDH2 has been shown to bind to nucleic acids, including RNA, a feature often found in stress granule proteins[215]. However, IMPDH2 does not contain an RNA-binding domain or recognition motif identified by PFAM. Further supporting evidence that IMPDH2 may be recruited to stress granules is that it binds STAU1, a reliable stress granule protein that can help regulate their formation (Figure 16)[216–218]. Other purine synthetic enzymes (PPAT,PFAS, GART & ADSL) also bind to STAU1, potentially linking them to stress granule formation as well[218]. Additionally, PPAT also presents some possible LCDs, although it is not definitive (Figure 18B).

These findings make it tempting to suggest that this is an indication of stress granule degradation and further implication of IMPDH1/2 localization to mammalian stress granules. However, it is unclear from our data whether entire stress granules are degraded by autophagy because classical stress granule markers including G3BP1/2, TIA1 and PABP were not identified as lysosomal proteins in any treatment condition, including sodium arsenite. One potential explanation is that whole stress granules are not degraded by autophagy. In fact live-cell imaging does indicate that stress granules are degraded in a piecemeal fashion that can take well over an hour[138]. Therefore, while autophagy is well-documented to degrade stress granules, this may occur in pieces rather than all at once. Additionally, literature indicates that stress granules are not one homogenous structure, but rather contain several dense, stable cores surrounded by a dynamic shell[106]. Both PABP and G3BP were found to localize

within stable cores, that can remain intact for over an hour in solution[106]. Therefore, we theorize that the reason why classic stress granule markers were not identified within our data as lysosomal was due to the stability of these cores. In the future we could address this by lengthening the recovery period and repeating the experiment to ensure that the entirety of the stress granules are degraded.

Another link to stress granules from the purine biosynthesis pathway occurs through TNFa (Figure 16). TNFa has been shown to enhance the formation of stress granules[219]. Interestingly, two purine biosynthesis enzymes (AICAR[220], IMPDH2[221]) and two purine biosynthesis byproducts (AMP[222], ADP[223]) all decrease the expression of TNFa. In theory, these molecules could limit stress granule formation through action against TNFa.

Finally, L-glutamic acid (glutamate/L-glutamate) provides another link from the purine biosynthesis pathway to both stress granule formation and ALS (Figure 16 & Figure 17). Glutamate is a byproduct of the purine biosynthesis pathway, so when the pathway is activated glutamate is produced. Treating primary cortical neurons with glutamate resulted in increased translocation of TDP-43 from the nucleus to the cytoplasm[224]. This mislocalization is as previously stated, linked to ALS and stress granule formation[195]. Should oxidative stress activate the purine biosynthesis pathway, it is possible that the production of glutamate may contribute to increasing levels of cytoplasmic TDP-43. However, excess glutamate in ALS patients is typically attributed to altered expression of EAAT2, a glutamate transporter[172]. Additionally, glutamate is involved in so many cellular processes that association between glutamate, ALS and the purine biosynthesis pathway would require further study before coming to any conclusions.

#### *4.4.1.2 Amyotrophic lateral sclerosis*

Glutamate can additionally be directly linked to ALS, as a prevalent theory behind the disease is that excess glutamate causes excitotoxicity resulting in cell death

(Figure 17)[173]. Riluzole, one of the few drugs available to ALS patients slows disease progression and elongates lifespan by a few months. This drug is proposed to function by attenuating glutamatergic excitotoxicity[173,225].

Furthermore, some key purine synthesis pathway proteins have been found to bind to ALS-linked proteins, such as IMPDH2 binding SQSTM1[226], UBQLN2[227] and SOD1[228], and PPAT binding ATXN1[229] (Figure 17).

There is literature discussion of a purinergic effect in ALS, however it primarily focuses on the adenylate arm of the pathway. This is likely due to ATP's fundamental role as an energy source, as well as it and adenosine's role as signalling molecules[230]. Notably, the purine metabolism pathway was significantly enriched in Parkinson's disease, Alzheimer's disease and ALS when analyzing metabolite markers[231]. For example, in SOD1 mutants increased levels of extracellular ATP and increased levels of purinergic receptors have been found in microglia, suggesting that cells became oversensitive to these signals[232].

One study looked at the effectiveness of a class of drugs targeting purine catabolism in a mutant SOD1 ALS model, by inhibiting this catabolism they were able to significantly extend the life of the mice and maintain better histopathological and physiological makeups[233]. The authors theorize that this may be due to increased efficiency of the purine salvage pathway, resulting in increased ATP and GTP. The sum of these results, and the literature, indicates that purine metabolism may have a role in ALS.

Relatedly, alterations in homeostatic GTPase and guanine nucleotide exchange factor function has been implicated in ALS. ALS2, for example, is caused by mutations to the Alsin2 protein that functions as a guanine nucleotide exchange factor[234]. Additionally, dysregulation of Rac and Rho, two subfamilies of Rho GTPases cause motor neuron death and inactivation of Rac is found mutant SOD1 mice[235]. Therefore, the role of guanylate purines may be of particular interest[234–236]. Notably, Rho family

signalling and RhoA signalling were found to be significantly enriched in sodium arsenite lysosomes according to IPA (Figure 11B)

#### 4.4.2 The enrichment of the purine biosynthesis pathway is dependent *on* ATG7

Absence of ATG7 results in an intense decrease in the enrichment of the purine biosynthesis pathway (Figure 15B, Figure 20), with 8 out of 11 proteins less enriched than in the HEK293 LysoIP lysosomes. This indicates that the majority of these proteins are dependent on macroautophagy for their localization to the lysosome.

The impact of ATG7 is primarily visible when looking at the pathway as a whole, as most of the individual proteins were not significantly impacted (Figure 21). Nearly all of the proteins trended towards being reduced in lysosomes from *ATG7*$^{-/-}$ cells, however only IMPDH2 and GART were significantly reduced within the lysosome when analyzing their LC-MS intensities.

##### *4.4.2.1 IMPDH2 is an autophagic substrate partially dependent on ATG7 for localization to the lysosome*

IMPDH2 represents a particularly interesting protein in this analysis. For one, its role in the purine biosynthesis pathway is the rate-limiting step for guanylate synthesis. Furthermore, not only is it known to bind several important ALS-linked and stress granule localized proteins, but mammalian IMPDH2 and its yeast homolog localize to stress granules as well[106]. This presents an interesting opportunity to analyze a critical enzyme in GTP synthesis during the response to stress.

The intensity measurements of IMPDH2 support the notion that the protein is degraded by an ATG7 dependent system, as it is significantly decreased in the *ATG7*$^{-/-}$ lysosomes (Figure 21).

Western blot analysis demonstrated that IMPDH2 was present in the lysosomes under all conditions, however it was significantly enriched in those from sodium arsenite treated cells (Figure 22A). Additionally, its localization was significantly

decreased in the absence of ATG7 in the sodium arsenite condition (Figure 22A). Interestingly, there was still a strong signal in the *ATG7*$^{-/-}$ lysosomal fraction, indicating that while some of IMPDH2 may be trafficked to the lysosome by macroautophagy other mechanisms may also be at play. One intriguing possibility is that it is degraded by CMA. This is certainly possible as the protein contains numerous KFERQ-like motifs (Figure 24). To further understand the degradation pattern of IMPDH2, it would be beneficial to assess the role of CMA in its catabolism. One possibility would be to produce a *LAMP2A*$^{-/-}$ LysoIP cell line and assess IMPDH2's lysosomal levels in those cells.

The whole cell levels of IMPDH2 were not significantly altered across cell types or treatment conditions. All the cells were treated with bafilomycin $A_1$, which blocks the degradation of autophagy and lysosome substrates, which would render it impossible to observe an accumulation of IMPDH2 in *ATG7*$^{-/-}$ cells. What is interesting is that the levels across the treatment conditions, bafilomycin $A_1$, sodium arsenite or HBSS, were not altered. These results suggest that IMPDH2 is not enriched in lysosomes due to increased whole cell expression under oxidative stress, but rather it is increasingly targeted for degradation.

#### *4.4.2.2 PPAT represents an intriguing autophagy substrate*

Similarly to IMPDH2, the importance of PPAT in the purine biosynthesis pathway makes it an interesting hit. PPAT is the rate-limiting step for the entirety of the pathway, and thus contributes to determining adenylate and guanylate levels. Furthermore, PPAT was only found in the sodium arsenite treated condition, it was not present at all under any other treatment (Figure 14). The uniqueness of this, and its association with ALS and stress granule linked proteins prompted us to take a closer look.

Based on LC-MS intensities, PPAT was not significantly dependent on ATG7 for its localization to the lysosome (Figure 21). PPAT does contain some KFERQ-like motifs, so it would be beneficial to analyze its response to the absence of LAMP2A in order to

gain a better understanding of how it localizes to the lysosome (Figure 24).

As we observed with IMPDH2, whole cell levels of PPAT did not differ across cellular conditions (Figure 23A). This is especially surprising as PPAT levels are reported to be directly regulated by NRF2 which is activated by oxidative stress. It could be interesting to knockdown NRF2 under these conditions and observe how that impacts PPAT and IMPDH2 levels.

#### *4.4.2.3 Determining whether PPAT and IMPDH2 localize to stress granules*

It would be valuable to perform immunofluorescence experiments to determine if IMPDH2 and/or PPAT co-localizes with stress granule markers during oxidative stress. This would provide some clarity as to whether these proteins are trafficked to the lysosome as part of stress granules, or whether they are cytoplasmic – or perhaps forming metabolic enzyme condensates. Recruitment into stress granules could also explain why IMPDH2 is enriched in sodium arsenite lysosomes, despite sodium arsenite treatment not increasing IMDPH2 levels as compared to bafilomycin $A_1$ or HBSS treatments (Figure 22B). Of course, due to the bafilomycin $A_1$ treatment across the board we can not assess whether degradation rate was impacted. If IMPDH2 localizes to stress granules then it may have been preferentially targeted for granulophagy. This would be particularly interesting for IMPDH2 because the mammalian version as well as its yeast homolog have been found to localize to stress granules[106]. It may be possible that the fraction of IMPDH2 sequestered in stress granules is degraded by granulophagy, and the free cytoplasmic IMPDH2 is degraded by CMA. This would explain why only a fraction of IMPDH2 accumulation in lysosomes is dependent on ATG7.

## 4.5 ALS-Linked genes are enriched in lysosomes from sodium arsenite treated cells

While we previously discussed the many links between purines and ALS, there are some proteins which are causes or risk factors for ALS that were also enriched in the sodium arsenite treated lysosomes. Some of these proteins were also enriched in the starvation condition, namely TMEM106B and SQSTM1/p62 (Table 3). This makes sense as TMEM106B, while an ALS-linked protein, is additionally localized to the lysosome so one would expect it to be consistently in LysoIP samples[237]. SQSTM1/p62 is a well-documented selective macroautophagy receptor, and is engaged in both mitophagy and granulophagy[41,238]. Our data also shows that the presence of SQSTM1/p62 in the lysosome was dependent on ATG7, validating its role as being macroautophagy dependent.

Amongst the other ALS-linked proteins there aren't any significant surprises, SOD1 is a documented autophagy substrate[239,240]. Several of the proteins we detected in LysoIP samples from sodium arsenite-treated cells have been shown to co-localize with stress granules (PFN1[241], DCTN[106], TUBA4A[106], VCP[242], TDP-43[162]), and therefore granulophagy may account for their localization to lysosomes. Interestingly, wild-type DCTN is typically degraded by the ubiquitin-proteasome system, however mutant DCTN aggregates are degraded by autophagy[239]. This may be an indication that DCTN is indeed being degraded due to its association with stress granules. For the remaining two proteins, VAPB and CHMP2B, it is less clear how they localized to the lysosome although they are involved in the regulation of autophagy (VAPB[243], CHMP2B[244]).

### 4.5.1 SOD1 is a lysosomal substrate under sodium arsenite conditions

SOD1 was selected as a protein to further analyze due to its significant enrichment in the sodium arsenite lysosomes (Figure 14, Table 3).

LC-MS analysis indicates that SOD1 is heavily dependent on ATG7 for its localization to the lysosome – it was not detected at all in the *ATG7*$^{-/-}$ lysosomes. This

aligns with the fact that SOD1 does not contain a KFERQ-like motif, making it unable to be transported by the CMA pathway. Unfortunately, the sensitivity at the western blot level was not sufficient to detect SOD1 within lysosomes. In the future, we wish to repeat these experiments with a greater sample amount to confirm the LC-MS results.

Treatment with bafilomycin $A_1$ makes analyzing whole cell levels between wild type and *ATG7*$^{-/-}$ useless. Whole cell analysis of SOD1 levels indicate that SOD1 levels may not differ across treatment conditions (bafilomycin $A_1$, sodium arsenite, HBSS), however statistical analysis was not able to be performed (Figure 23B). Future experiments should explore the levels of SOD1 in the lysosomes under sodium arsenite treatment in the wild-type and *ATG7*$^{-/-}$ cells.

## 4.6 Enrichment of small GTPases in lysosomes from sodium arsenite treated cells

While the majority of this thesis concentrated on the purine biosynthesis pathway and its related molecules, we would be remiss if we did not also briefly mention the enrichment of small GTPase related pathways in sodium arsenite lysosomes as identified by IPA canonical pathway analysis (Figure 11). RhoA is a member of the Rho family, which is made up of small GTPases, therefore it is likely that the pathways 'Signaling by Rho Family GTPases' and 'RHOA Signaling' identified by IPA have a significant number of overlapping proteins. The Rho family is a family of small GTPases compromised of RhoA (sodium arsenite MIST score: 0.63), Rac (sodium arsenite MIST score: 0.62) and CDC42 (sodium arsenite MIST score: 0.80). All three were found to be enriched in the sodium arsenite lysosomes but none were enriched in the bafilomycin $A_1$ or HBSS condition. Not only has the absence of RhoA been shown to compromise stress granule formation, but the activated form has been shown to localize to the granules as well[245]. In order to function, Rho GTPases need to be bound to GTP as hydrolysis of GTP to GDP releases energy. The GDP is regularly replaced with GTP in order to maintain activation of the GTPase[246].

RhoA is linked to numerous neurodegenerative diseases including ALS, Parkinson's disease, Alzheimer's disease and Huntington's disease[246]. RhoA is primarily linked to ALS through ROCK, an effector of RhoA's. RhoA/ROCK activity inhibits autophagy, and increased levels of ROCK1 are found in SOD1 mouse models and sporadic ALS patients[247,248]. In turn, ROCK inhibition led to improved lifespan, symptom onset and pathology of mutant SOD1 mice[249,250]. It is possible that the enrichment of this signalling pathway in lysosomes is, at least in part, a way of re-establishing homeostatic autophagy by degrading its inhibitors.

It is tempting to hypothesize that there is a link between the purine biosynthesis pathway producing guanylates, and the enrichment of GTPases as well. It would be interesting to conduct an experiment to determine if overexpression of IMPDH2 led to inhibition of autophagy, through increased production of GTP and therefore more active RhoA. Autophagic flux, level of GTP and direct RhoA activation could be measured[251–253].

## 4.7 Limitations and Future Directions

### 4.7.1 Limitations and how to address them

One of the primary limitations with this thesis is that the level of TMEM192-3xHA is lower in the *ATG7*$^{-/-}$ cells compared to wild-type cells (Figure 4E). This makes it possible that decreased amounts of proteins in LysoIP from ATG7$^{-/-}$ cells could be due to decreased pulldown of lysosomes rather than autophagy-dependent localization of the protein to lysosomes. In the LC-MS data of LysoIP samples, both LAMP1 and RAB9A, two lysosomal markers, are not significantly altered between cell types. By western blot LAMP1 levels appear similar, although perhaps slightly reduced in the *ATG7*$^{-/-}$ lysosomal fraction as compared to wild-type (Figure 22A). TMEM192 is substantially depleted in LC-MS analysis of the *ATG7*$^{-/-}$ cells despite the data being normalized (Figure 21). In order to further assess the situation, it would be beneficial

to do some western blots for TMEM192 levels in the lysosomal pulldowns and see how they compare to LAMP1. LAMP1 was utilized to normalize the western blot signal in the quantification of lysosomal IMPDH2, so it would be of benefit to ensure that the effect is real by normalizing to TMEM192 (Figure 22A). What is a positive indication that IMPDH2 is genuinely degraded by autophagy is that the LAMP1 levels appear to be slightly lower in the *ATG7*$^{-/-}$ samples, which may help account for any differences in TMEM192-3xHA.

Another limitation was the complete absence of classic stress granule markers in the sodium arsenite treated lysosomes. While numerous proteins reported to localize to stress granules were found, it makes it more difficult to believe that granulophagy is genuinely occurring without detecting markers such as G3BP1/2, TIA-1 or PABP. As previously mentioned, this may be due to their localization within stress granule cores and/or the piecemeal degradation of stress granules. However, to further explore this result, it would be interesting to probe for these proteins in the lysosomal fractions by western blot. While LC-MS is extremely sensitive, it would be of use to have another method of quantification to compare results. Additionally, G3BP1/2, TIA-1 and PABP were all detected by LC-MS, however they did not reach the MIST score threshold to be identified as lysosomal. It is possible that the MIST score was too stringent to properly identify all lysosomal proteins.

Finally, the use of bafilomycin $A_1$ only, as opposed to untreated, as a control limits the ability to make confident statements regarding some of the results. While it was necessary to utilize a bafilomycin $A_1$ only treatment as the control to increase the yield when precipitating lysosomes (Figure 3B), it is not the best control for comparing whole cell levels between wild-type and *ATG7*$^{-/-}$ samples. Additionally, some may be concerned because bafilomycin $A_1$ is reported to not only inhibit acidification of the lysosome, but to inhibit fusion of the lysosome with autophagosomes as well. Thankfully, that seems to occur primarily in longer incubations with bafilomycin (6-12

hours), whereas the incubation in this study was limited to 1 hour[254]. Bafilomycin is frequently used to accumulate cargo within the lysosomes as part of many experiments related to autophagy[255]. However, repeating the western blots of IMPDH2, PPAT and SOD1 whole cell levels would best be done with an untreated sample as bafilomycin $A_1$ treatment makes it difficult to observe the effect of *ATG7*$^{-/-}$ on these protein levels.

### 4.7.2 Future Directions

A number of potential future directions were mentioned in the discussion above, including determining if IMPDH2 and PPAT localize to stress granules, and trying to determine if there is a link between the purine biosynthesis pathway and GTPases.

However, there are a few more future directions that would be interesting that are not directly related to our data. Firstly, it would be valuable to utilize the LysoIP system to look at the metabolomics data across these conditions. This could provide some additional information about the purine biosynthesis pathway, as well as a plethora of other information. It would additionally be beneficial to adapt this technique to isolate RNA from lysosomes. Despite early evidence that autophagy contributes to RNA degradation, the topic remains substantially less studied than protein degradation by autophagy[256]. However, RNA degradation by autophagy has continued to demonstrate its importance in development, maintenance of homeostasis and in response to stress[161,256,257]. By isolating RNA from the lysosomes it would be possible to provide the full scope as to what is being degraded by autophagy by using RNA-seq.

Furthermore, this technique could be used to further define the lysosomal proteome under various conditions. This could include analyzing the changes between cell types (e.g. motor neurons vs. cortical neurons), different stress conditions (e.g. heat shock, hypoxia, etc.) and cellular models of disease. Finally, it would be interesting to use this technique *in vivo* through transgenic mice – mice which recently

became available through the Jackson Laboratory. These mice conditionally express a Tmem192-3xHA tag, thus allowing the isolation of lysosomes from various tissues (Strain: 035401). It would be interesting to use these mice to further explore the lysosomal proteome under the conditions described above.

# Chapter 5: Conclusion

One commonality across most fields in medical research is the immense complexity of disease. Processes or molecules once thought to be simple or straightforward can, with more research and development, turn out to be much more complex. These are themes that we have seen emerge in the study of autophagy, as the complexities of this recycling mechanism are further elucidated and linked to diseases from cancer to viral infection. This thesis successfully demonstrates that the lysosomal proteome is dependent upon cellular conditions, and that starvation and oxidative stress can induce accumulation of distinct substrates in lysosomes. These differences often align with what we know regarding the stress response to these two offences.

A subset of causative ALS proteins/risk factors were also shown to localize to the lysosome when treated with sodium arsenite. This supports the idea that autophagy plays a large role in ALS pathology and stress granule degradation.

While several pathways were differentially enriched, we took note of the purine biosynthesis pathway in particular as it, and its individual components, were highly enriched in LysoIP samples in the sodium arsenite condition. The localization of this pathway's proteins were quite heavily dependent on macroautophagy. Interestingly, one of these pathway's proteins, IMPDH2, the rate-limiting step of guanylate synthesis, was only partially dependent on macroautophagy suggesting a secondary mechanism for its degradation. Due to the presence of multiple KFERQ-like motifs, it is hypothesized that CMA participated in localizing IMPDH2 to the lysosome.

The identification of the purine synthesis pathway as being targeted by autophagy under oxidative stress presents an interesting set of proteins to further analyze for their roles in the stress response, stress granules and ALS.


**Supplemental Figure 1: All canonical pathways differentially regulated between sodium arsenite and HBSS treated lysosomes.** Highlighted in red are the pathways selected to show in Figure 11.


**Supplemental Figure 2: Low complexity domains in TDP43.** This graphic demonstrates how LCD analysis may appear in a protein with confirmed LCDs and prion-like activity. It serves as a comparison to the LCD analysis performed on PPAT and IMPDH2.

# References


1. Dikic I, Elazar Z. Mechanism and medical implications of mammalian autophagy. *Nat Rev Mol Cell Biol*. 2018;19(6):349-364. doi:10.1038/s41580-018-0003-4
2. Bolt AM, Zhao F, Pacheco S, Klimecki WT. Arsenite-induced autophagy is associated with proteotoxicity in human lymphoblastoid cells. *Toxicol Appl Pharmacol*. 2012;264(2):255-261. doi:10.1016/j.taap.2012.08.006
3. Chen C, Ma J, Miao CS, et al. Trigonelline induces autophagy to protect mesangial cells in response to high glucose via activating the miR-5189-5p-AMPK pathway. *Phytomedicine*. 2021;92(February):153614. doi:10.1016/j.phymed.2021.153614
4. Back MJ, Ha HC, Fu Z, et al. Activation of neutral sphingomyelinase 2 by starvation induces cell-protective autophagy via an increase in Golgi-localized ceramide article. *Cell Death Dis*. 2018;9(6). doi:10.1038/s41419-018-0709-4
5. Karabiyik C, Vicinanza M, Son SM, Rubinsztein DC. Glucose starvation induces autophagy via ULK1-mediated activation of PIKfyve in an AMPK-dependent manner. *Dev Cell*. 2021;56(13):1961-1975.e5. doi:10.1016/j.devcel.2021.05.010
6. Wyant GA, Abu-Remaileh M, Frenkel EM, et al. NUFIP1 is a ribosome receptor for starvation-induced ribophagy. *Science (80- )*. 2018;176(3):139-148. doi:10.1126/science.aar2663.NUFIP1
7. Parzych KR, Klionsky DJ. An overview of autophagy: Morphology, mechanism, and regulation. *Antioxidants Redox Signal*. 2014;20(3):460-473. doi:10.1089/ars.2013.5371
8. Mehta A, Beck M, Sunder-Plassmann G. Physiology of the lysosome. In: *Fabry Disease: Perspectives from 5 Years of FOS.* Oxford: Oxford PharmaGenesis; 2006. https://www.ncbi.nlm.nih.gov/books/NBK11604/.
9. Rostislavleva K, Soler N, Ohashi Y, et al. Structure and flexibility of the endosomal Vps34 complex reveals the basis of its function on membranes. *Science (80- )*. 2015;350(6257):1-25. doi:10.1126/science.aac7365
10. Itakura E, Kishi C, Inoue K, Mizushima N. Beclin 1 Forms Two Distinct Phosphatidylinositol 3-Kinase Complexes with Mammalian Atg14 and UVRAG. *Mol Biol Cell*. 2008;19(December):5360-5372. doi:10.1091/mbc.E08
11. Song Y, Quach C, Liang C. UVRAG in autophagy, inflammation, and cancer. *Autophagy*. 2020;16(2):387-388. doi:10.1080/15548627.2019.1709768
12. Liang C, Feng P, Ku B, et al. Autophagic and tumour suppressor activity of a novel Beclin1-binding protein UVRAG. *Nat Cell Biol*. 2006;8(7):688-698. doi:10.1038/ncb1426
13. Mizushima N, Kuma A, Kobayashi Y, et al. Mouse Apg16L, a novel WD-repeat protein, targets to the autophagic isolation membrane with the Apg12-Apg5 conjugate. *J Cell Sci*. 2003;116(9):1679-1688. doi:10.1242/jcs.00381
14. Ichimura Y, Kirisako T, Takao T, et al. A ubiquitin-like system mediates protein lipidation. *Nature*. 2000;408(6811):488-492.
15. Fujita N, Itoh T, Omori H, Fukuda M, Noda T, Yoshimori T. The Atg16L Complex Specifies the Site of LC3 Lipidation for Membrane Biogenesis in Autophagy. *Mol Biol Cell*. 2008;19(May):2092-2100. doi:10.1091/mbc.E07
16. Kabeya Y, Mizushima N, Ueno T, et al. LC3, a mammalian homolog of yeast Apg8p, is localized in autophagosome membranes after processing. *EMBO J*. 2000;19(21):5720-5728. doi:10.1093/emboj/cdg454
17. Kirisako T, Ichimura Y, Okada H, et al. The reversible modification regulates the membrane-binding state of Apg8/Aut7 essential for autophagy and the cytoplasm to vacuole targeting pathway. *J Cell*

*Biol*. 2000;151(2):263-275. doi:10.1083/jcb.151.2.263
18. Nakatogawa H, Ishii J, Asai E, Ohsumi Y. Atg4 recycles inappropriately lipidated Atg8 to promote autophagosome biogenesis. *Autophagy*. 2012;8(2). doi:10.4161/auto.8.2.18373
19. Agrotis A, Pengo N, Burden JJ, Ketteler R. Redundancy of human ATG4 protease isoforms in autophagy and LC3/GABARAP processing revealed in cells. *Autophagy*. 2019;15(6):976-997. doi:10.1080/15548627.2019.1569925
20. Matoba K, Kotani T, Tsutsumi A, et al. Atg9 is a lipid scramblase that mediates autophagosomal membrane expansion. *Nat Struct Mol Biol*. 2020;27(December). doi:10.1038/s41594-020-00518-w
21. Velikkakath AKG, Nishimura T, Oita E, Ishihara N, Mizushima N. Mammalian Atg2 proteins are essential for autophagosome formation and important for regulation of size and distribution of lipid droplets. *Mol Biol Cell*. 2012;23(5):896-909. doi:10.1091/mbc.E11-09-0785
22. Kishi-Itakura C, Koyama-Honda I, Itakura E, Mizushima N. Ultrastructural analysis of autophagosome organization using mammalian autophagy-deficient cells. *J Cell Sci*. 2014;127:4089-4102. doi:10.1242/jcs.164293
23. Lu Y, Zhang Z, Sun D, Sweeney ST, Gao F-B. Syntaxin 13, a genetic modifier of mutant CHMP2B in frontotemporal dementia, is required for autophagosome maturation. *Mol Cell*. 2013;52(2). doi:10.1016/j.molcel.2013.08.041.Syntaxin
24. Takahashi Y, Liang X, Hattori T, et al. VPS37A directs ESCRT recruitment for phagophore closure. *J Cell Biol*. 2019;218(10):3336-3354. doi:10.1083/JCB.201902170
25. Takahashi Y, He H, Tang Z, et al. An autophagy assay reveals the ESCRT-III component CHMP2A as a regulator of phagophore closure. *Nat Commun*. 2018;9(1). doi:10.1038/s41467-018-05254-w
26. Jiang W, Chen X, Ji C, et al. Key regulators of autophagosome closure. *Cells*. 2021;10(11):1-13. doi:10.3390/cells10112814
27. Itakura E, Kishi-Itakura C, Mizushima N. The hairpin-type tail-anchored SNARE syntaxin 17 targets to autophagosomes for fusion with endosomes/lysosomes. *Cell*. 2012;151(6):1256-1269. doi:10.1016/j.cell.2012.11.001
28. Takáts S, Nagy P, Varga Á, et al. Autophagosomal Syntaxin17-dependent lysosomal degradation maintains neuronal function in Drosophila. *J Cell Biol*. 2013;201(4):531-539. doi:10.1083/jcb.201211160
29. Frank M, Duvezin-Caubet S, Koob S, et al. Mitophagy is triggered by mild oxidative stress in a mitochondrial fission dependent manner. *Biochim Biophys Acta - Mol Cell Res*. 2012;1823(12):2297-2310. doi:10.1016/j.bbamcr.2012.08.007
30. An H, Harper JW. Systematic analysis of ribophagy in human cells reveals bystander flux during selective autophagy. *Nat Cell Biol*. 2018;20(2):135-143. doi:10.1038/s41556-017-0007-x
31. Kirkin V. History of the Selective Autophagy Research: How Did It Begin and Where Does It Stand Today? *J Mol Biol*. 2020;432(1):3-27. doi:10.1016/j.jmb.2019.05.010
32. Smith MD, Harley ME, Kemp AJ, et al. CCPG1 Is a Non-canonical Autophagy Cargo Receptor Essential for ER-Phagy and Pancreatic ER Proteostasis. *Dev Cell*. 2018;44(2):217-232.e11. doi:10.1016/j.devcel.2017.11.024
33. Turco E, Witt M, Abert C, et al. FIP200 Claw Domain Binding to p62 Promotes Autophagosome Formation at Ubiquitin Condensates. *Mol Cell*. 2019;74(2):330-346.e11. doi:10.1016/j.molcel.2019.01.035
34. Bjørkøy G, Lamark T, Brech A, et al. p62/SQSTM1 forms protein aggregates degraded by autophagy and has a protective effect on huntingtin-induced cell death. *J Cell Biol*. 2005;171(4):603-614. doi:10.1083/jcb.200507002
35. Zaffagnini G, Savova A, Danieli A, et al. P62 Filaments Capture and Present Ubiquitinated Cargos

for Autophagy. *EMBO J*. 2018;37(5):1-21. doi:10.15252/embj.201798308
36. Khaminets A, Behl C, Dikic I. Ubiquitin-Dependent And Independent Signals In Selective Autophagy. *Trends Cell Biol*. 2016;26(1):6-16. doi:10.1016/j.tcb.2015.08.010
37. Sarraf SA, Raman M, Guarani-Pereira V, et al. Landscape of the PARKIN-dependent ubiquitylome in response to mitochondrial depolarization. *Nature*. 2013;496(7445):372-376. doi:10.1038/nature12043
38. Lazarou M, Sliter DA, Kane LA, et al. The ubiquitin kinase PINK1 recruits autophagy receptors to induce mitophagy. *Physiol Behav*. 2015;524(7565):309-314. doi:10.1038/nature14893.The
39. Wong YC, Holzbaur ELF. Optineurin is an autophagy receptor for damaged mitochondria in parkin-mediated mitophagy that is disrupted by an ALS-linked mutation. *Proc Natl Acad Sci U S A*. 2014;111(42):E4439-E4448. doi:10.1073/pnas.1405752111
40. Liu L, Feng D, Chen G, et al. Mitochondrial outer-membrane protein FUNDC1 mediates hypoxia-induced mitophagy in mammalian cells. *Nat Cell Biol*. 2012;14(2):177-185. doi:10.1038/ncb2422
41. Chitiprolu M, Jagow C, Tremblay V, et al. A complex of C9ORF72 and p62 uses arginine methylation to eliminate stress granules by autophagy. *Nat Commun*. 2018;9(1). doi:10.1038/s41467-018-05273-7
42. Kiffin R, Christian C, Knecht E, Cuervo AM. Activation of Chaperone-mediated Autophagy during Oxidative Stress. *Mol Biol Cell*. 2004;15(November):4829-4840. doi:10.1091/mbc.E04
43. Ferreira JV, Fofo H, Bejarano E, et al. STUB1/CHIP is required for HIF1A degradation by chaperone-mediated autophagy. *Autophagy*. 2013;9(9):1349-1366. doi:10.4161/auto.25190
44. Qi L, Zhang XD, Wu JC, et al. The Role of Chaperone-Mediated Autophagy in Huntingtin Degradation. *PLoS One*. 2012;7(10):1-16. doi:10.1371/journal.pone.0046834
45. Huang CC, Bose JK, Majumder P, et al. Metabolism and mis-metabolism of the neuropathological signature protein TDP-43. *J Cell Sci*. 2014;127(14):3024-3038. doi:10.1242/jcs.136150
46. Bauer PO, Goswami A, Wong HK, et al. Harnessing chaperone-mediated autophagy for the selective degradation of mutant huntingtin protein. *Nat Biotechnol*. 2010;28(3):256-263. doi:10.1038/nbt.1608
47. Cuervo A, Stefanis L, Fredenburg R, Lansbury PT, Sulzer D. Impaired Degradation of Mutant α-Synuclein by Chaperone-Mediated Autophagy Published by : American Association for the Advancement of Science Stable URL : http://www.jstor.org/stable/3837669 . *Sceince*. 2004;305(5688):1292-1295.
48. Yim WWY, Mizushima N. Lysosome biology in autophagy. *Cell Discov*. 2020;6(1). doi:10.1038/s41421-020-0141-7
49. Cuervo AM, Wong E. Chaperone-mediated autophagy: Roles in disease and aging. *Cell Res*. 2014;24(1):92-104. doi:10.1038/cr.2013.153
50. Jackson MP, Hewitt EW. Cellular proteostasis: Degradation of misfolded proteins by lysosomes. *Essays Biochem*. 2016;60(2):173-180. doi:10.1042/EBC20160005
51. Kirchner P, Bourdenx M, Madrigal-Matute J, et al. Proteome-wide analysis of chaperone-mediated autophagy targeting motifs. *PLoS Biol*. 2019;17(5):1-27. doi:10.1371/JOURNAL.PBIO.3000301
52. Kenney DL, Benarroch EE. The autophagy-lysosomal pathway: General concepts and clinical implications. *Neurology*. 2015;85:634-645.
53. Martinez-Vicente M, Talloczy Z, Kaushik S, et al. Dopamine-modified α-synuclein blocks chaperone-mediated autophagy. *J Clin Invest*. 2008;118(2):777-778. doi:10.1172/JCI32806
54. Caballero B, Bourdenx M, Luengo E, et al. Acetylated tau inhibits chaperone-mediated autophagy and promotes tau pathology propagation in mice. *Nat Commun*. 2021;12(1):1-18. doi:10.1038/s41467-021-22501-9

55. Dice JF. Peptide sequences that target cytosolic proteins for lysosomal proteolysis. *Tibs*. 1990:305-309.
56. Mijaljica D, Prescott M, Devenish RJ. Microautophagy in mammalian cells: Revisiting a 40-year-old conundrum. *Autophagy*. 2011;7(7):673-682. doi:10.4161/auto.7.7.14733
57. Sato M, Seki T, Konno A, et al. Rapamycin activates mammalian microautophagy. *J Pharmacol Sci*. 2019;140(2):201-204. doi:10.1016/j.jphs.2019.05.007
58. Schuck S. Microautophagy – distinct molecular mechanisms handle cargoes of many sizes. *J Cell Sci*. 2020;133(17). doi:10.1242/jcs.246322
59. Sahu R, Kaushik S, Clement CC, et al. Microautophagy of Cytosolic Proteins by Late Endosomes. *Dev Cell*. 2011;20(1):131-139. doi:10.1016/j.devcel.2010.12.003
60. Schneider JL, Suh Y, Cuervo AM. Deficient chaperone-mediated autophagy in liver leads to metabolic dysregulation. *Cell Metab*. 2014;20(3):417-432. doi:10.1016/j.cmet.2014.06.009.Deficient
61. Qiao L, Ma J, Zhang Z, et al. Deficient chaperone-mediated autophagy promotes inflammation and atherosclerosis. *Circ Res*. 2021;129(12):1141-1157. doi:10.1161/CIRCRESAHA.121.318908
62. Bae H, Guan J-L. Suppression of autophagy by FIP200 deletion impairs DNA damage repair and increases cell death upon treatments with anti-cancer agents. *Mol Cancer Res*. 2011;9(9):1232-1241. doi:10.1158/1541-7786.MCR-11-0098.Suppression
63. Komatsu M, Waguri S, Ueno T, et al. Impairment of starvation-induced and constitutive autophagy in Atg7-deficient mice. *J Cell Biol*. 2005;169(3):425-434. doi:10.1083/jcb.200412022
64. Ye X, Zhou XJ, Zhang H. Exploring the role of autophagy-related gene 5 (ATG5) yields important insights into autophagy in autoimmune/autoinflammatory diseases. *Front Immunol*. 2018;9(OCT):1-15. doi:10.3389/fimmu.2018.02334
65. Sato M, Seki T, Konno A, et al. Fluorescent-based evaluation of chaperone-mediated autophagy and microautophagy activities in cultured cells. *Genes to Cells*. 2016;21(8):861-873. doi:10.1111/gtc.12390
66. Razi M, Futter CE. Distinct Roles for Tsg101 and Hrs in Multivesicular Body Formation and Inward Vesiculation. *Mol Biol Cell*. 2006;17(August):3469-3483. doi:10.1091/mbc.E05
67. Williams RL, Urbé S. The emerging shape of the ESCRT machinery. *Nat Rev Mol Cell Biol*. 2007;8(5):355-368. doi:10.1038/nrm2162
68. Gurung S, Perocheau D, Touramanidou L, Baruteau J. The exosome journey: from biogenesis to uptake and intracellular signalling. *Cell Commun Signal*. 2021;19(1):1-19. doi:10.1186/s12964-021-00730-1
69. Nishida Y, Arakawa S, Fujitani K, et al. Discovery of Atg5/Atg7-independent alternative macroautophagy. *Nature*. 2009;461(7264):654-658. doi:10.1038/nature08455
70. Cuervo AM, Dice JF, Knecht E. A population of rat liver lysosomes responsible for the selective uptake and degradation of cytosolic proteins. *J Biol Chem*. 1997;272(9):5606-5615. doi:10.1074/jbc.272.9.5606
71. Loos B, Du Toit A, Hofmeyr JHS. Defining and measuring autophagosome flux - Concept and reality. *Autophagy*. 2014;10(11):2087-2096. doi:10.4161/15548627.2014.973338
72. Kim DH, Sarbassov DD, Ali SM, et al. mTOR interacts with raptor to form a nutrient-sensitive complex that signals to the cell growth machinery. *Cell*. 2002;110(2):163-175. doi:10.1016/S0092-8674(02)00808-5
73. Kim D, Sarbassov DD, Ali SM, et al. GBL, a Positive Regulator of the Rapamycin- Sensitive Pathway Required for the Nutrient- Sensitive Interaction between Raptor and mTOR. 2003;11:895-904. http://www.molecule.org/cgi/.
74. Saxton RA, Sabatini DM. mTOR Signaling in Growth, Metabolism, and Disease. *Cell*.

2017;168(6):960-976. doi:10.1016/j.cell.2017.02.004
75. Sardiello M, Palmieri M, di Ronza A, et al. A Gene Network Regulating Lysosomal Biogenesis and Function. *Science (80- )*. 2009;325:473-476.
76. Settembre C, Di Malta C, Polito VA, et al. TFEB Links Autophagy to Lysosomal Biogenesis. *Science (80- )*. 2011;332(6036):1429-1433. doi:10.1126/science.1204592.TFEB
77. Martina JA, Chen Y, Gucek M, Puertollano R. MTORC1 functions as a transcriptional regulator of autophagy by preventing nuclear transport of TFEB. *Autophagy*. 2012;8(6):903-914. doi:10.4161/auto.19653
78. Settembre C, Zoncu R, Medina DL, et al. A lysosome-to-nucleus signalling mechanism senses and regulates the lysosome via mTOR and TFEB. *EMBO J*. 2012;31(5):1095-1108. doi:10.1038/emboj.2012.32
79. Hoxhaj G, Hughes-Hallett J, Timson RC, et al. The mTORC1 Signaling Network Senses Changes in Cellular Purine Nucleotide Levels. *Cell Rep*. 2017;21(5):1331-1346. doi:10.1016/j.celrep.2017.10.029
80. Bar-Peled L, Chantranupong L, Cherniack AD, et al. A tumor suppressor complex with GAP activity for the Rag GTPases that signal amino acid sufficiency to mTORC1. *Science (80- )*. 2013;340(6136):1100-1106. doi:10.1126/science.1232044.A
81. Tsun Z-Y, Bar-Peled L, Chantranupong L, et al. The Folliculin tumor suppressor is a GAP for RagC/D GTPases that signal amino acid levels to mTORC1. *Mol Cell*. 2013;52(4). doi:10.1016/j.molcel.2013.09.016.The
82. Dibble CC, Elis W, Menon S, et al. TBC1D7 Is a Third Subunit of the TSC1-TSC2 Complex Upstream of mTORC1. *Mol Cell*. 2012;47(4):535-546. doi:10.1016/j.molcel.2012.06.009
83. Sancak Y, Peterson TR, Shaul YD, et al. The Rag GTPases bind raptor and mediate amino acid signaling to mTORC1. *Science (80- )*. 2008;320(5882):1496-1501. doi:10.1126/science.1157535
84. Kim E, Goraksha-Hicks P, Li L, Neufeld TP, Guan KL. Regulation of TORC1 by Rag GTPases in nutrient response. *Nat Cell Biol*. 2008;10(8):935-945. doi:10.1038/ncb1753
85. Yang H, Jiang X, Li B, et al. Mechanisms of mTORC1 activation by RHEB and inhibition by PRAS40. *Nature*. 2017;552(7685):368-373. doi:10.1038/nature25023
86. Bar-Peled L, Sabatini DM. Regulation of mTORC1 by amino acids. *Trends Cell Biol*. 2014;24(7):400-406. doi:10.1016/j.tcb.2014.03.003
87. Sancak Y, Bar-Peled L, Zoncu R, Markhard AL, Nada S, Sabatini DM. Ragulator-rag complex targets mTORC1 to the lysosomal surface and is necessary for its activation by amino acids. *Cell*. 2010;141(2):290-303. doi:10.1016/j.cell.2010.02.024
88. Chen J, Ou Y, Luo R, et al. SAR1B senses leucine levels to regulate mTORC1 signalling. *Nature*. 2021;596(7871):281-284. doi:10.1038/s41586-021-03768-w
89. Parmigiani A, Nourbakhsh A, Ding B, et al. Sestrins Inhibit mTORC1 Kinase Activation Through the GATOR Complex. *Cell Rep*. 2014;9(4):1281-1291. doi:10.1016/j.celrep.2014.10.019.Sestrins
90. Wolfson RL, Chantranupong L, Saxton RA, et al. Sestrin2 is a leucine sensor for the mTORC1 pathway. *Science (80- )*. 2016;351(6268). doi:10.1126/science.aab2674.Sestrin2
91. Chantranupong L, Scaria SM, Saxton RA, et al. The CASTOR proteins are arginine sensors for the mTORC1 pathway. *Cell*. 2016;165(1):153-164. doi:10.1016/j.cell.2016.02.035.The
92. Mimura K, Sakamaki JI, Morishita H, Kawazu M, Mano H, Mizushima N. Genome-wide CRISPR screening reveals nucleotide synthesis negatively regulates autophagy. *J Biol Chem*. 2021;296:100780. doi:10.1016/j.jbc.2021.100780
93. Cuervo AM, Knecht E, Terlecky SR, Dice JF. Activation of a selective pathway of lysosomal proteolysis in rat liver by prolonged starvation. *Am J Physiol - Cell Physiol*. 1995;269(5 38-5).

doi:10.1152/ajpcell.1995.269.5.c1200
94. Dohi E, Tanaka S, Seki T, et al. Hypoxic stress activates chaperone-mediated autophagy and modulates neuronal cell survival. *Neurochem Int*. 2012;60(4):431-442. doi:10.1016/j.neuint.2012.01.020
95. Cuervo AM, Dice JF. Regulation of Lamp2a levels in the lysosomal membrane. *Traffic*. 2000;1(7):570-583. doi:10.1034/j.1600-0854.2000.010707.x
96. Cuervo AM, Hu W, Lim B, Dice JF. IκB is a substrate for a selective pathway of lysosomal proteolysis. *Mol Biol Cell*. 1998;9(8):1995-2010. doi:10.1091/mbc.9.8.1995
97. Mejlvang J, Olsvik H, Svenning S, et al. Starvation induces rapid degradation of selective autophagy receptors by endosomal microautophagy. *J Cell Biol*. 2018;217(10):3640-3655. doi:10.1083/JCB.201711002
98. Mukherjee A, Patel B, Koga H, Cuervo AM, Jenny A. Selective endosomal microautophagy is starvation-inducible in Drosophila. *Autophagy*. 2016;12(11):1984-1999. doi:10.1080/15548627.2016.1208887
99. Hatakeyama R, De Virgilio C. TORC1 specifically inhibits microautophagy through ESCRT-0. *Curr Genet*. 2019;65(5):1243-1249. doi:10.1007/s00294-019-00982-y
100. Thoreen CC, Kang SA, Chang JW, et al. An ATP-competitive mammalian target of rapamycin inhibitor reveals rapamycin-resistant functions of mTORC1. *J Biol Chem*. 2009;284(12):8023-8032. doi:10.1074/jbc.M900301200
101. Singh J, Kaade E, Muntel J, et al. Systematic Comparison of Strategies for the Enrichment of Lysosomes by Data Independent Acquisition. *J Proteome Res*. 2020;19(1):371-381. doi:10.1021/acs.jproteome.9b00580
102. Walker MW, Lloyd-Evans E. *A Rapid Method for the Preparation of Ultrapure, Functional Lysosomes Using Functionalized Superparamagnetic Iron Oxide Nanoparticles*. Vol 126. Elsevier Ltd; 2015. doi:10.1016/bs.mcb.2014.10.019
103. Diettrich O, Mills K, Johnson AW, Hasilik A, Winchester BG. Application of magnetic chromatography to the isolation of lysosomes from fibroblasts of patients with lysosomal storage disorders. *FEBS Lett*. 1998;441(3):369-372. doi:10.1016/S0014-5793(98)01578-6
104. Abu-Remaileh M, Wyant GA, Kim C, et al. Lysosomal metabolomics reveals V-ATPase and mTOR- dependent regulation of amino acid efflux from lysosomes. *Science (80- )*. 2017;358(6364):807-813.
105. Ivanov P, Kedersha N, Anderson P. Stress granules and processing bodies in translational control. *Cold Spring Harb Perspect Biol*. 2019;11(5):1-18. doi:10.1101/cshperspect.a032813
106. Jain S, Wheeler JR, Walters RW, Agrawal A, Barsic A, Parker R. ATPase modulated stress granules contain a diverse proteome and substructure. *Cell*. 2016;164(3):487-498. doi:10.1016/j.cell.2015.12.038.ATPase
107. Molliex A, Temirov J, Lee J, et al. Phase Separation by Low Complexity Domains Promotes Stress Granule Assembly and Drives Pathological Fibrillization. *Cell*. 2015;163(1):123-133. doi:10.1016/j.cell.2015.09.015
108. Jain S, Wheeler JR, Walters RW, Agrawal A, Barsic A, Parker R. ATPase-Modulated Stress Granules Contain a Diverse Proteome and Substructure. *Cell*. 2016;164(3):487-498. doi:10.1016/j.cell.2015.12.038
109. Youn JY, Dyakov BJA, Zhang J, et al. Properties of Stress Granule and P-Body Proteomes. *Mol Cell*. 2019;76(2):286-294. doi:10.1016/j.molcel.2019.09.014
110. Wolozin B, Ivanov P. Stress granules and neurodegeneration. *Nat Rev Neurosci*. 2019;20(11):649-666. doi:10.1038/s41583-019-0222-5

111. Radford H, Moreno JA, Verity N, Halliday M, Mallucci GR. PERK inhibition prevents tau-mediated neurodegeneration in a mouse model of frontotemporal dementia. *Acta Neuropathol*. 2015;130(5):633-642. doi:10.1007/s00401-015-1487-z
112. Kim H, Raphael AR, Ladow ES, et al. Therapeutic modulation of eIF2α-phosphorylation rescues TDP-43 toxicity in amyotrophic lateral sclerosis disease models. *Nat Genet*. 2014;46(2):152-160. doi:10.1038/ng.2853.Therapeutic
113. Buchan JR, Kolaitis RM, Taylor JP, Parker R. Eukaryotic stress granules are cleared by autophagy and Cdc48/VCP function. *Cell*. 2013;153(7):1461. doi:10.1016/j.cell.2013.05.037
114. Wang B, Zhang L, Dai T, et al. Liquid–liquid phase separation in human health and diseases. *Signal Transduct Target Ther*. 2021;6(1). doi:10.1038/s41392-021-00678-1
115. Banani SF, Lee HO, Hyman AA, Rosen MK. *Biomolecular Condensates: Organizers of Cellular Biochemistry*. Vol 18.; 2017. doi:10.1038/nrm.2017.7
116. Bergeron-Sandoval LP, Safaee N, Michnick SW. Mechanisms and Consequences of Macromolecular Phase Separation. *Cell*. 2016;165(5):1067-1079. doi:10.1016/j.cell.2016.05.026
117. Jin M, Han T, Yao Y, et al. Glycolytic Enzymes Coalesce in G Bodies under Hypoxic Stress. *Cell Rep*. 2017;20(4):895-908. doi:10.1016/j.celrep.2017.06.082
118. Noree C, Begovich K, Samilo D, Broyer R, Monfort E, Wilhelm JE. A quantitative screen for metabolic enzyme structures reveals patterns of assembly across the yeast metabolic network. *Mol Biol Cell*. 2019;30(21):2721-2736. doi:10.1091/mbc.E19-04-0224
119. Barry RM, Bitbol AF, Lorestani A, et al. Large-scale filament formation inhibits the activity of CTP synthetase. *Elife*. 2014;3(July2014):1-19. doi:10.7554/eLife.03638
120. Begovich K, Vu AQ, Yeo G, Wilhelm JE. Conserved metabolite regulation of stress granule assembly via AdoMet. *J Cell Biol*. 2020;219(8 August). doi:10.1083/JCB.201904141
121. Komatsu M, Waguri S, Chiba T, et al. Loss of autophagy in the central nervous system causes neurodegeneration in mice. *Nature*. 2006;441(7095):880-884. doi:10.1038/nature04723
122. Menzies FM, Fleming A, Caricasole A, et al. Autophagy and Neurodegeneration: Pathogenic Mechanisms and Therapeutic Opportunities. *Neuron*. 2017;93(5):1015-1034. doi:10.1016/j.neuron.2017.01.022
123. Ormeño F, Hormazabal J, Moreno J, et al. Chaperone Mediated Autophagy Degrades TDP-43 Protein and Is Affected by TDP-43 Aggregation. *Front Mol Neurosci*. 2020;13(February):1-17. doi:10.3389/fnmol.2020.00019
124. Xu X, Sun Y, Cen X, et al. Metformin activates chaperone-mediated autophagy and improves disease pathologies in an Alzheimer disease mouse model. *Protein Cell*. 2021;12(10):769-787. doi:10.1007/s13238-021-00858-3
125. Hardiman O, Al-Chalabi A, Chio A, et al. Amyotrophic lateral sclerosis. *Nat Rev Dis Prim*. 2017:1-5. doi:10.1016/B978-008055232-3.60661-0
126. Wolozin B. The Evolution of Phase-Separated TDP-43 in Stress. *Neuron*. 2019;102(2):265-267. doi:10.1016/j.neuron.2019.03.041
127. Chia R, Chiò A, Traynor BJ. Novel genes associated with amyotrophic lateral sclerosis: diagnostic and clinical implications. *Lancet Neurol*. 2017;17(1):94-102. doi:10.1016/S1474-4422(17)30401-5. Novel
128. Wils H, Kleinberger G, Janssens J, et al. TDP-43 transgenic mice develop spastic paralysis and neuronal inclusions characteristic of ALS and frontotemporal lobar degeneration. *Proc Natl Acad Sci U S A*. 2010;107(8):3858-3863. doi:10.1073/pnas.0912417107
129. Wijesekera LC, Leigh PN. Amyotrophic lateral sclerosis. *Orphanet J Rare Dis*. 2009;4(1):1-22. doi:10.1186/1750-1172-4-3

130. Blokhuis AM, Groen EJN, Koppers M, Van Den Berg LH, Pasterkamp RJ. Protein aggregation in amyotrophic lateral sclerosis. *Acta Neuropathol*. 2013;125(6):777-794. doi:10.1007/s00401-013-1125-6
131. Baradaran-Heravi Y, Van Broeckhoven C, van der Zee J. Stress granule mediated protein aggregation and underlying gene defects in the FTD-ALS spectrum. *Neurobiol Dis*. 2020;134(September 2019):104639. doi:10.1016/j.nbd.2019.104639
132. Zhang Y, Gu J, Sun Q. Aberrant stress granule dynamics and aggrephagy in ALS pathogenesis. *Cells*. 2021;10(9):1-13. doi:10.3390/cells10092247
133. Markmiller S, Sathe S, Server KL, et al. Persistent mRNA localization defects and cell death in ALS neurons caused by transient cellular stress. *Cell Rep*. 2021;36(10). doi:10.1016/j.celrep.2021.109685
134. Ravanan P, Srikumar IF, Talwar P. Autophagy: The spotlight for cellular stress responses. *Life Sci*. 2017;188(August):53-67. doi:10.1016/j.lfs.2017.08.029
135. Markovinovic A, Cimbro R, Ljutic T, Kriz J, Rogelj B, Munitic I. Optineurin in amyotrophic lateral sclerosis: Multifunctional adaptor protein at the crossroads of different neuroprotective mechanisms. *Prog Neurobiol*. 2017;154:1-20. doi:10.1016/j.pneurobio.2017.04.005
136. Fay MM, Anderson PJ, Ivanov P. ALS/FTD-Associated C9ORF72 Repeat RNA Promotes Phase Transitions In Vitro and in Cells. *Cell Rep*. 2017;21(12):3573-3584. doi:10.1016/j.celrep.2017.11.093
137. Gal J, Strom A-L, Kwinter DM, et al. Sequestosome 1/p62 links familial ALS mutant SOD1 to LC3 via an ubiquitin-independent mechanism. *J Neurochem*. 2009;111(4):1062-1073. doi:10.1111/j.1471-4159.2009.06388.x.Sequestosome
138. Wheeler JR, Matheny T, Jain S, Abrisch R, Parker R. Distinct stages in stress granule assembly and disassembly. *Elife*. 2016;5(Se):1-25. doi:10.7554/eLife.18413
139. Ran FA, Hsu PD, Wright J, Agarwala V, Scott DA, Zhang F. Genome engineering using the CRISPR-Cas9 system. *Nat Protoc*. 2013;8(11):2281-2308. doi:10.1038/nprot.2013.143
140. Laflamme C, McKeever PM, Kumar R, et al. Implementation of an antibody characterization procedure and application to the major ALS/FTD disease gene C9ORF72. *Elife*. 2019;8. doi:10.7554/eLife.48363
141. Yambire KF, Rostosky C, Watanabe T, et al. Impaired lysosomal acidification triggers iron deficiency and inflammation in vivo. *Elife*. 2019;8:1-36. doi:10.7554/eLife.51031
142. Cox J, Mann M. MaxQuant enables high peptide identification rates, individualized p.p.b.-range mass accuracies and proteome-wide protein quantification. *Nat Biotechnol*. 2008;26(12):1367-1372. doi:10.1038/nbt.1511
143. Afgan E, Baker D, Batut B, et al. The Galaxy platform for accessible, reproducible and collaborative biomedical analyses: 2018 update. *Nucleic Acids Res*. 2018;46(W1):W537-W544. doi:10.1093/nar/gky379
144. Föll M, Fahrner M. Label-free data analysis using MaxQuant (Galaxy Training Materials). 2021. https://training.galaxyproject.org/training-material/topics/proteomics/tutorials/maxquant-label-free/tutorial.html.
145. Gierlinski M, Gastaldello F, Cole C, Barton GJ. Proteus: an R package for downstream analysis of MaxQuant output. *bioRxiv*. 2018:416511. https://www.biorxiv.org/content/10.1101/416511v2%0Ahttps://www.biorxiv.org/content/10.1101/416511v2.abstract.
146. Jäger S, Cimermancic P, Gulbahce N, et al. Global landscape of HIV-human protein complexes. *Nature*. 2012;481(7381):365-370. doi:10.1038/nature10719
147. Shannon P, Markiel A, Ozier O, et al. Cytoscape: A Software Environment for Integrated Models.

*Genome Res*. 2003;13:2498-2504. doi:10.1101/gr.1239303.metabolite
148. Doncheva NT, Morris JH, Gorodkin J, Jensen LJ. Cytoscape StringApp: Network Analysis and Visualization of Proteomics Data. *J Proteome Res*. 2019;18(2):623-632. doi:10.1021/acs.jproteome.8b00702
149. Morris JH, Apeltsin L, Newman AM, et al. ClusterMaker: A multi-algorithm clustering plugin for Cytoscape. *BMC Bioinformatics*. 2011;12. doi:10.1186/1471-2105-12-436
150. Binder JX, Pletscher-Frankild S, Tsafou K, et al. COMPARTMENTS: Unification and visualization of protein subcellular localization evidence. *Database*. 2014;2014:1-9. doi:10.1093/database/bau012
151. Liao Y, Wang J, Jaehnig EJ, Shi Z, Zhang B. WebGestalt 2019: gene set analysis toolkit with revamped UIs and APIs. *Nucleic Acids Res*. 2019;47(W1):W199-W205. doi:10.1093/nar/gkz401
152. Jarnot P, Ziemska-Legiecka J, Dobson L, et al. PlaToLoCo: The first web meta-server for visualization and annotation of low complexity regions in proteins. *Nucleic Acids Res*. 2020;48(W1):W77-W84. doi:10.1093/NAR/GKAA339
153. Jia J, Claude-Taupin A, Gu Y, et al. Galectin-3 Coordinates a Cellular System for Lysosomal Repair and Removal. *Dev Cell*. 2020;52(1):69-87.e8. doi:10.1016/j.devcel.2019.10.025
154. Devenport SN, Singhal R, Radyk MD, et al. Colorectal cancer cells utilize autophagy to maintain mitochondrial metabolism for cell proliferation under nutrient stress. *JCI Insight*. 2021;6(14). doi:10.1172/jci.insight.138835
155. Cui W, Sathyanarayan A, Lopresti M, Aghajan M, Chen C, Mashek DG. Lipophagy-derived fatty acids undergo extracellular efflux via lysosomal exocytosis. *Autophagy*. 2021;17(3):690-705. doi:10.1080/15548627.2020.1728097
156. Mackenzie IR, Nicholson AM, Sarkar M, et al. TIA1 mutations in amyotrophic lateral sclerosis and frontotemporal dementia promote phase separation and alter stress granule dynamics. 2018;95(4):808-816. doi:10.1016/j.neuron.2017.07.025.TIA1
157. Yoshimori T, Yamamoto A, Moriyama Y, Futai M, Tashiro Y. Bafilomycin A1, a specific inhibitor of vacuolar-type H+-ATPase, inhibits acidification and protein degradation in lysosomes of cultured cells. J Biol Chem. 1991;266(26):17707-17712. doi:10.1016/s0021-9258(19)47429-2
158. Bolt AM, Douglas RR, Klimecki WT. Arsenite exposure in human lymphoblastoid cell lines induces autophagy and coordinated induction of lysosomal genes. *Toxicol Lett*. 2010;199(2):153-159. doi:10.1016/j.toxlet.2010.08.017.Arsenite
159. Scherr AL, Jassowicz A, Pató A, et al. Knockdown of Atg7 induces nuclear-LC3 dependent apoptosis and augments chemotherapy in colorectal cancer cells. *Int J Mol Sci*. 2020;21(3):1-15. doi:10.3390/ijms21031099
160. Zhou H, Qian X, Xu N, et al. Disruption of Atg7-dependent autophagy causes electromotility disturbances, outer hair cell loss, and deafness in mice. *Cell Death Dis*. 2020;11(10). doi:10.1038/s41419-020-03110-8
161. Liu Y, Zou W, Yang P, et al. Autophagy-dependent ribosomal RNA degradation is essential for maintaining nucleotide homeostasis during C. Elegans development. *Elife*. 2018;7:1-22. doi:10.7554/eLife.35373
162. Zhang K, Daigle JG, Cunningham KM, et al. Stress Granule Assembly Disrupts Nucleocytoplasmic Transport. *Cell*. 2018;173(4):958-971.e17. doi:10.1016/j.cell.2018.03.025
163. Easterling MR, Styblo M, Evans M V., Kenyon EM. Pharmacokinetic modeling of arsenite uptake and metabolism in hepatocytes - Mechanistic insights and implications for further experiments. *J Pharmacokinet Pharmacodyn*. 2002;29(3):207-234. doi:10.1023/A:1020248922689
164. Janasik B, Reszka E, Stanislawska M, et al. Effect of Arsenic Exposure on NRF2-KEAP1 Pathway

and Epigenetic Modification. *Biol Trace Elem Res*. 2018;185(1):11-19. doi:10.1007/s12011-017-1219-4
165. Park WH. Upregulation of thioredoxin and its reductase attenuates arsenic trioxide-induced growth suppression in human pulmonary artery smooth muscle cells by reducing oxidative stress. *Oncol Rep*. 2020;43(1):358-367. doi:10.3892/or.2019.7414
166. Mitchell J, Morris A, de Belleroche J. Thioredoxin reductase 1 haplotypes modify familial amyotrophic lateral sclerosis onset. *Free Radic Biol Med*. 2009;46(2):202-211. doi:10.1016/j.freeradbiomed.2008.09.041
167. Buchan JR, Kolaitis RM, Taylor JP, Parker R. Eukaryotic stress granules are cleared by autophagy and Cdc48/VCP function. *Cell*. 2013;153(7):1461. doi:10.1016/j.cell.2013.05.037
168. Da Ros M, Deol HK, Savard A, Guo H, Meiering EM, Gibbings D. Wild-type and mutant SOD1 localizes to RNA-rich structures in cells and mice but does not bind RNA. *J Neurochem*. 2020;156(4):524-538. doi:10.1111/jnc.15126
169. Lee DY, Jeon GS, Sung JJ. ALS-Linked Mutant SOD1 Associates with TIA-1 and Alters Stress Granule Dynamics. *Neurochem Res*. 2020;45(12):2884-2893. doi:10.1007/s11064-020-03137-5
170. Mateju D, Franzmann TM, Patel A, et al. An aberrant phase transition of stress granules triggered by misfolded protein and prevented by chaperone function. *EMBO J*. 2017;36(12):1669-1687. doi:10.15252/embj.201695957
171. Cluskey S, Ramsden DB. Mechanisms of neurodegeneration in amyotrophic lateral sclerosis. *J Clin Pathol - Mol Pathol*. 2001;54(6):386-392.
172. Bruijn LI, Miller TM, Cleveland DW. Unraveling the mechanisms involved in motor neuron degeneration in ALS. *Annu Rev Neurosci*. 2004;27:723-749. doi:10.1146/annurev.neuro.27.070203.144244
173. Van Den Bosch L, Van Damme P, Bogaert E, Robberecht W. The role of excitotoxicity in the pathogenesis of amyotrophic lateral sclerosis. *Biochim Biophys Acta - Mol Basis Dis*. 2006;1762(11-12):1068-1082. doi:10.1016/j.bbadis.2006.05.002
174. Hansen JP. Can't miss: conquer any number task by making important statistics simple. Part 6. Tests of statistical significance (z test statistic, rejecting the null hypothesis, p value), t test, z test for proportions, statistical significance versus meaningful dif. *J Healthc Qual*. 2004;26(4):43-53. doi:10.1111/j.1945-1474.2004.tb00507.x
175. Mistry J, Chuguransky S, Williams L, et al. Pfam: The protein families database in 2021. *Nucleic Acids Res*. 2021;49(D1):D412-D419. doi:10.1093/nar/gkaa913
176. Spector JM, Harrison RS, Fishman MC. Fundamental science behind today's important medicines. *Sci Transl Med*. 2018;10(438):1-5. doi:10.1126/scitranslmed.aaq1787
177. Deltcheva E, Chylinski K, Sharma CM, et al. CRISPR RNA maturation by trans-encoded small RNA and host factor RNase III. *Nature*. 2011;471(7340):602-607. doi:10.1038/nature09886
178. De Duve C, Pressman BC, Gianetto R, Wattiaux R, Appelmans F. Tissue fractionation studies. 6. Intracellular distribution patterns of enzymes in rat-liver tissue. *Biochem J*. 1955;60(4):604-617. doi:10.1042/bj0600604
179. Takeshige K, Baba M, Tsuboi S, Noda T, Ohsumi Y. Autophagy in yeast demonstrated with proteinase-deficient mutants and conditions for its induction. *J Cell Biol*. 1992;119(2):301-312. doi:10.1083/jcb.119.2.301
180. Guo H, Chitiprolu M, Gagnon D, et al. Autophagy supports genomic stability by degrading retrotransposon RNA. *Nat Commun*. 2014;5. doi:10.1038/ncomms6276
181. Saiz-Baggetto S, Méndez E, Quilis I, Igual JC, Bañó MC. Chimeric proteins tagged with specific 3xHA cassettes may present instability and functional problems. *PLoS One*. 2017;12(8):1-12. doi:10.1371/journal.pone.0183067

182. Matsuki H, Takahashi M, Higuchi M, Makokha GN, Oie M, Fujii M. Both G3BP1 and G3BP2 contribute to stress granule formation. *Genes to Cells*. 2013;18(2):135-146. doi:10.1111/gtc.12023
183. Eiyama A, Kondo-Okamoto N, Okamoto K. Mitochondrial degradation during starvation is selective and temporally distinct from bulk autophagy in yeast. *FEBS Lett*. 2013;587(12):1787-1792. doi:10.1016/j.febslet.2013.04.030
184. Wadgaonkar P, Chen F. Connections between endoplasmic reticulum stress-associated unfolded protein response, mitochondria, and autophagy in arsenic-induced carcinogenesis. *Semin Cancer Biol*. 2021;76:258-266. doi:10.1016/j.semcancer.2021.04.004
185. Grumati P, Morozzi G, Hölper S, et al. Full length RTN3 regulates turnover of tubular endoplasmic reticulum via selective autophagy. *Elife*. 2017;6:1-32. doi:10.7554/eLife.25555
186. Fumagalli F, Noack J, Bergmann TJ, et al. Translocon component Sec62 acts in endoplasmic reticulum turnover during stress recovery. *Nat Cell Biol*. 2016;18(11):1173-1184. doi:10.1038/ncb3423
187. An H, Ordureau A, Paulo JA, Shoemaker CJ, Denic V, Harper JW. TEX264 is an ER-resident ATG8-interacting protein critical for endoplasmic reticulum remodeling during nutrient stress Heeseon. *Mol Cell*. 2019;74(5):891-908. doi:10.1016/j.molcel.2019.03.034.TEX264
188. Chen Q, Xiao Y, Chai P, Zheng P, Teng J, Chen J. ATL3 Is a Tubular ER-Phagy Receptor for GABARAP-Mediated Selective Autophagy. *Curr Biol*. 2019;29(5):846-855.e6. doi:10.1016/j.cub.2019.01.041
189. Yang M, Luo S, Wang X, et al. ER-Phagy: A New Regulator of ER Homeostasis. *Front Cell Dev Biol*. 2021;9(July):1-10. doi:10.3389/fcell.2021.684526
190. Rørvig S, Honore C, Larsson L-I, et al. Ficolin-1 is present in a highly mobilizable subset of human neutrophil granules and associates with the cell surface after stimulation with fMLP. *J Leukoc Biol*. 2009;86(6):1439-1449. doi:10.1189/jlb.1008606
191. Tausk FA, Milgram SL, Mains RE, Eipper BA. Expression of a peptide processing enzyme in cultured cells: Truncation mutants reveal a routing domain. *Mol Endocrinol*. 1992;6(12):2185-2196. doi:10.1210/mend.6.12.1491698
192. Bäck N, Kanerva K, Kurutihalli V, et al. The endocytic pathways of a secretory granule membrane protein in HEK293 cells: PAM and EGF traverse a dynamic multivesicular body network together. 2018;96(5):407-417. doi:10.1016/j.ejcb.2017.03.007.The
193. Waite KA, Burris A, Vontz G, Lang A, Roelofs J. Proteaphagy is specifically regulated and requires factors dispensable for general autophagy. *J Biol Chem*. 2022;298(1):101494. doi:10.1016/j.jbc.2021.101494
194. Barmada SJ, Skibinski G, Korb E, Rao EJ, Wu JY, Finkbeiner S. Cytoplasmic mislocalization of TDP-43 is toxic to neurons and enhanced by a mutation associated with familial amyotrophic lateral sclerosis. *J Neurosci*. 2010;30(2):639-649. doi:10.1523/JNEUROSCI.4988-09.2010
195. Uchida A, Sasaguri H, Kimura N, et al. Non-human primate model of amyotrophic lateral sclerosis with cytoplasmic mislocalization of TDP-43. *Brain*. 2012;135(3):833-846. doi:10.1093/brain/awr348
196. Gonzalez A, Mannen T, Çağatay T, et al. Mechanism of karyopherin-β2 binding and nuclear import of ALS variants FUS(P525L) and FUS(R495X). *Sci Rep*. 2021;11(1):1-15. doi:10.1038/s41598-021-83196-y
197. Walker AK, Spiller KJ, Ge G, et al. Functional recovery in new mouse models of ALS/FTLD after clearance of pathological cytoplasmic TDP-43. *Acta Neuropathol*. 2015;130(5):643-660. doi:10.1007/s00401-015-1460-x
198. Lange A, Mills RE, Lange CJ, Stewart M, Devine SE, Corbett AH. Classical nuclear localization signals: Definition, function, and interaction with importin α. *J Biol Chem*. 2007;282(8):5101-5105. doi:10.1074/jbc.R600026200

199. Imasaki T, Shimizu T, Hashimoto H, et al. Structural Basis for Substrate Recognition and Dissociation by Human Transportin 1. *Mol Cell*. 2007;28(1):57-67. doi:10.1016/j.molcel.2007.08.006
200. Nishimura AL, Upunski V, Troakes C, et al. Nuclear import impairment causes cytoplasmic trans-activation response DNA-binding protein accumulation and is associated with frontotemporal lobar degeneration. *Brain*. 2010;133(6):1763-1771. doi:10.1093/brain/awq111
201. Pinarbasi ES, Cağatay T, Fung HYJ, Li YC, Chook YM, Thomas PJ. Active nuclear import and passive nuclear export are the primary determinants of TDP-43 localization. *Sci Rep*. 2018;8(1):1-16. doi:10.1038/s41598-018-25008-4
202. Mahboubi H, Seganathy E, Kong D, Stochaj U. Identification of Novel Stress Granule Components That Are Involved in Nuclear Transport. *PLoS One*. 2013;8(6). doi:10.1371/journal.pone.0068356
203. Córdova EJ, Martínez-Hernández A, Uribe-Figueroa L, et al. The NRF2-KEAP1 pathway is an early responsive gene network in arsenic exposed lymphoblastoid cells. *PLoS One*. 2014;9(2). doi:10.1371/journal.pone.0088069
204. Komatsu M, Kurokawa H, Waguri S, et al. The selective autophagy substrate p62 activates the stress responsive transcription factor Nrf2 through inactivation of Keap1. *Nat Cell Biol*. 2010;12(3):213-223. doi:10.1038/ncb2021
205. Ichimura Y, Komatsu M. Activation of p62/SQSTM1-keap1-nuclear factor erythroid 2-related factor 2 pathway in cancer. *Front Oncol*. 2018;8(JUN):1-8. doi:10.3389/fonc.2018.00210
206. Fu J, Xiong Z, Huang C, et al. Hyperactivity of the transcription factor Nrf2 causes metabolic reprogramming in mouse esophagus. *J Biol Chem*. 2019;294(1):327-340. doi:10.1074/jbc.RA118.005963
207. Sakurai A, Nishimoto M, Himeno S, et al. Transcriptional regulation of thioredoxin reductase 1 expression by cadmium in vascular endothelial cells: Role of NF-E2-related factor-2. *J Cell Physiol*. 2005;203(3):529-537. doi:10.1002/jcp.20246
208. Kim YJ, Ahn JY, Liang P, Ip C, Zhang Y, Park YM. Human prx1 gene is a target of Nrf2 and is up-regulated by hypoxia/reoxygenation: Implication to tumor biology. *Cancer Res*. 2007;67(2):546-554. doi:10.1158/0008-5472.CAN-06-2401
209. He F, Antonucci L, Karin M. NRF2 as a regulator of cell metabolism and inflammation in cancer. *Carcinogenesis*. 2020;41(4):405-416. doi:10.1093/carcin/bgaa039
210. Markmiller S, Soltanieh S, Server KL, et al. Context-Dependent and Disease-Specific Diversity in Protein Interactions within Stress Granules. *Cell*. 2018;172(3):590-604.e13. doi:10.1016/j.cell.2017.12.032
211. Mitsuishi Y, Taguchi K, Kawatani Y, et al. Nrf2 Redirects Glucose and Glutamine into Anabolic Pathways in Metabolic Reprogramming. *Cancer Cell*. 2012;22(1):66-79. doi:10.1016/j.ccr.2012.05.016
212. Jiménez-Villegas J, Ferraiuolo L, Mead RJ, Shaw PJ, Cuadrado A, Rojo AI. NRF2 as a therapeutic opportunity to impact in the molecular roadmap of ALS. *Free Radic Biol Med*. 2021;173:125-141. doi:10.1016/j.freeradbiomed.2021.07.022
213. Bergström P, Von Otter M, Nilsson S, et al. Association of NFE2L2 and KEAP1 haplotypes with amyotrophic lateral sclerosis. *Amyotroph Lateral Scler Front Degener*. 2014;15(1-2):130-137. doi:10.3109/21678421.2013.839708
214. Zhang D, Xiao Y, Lv P, et al. Edaravone attenuates oxidative stress induced by chronic cerebral hypoperfusion injury: role of ERK/Nrf2/HO-1 signaling pathway. *Neurol Res*. 2018;40(1):1-10. doi:10.1080/01616412.2017.1376457
215. McLean JE, Hamaguchi N, Belenky P, Mortimer SE, Stanton M, Hedstrom L. Inosine 5′-monophosphate dehydrogenase binds nucleic acids in vitro and in vivo. *Biochem J*. 2004;379(2):243-

251. doi:10.1042/BJ20031585
216. Martinez Tosar LJ, Thomas MG, Baez MV, Ibanez I, Chernomoretz A, Boccaccio GL. Staufen: from embryo polarity to cellular stress and neurodegeneration Leandro. *Front Biosci*. 2012;4:432-451. doi:10.1109/epqu.2011.6128966
217. Paul S, Dansithong W, Figueroa KP, Scoles DR, Pulst SM. Staufen1 links RNA stress granules and autophagy in a model of neurodegeneration. *Nat Commun*. 2018;9(1). doi:10.1038/s41467-018-06041-3
218. Lee S, Mayr C. Gain of additional BIRC3 protein functions through 3′UTR- mediated protein complex formation. *Mol Cell*. 2019;74(4):701-712. doi:10.1016/j.molcel.2019.03.006.Gain
219. Hu S, Claud EC, Musch MW, Chang EB. Stress granule formation mediates the inhibition of colonic Hsp70 translation by interferon-γ and tumor necrosis factor-α. *Am J Physiol - Gastrointest Liver Physiol*. 2010;298(4):481-492. doi:10.1152/ajpgi.00234.2009
220. Ma A, Wang J, Yang L, An Y, Zhu H. AMPK activation enhances the anti-atherogenic effects of high density lipoproteins in apoE-/- mice. *J Lipid Res*. 2017;58(8):1536-1547. doi:10.1194/jlr.M073270
221. Liao LX, Song XM, Wang LC, et al. Highly selective inhibition of IMPDH2 provides the basis of antineuroinflammation therapy. *Proc Natl Acad Sci U S A*. 2017;114(29):E5986-E5994. doi:10.1073/pnas.1706778114
222. Panther E, Dürk T, Ferrari D, et al. AMP affects intracellular CA2+ signaling, migration, cytokine secretion and T cell priming capacity of dendritic cells. *PLoS One*. 2012;7(5). doi:10.1371/journal.pone.0037560
223. Feng C, Mery AG, Beller EM, Favot C, Boyce JA. Adenine Nucleotides Inhibit Cytokine Generation by Human Mast Cells through a G s -Coupled Receptor . *J Immunol*. 2004;173(12):7539-7547. doi:10.4049/jimmunol.173.12.7539
224. Tischbein M, Baron DM, Lin YC, et al. The RNA-binding protein FUS/TLS undergoes calcium-mediated nuclear egress during excitotoxic stress and is required for GRIA2 mRNA processing. *J Biol Chem*. 2019;294(26):10194-10210. doi:10.1074/jbc.RA118.005933
225. Bensimon G, Lacomblez L, Meininger V. A Controlled Trial of Riluzole in Amyotrophic Lateral Sclerosis. *N Engl J Med*. 1994;330(9):585-591.
226. Go CD, Knight JDR, Rajasekharan A, et al. A proximity-dependent biotinylation map of a human cell. *Nature*. 2021;595(7865):120-124. doi:10.1038/s41586-021-03592-2
227. Alexander EJ, Niaki AG, Zhang T, et al. Ubiquilin 2 modulates ALS/FTD-linked FUS–RNA complex dynamics and stress granule formation. *Proc Natl Acad Sci U S A*. 2018;115(49):E11485-E11494. doi:10.1073/pnas.1811997115
228. Malty RH Aoki H KAPSASZQMZGFMGWZA-THMMDVKSSVJMSNEXXVJPBFLJATGBYHB-GDNKPJBM. A Map of Human Mitochondrial Protein Interactions Linked to Neurodegeneration Reveals New Mechanisms of Redox Homeostasis and NF-?B Signaling. *Cell Syst*. 2017;5(6):564-577.e12. Epub 2017 Nov 8.
229. Suter B, Fontaine JF, Yildirimman R, et al. Development and application of a DNA microarray-based yeast two-hybrid system. *Nucleic Acids Res*. 2013;41(3):1496-1507. doi:10.1093/nar/gks1329
230. Cieślak M, Roszek K, Wujak M. Purinergic implication in amyotrophic lateral sclerosis—from pathological mechanisms to therapeutic perspectives. *Purinergic Signal*. 2019;15(1):1-15. doi:10.1007/s11302-018-9633-4
231. Kori M, Aydln B, Unal S, Arga KY, Kazan D. Metabolic Biomarkers and Neurodegeneration: A Pathway Enrichment Analysis of Alzheimer's Disease, Parkinson's Disease, and Amyotrophic Lateral

Sclerosis. *Omi A J Integr Biol*. 2016;20(11):645-661. doi:10.1089/omi.2016.0106
232. D'Ambrosi N, Finocchi P, Apolloni S, et al. The Proinflammatory Action of Microglial P2 Receptors Is Enhanced in SOD1 Models for Amyotrophic Lateral Sclerosis. *J Immunol*. 2009;183(7):4648-4656. doi:10.4049/jimmunol.0901212
233. Kato S, Kato M, Kusano T, Nishino T. New strategy that delays progression of amyotrophic lateral sclerosis in G1H-G93A transgenic mice: Oral administration of xanthine oxidoreductase inhibitors that are not substrates for the purine salvage pathway. *J Neuropathol Exp Neurol*. 2016;75(12):1124-1144. doi:10.1093/jnen/nlw088
234. Guiler W, Koehler A, Boykin C, Lu Q. Pharmacological Modulators of Small GTPases of Rho Family in Neurodegenerative Diseases. *Front Cell Neurosci*. 2021;15(May):1-18. doi:10.3389/fncel.2021.661612
235. Stankiewicz TR, Pena C, Bouchard RJ, Linseman DA. Dysregulation of Rac or Rho elicits death of motor neurons and activation of these GTPases is altered in the G93A mutant hSOD1 mouse model of amyotrophic lateral sclerosis. *Neurobiol Dis*. 2020;136. doi:10.1016/j.nbd.2020.104743. Dysregulation
236. Droppelmann CA, Campos-Melo D, Volkening K, Strong MJ, Volkening K, Strong MJ. The emerging role of guanine nucleotide exchange factors in ALS and other neurodegenerative diseases. *Front Cell Neurosci*. 2014;8(September):1-14. doi:10.3389/fncel.2014.00282
237. Brady OA, Zheng Y, Murphy K, Huang M, Hu F. The frontotemporal lobar degeneration risk factor, TMEM106B, regulates lysosomal morphology and function. *Hum Mol Genet*. 2013;22(4):685-695. doi:10.1093/hmg/dds475
238. Geisler S, Holmström KM, Skujat D, et al. PINK1/Parkin-mediated mitophagy is dependent on VDAC1 and p62/SQSTM1. *Nat Cell Biol*. 2010;12(2):119-131. doi:10.1038/ncb2012
239. Wang N, Ma Q, Peng P, et al. Autophagy and Ubiquitin-Proteasome System Coordinate to Regulate the Protein Quality Control of Neurodegenerative Disease-Associated DCTN1. *Neurotox Res*. 2020;37(1):48-57. doi:10.1007/s12640-019-00113-y
240. Meissner F, Molawi K, Zychlinsky A. Mutant superoxide dismutase 1-induced IL-1β accelerates ALS pathogenesis. *Proc Natl Acad Sci U S A*. 2010;107(29):13046-13050. doi:10.1073/pnas.1002396107
241. Figley MD, Bieri G, Kolaitis RM, Paul Taylor J, Gitler AD. Profilin 1 associates with stress granules and ALS-Linked mutations alter stress granule dynamics. *J Neurosci*. 2014;34(24):8083-8097. doi:10.1523/JNEUROSCI.0543-14.2014
242. Turakhiya A, Meyer SR, Marincola G, et al. ZFAND1 Recruits p97 and the 26S Proteasome to Promote the Clearance of Arsenite-Induced Stress Granules. *Mol Cell*. 2018;70(5):906-919.e7. doi:10.1016/j.molcel.2018.04.021
243. Tripathi P, Guo H, Dreser A, et al. Pathomechanisms of ALS8: altered autophagy and defective RNA binding protein (RBP) homeostasis due to the VAPB P56S mutation. *Cell Death Dis*. 2021;12(5). doi:10.1038/s41419-021-03710-y
244. Krasniak CS, Ahmad ST. The Role of CHMP2B Intron5 in Autophagy and Frontotemporal Dementia. *Brain Res*. 2016;1649(B):151-157. doi:10.1016/j.brainres.2016.02.051.The
245. Tsai N-P, Wei L-N. RhoA/ROCK1 signaling regulates stress granules formation and apoptosis. *Cell Signal*. 2010;22(4). doi:10.1016/j.cellsig.2009.12.001.RhoA/ROCK1
246. Schmidt SI, Blaabjerg M, Freude K. RhoA Signaling in Neurodegenerative Diseases. 2022:1-32.
247. Conti A, Riva N, Pesca M, et al. Increased expression of Myosin binding protein H in the skeletal muscle of amyotrophic lateral sclerosis patients. *Biochim Biophys Acta - Mol Basis Dis*. 2014;1842(1):99-106. doi:10.1016/j.bbadis.2013.10.013

248. Hu JH, Chernoff K, Pelech S, Krieger C. Protein kinase and protein phosphatase expression in the central nervous system of G93A mSOD over-expressing mice. *J Neurochem*. 2003;85(2):422-431. doi:10.1046/j.1471-4159.2003.01669.x
249. Tönges L, Günther R, Suhr M, et al. Rho kinase inhibition modulates microglia activation and improves survival in a model of amyotrophic lateral sclerosis. *Glia*. 2014;62(2):217-232. doi:10.1002/glia.22601
250. Joshi AR, Muke I, Bobylev I, Lehmann HC. ROCK inhibition improves axonal regeneration in a preclinical model of amyotrophic lateral sclerosis. *J Comp Neurol*. 2019;527(14):2334-2340. doi:10.1002/cne.24679
251. Mondal S, Hsiao K, Goueli SA. A Homogenous Bioluminescent System for Measuring GTPase, GTPase Activating Protein, and Guanine Nucleotide Exchange Factor Activities. *Assay Drug Dev Technol*. 2015;13(8):444-455. doi:10.1089/adt.2015.643
252. Bianchi-Smiraglia A, Rana MS, Foley CE, et al. Internally ratiometric fluorescent sensors for evaluation of intracellular GTP levels and distribution. *Nat Methods*. 2017;14(10):1003-1009. doi:10.1038/nmeth.4404
253. Nini L, Dagnino L. Accurate and reproducible measurements of RhoA activation in small samples of primary cells. *Anal Biochem*. 2010;398(1):135-137. doi:10.1016/j.ab.2009.11.011
254. Klionsky DJ, Elazar Z, Seglen PO, Rubinsztein DC. Does bafilomycin A1 block the fusion of autophagosomes with lysosomes? *Autophagy*. 2008;4(7):849-850. doi:10.4161/auto.6845
255. Klionsky DJ, Abdelmohsen K, Abe A, et al. Guidelines for the use and interpretation of assays for monitoring autophagy (3rd edition). *Autophagy*. 2016;12(1):1-222. doi:10.1080/15548627.2015.1100356
256. Heydrick SJ, Lardeux BR, Mortimore GE. Uptake and degradation of cytoplasmic RNA by hepatic lysosomes: Quantitative relationship to RNA turnover. *J Biol Chem*. 1991;266(14):8790-8796.
257. Floyd BE, Morriss SC, MacIntosh GC, Bassham DC. Evidence for autophagy-dependent pathways of rRNA turnover in Arabidopsis. *Autophagy*. 2015;11(12):2199-2212. doi:10.1080/15548627.2015.1106664